

NOTE TO USERS

This reproduction is the best copy available.

UMI[®]

**STUDIES ON THE EFFECT OF SODIUM IN
BRIDGMAN-GROWN CuInSe_2**

Hadley Franklin Myers (B.Eng., Concordia University, Canada),

Department of Electrical and Computer Engineering,

McGill University, Montreal

October, 2008.

A thesis submitted to McGill University in partial fulfillment of the requirements of
the degree of Master of Engineering.

© Hadley Franklin Myers 2008



Library and Archives
Canada

Published Heritage
Branch

395 Wellington Street
Ottawa ON K1A 0N4
Canada

Bibliothèque et
Archives Canada

Direction du
Patrimoine de l'édition

395, rue Wellington
Ottawa ON K1A 0N4
Canada

Your file *Votre référence*
ISBN: 978-0-494-66956-3
Our file *Notre référence*
ISBN: 978-0-494-66956-3

NOTICE:

The author has granted a non-exclusive license allowing Library and Archives Canada to reproduce, publish, archive, preserve, conserve, communicate to the public by telecommunication or on the Internet, loan, distribute and sell theses worldwide, for commercial or non-commercial purposes, in microform, paper, electronic and/or any other formats.

The author retains copyright ownership and moral rights in this thesis. Neither the thesis nor substantial extracts from it may be printed or otherwise reproduced without the author's permission.

In compliance with the Canadian Privacy Act some supporting forms may have been removed from this thesis.

While these forms may be included in the document page count, their removal does not represent any loss of content from the thesis.

AVIS:

L'auteur a accordé une licence non exclusive permettant à la Bibliothèque et Archives Canada de reproduire, publier, archiver, sauvegarder, conserver, transmettre au public par télécommunication ou par l'Internet, prêter, distribuer et vendre des thèses partout dans le monde, à des fins commerciales ou autres, sur support microforme, papier, électronique et/ou autres formats.

L'auteur conserve la propriété du droit d'auteur et des droits moraux qui protègent cette thèse. Ni la thèse ni des extraits substantiels de celle-ci ne doivent être imprimés ou autrement reproduits sans son autorisation.

Conformément à la loi canadienne sur la protection de la vie privée, quelques formulaires secondaires ont été enlevés de cette thèse.

Bien que ces formulaires aient inclus dans la pagination, il n'y aura aucun contenu manquant.


Canada

ABSTRACT

Ingots containing single crystals were grown from melts of Cu, In and Se in either stoichiometric proportions (CuInSe_2) or with an excess of Se ($\text{CuInSe}_{2.2}$). In addition, either sodium selenide (Na_2Se) or elemental sodium (Na^0) was introduced to both sets of compositions in concentrations ranging from 0 to 3 at. %. The starting constituents were placed in quartz ampoules, which were evacuated and sealed before undergoing a vertical-Bridgman growth procedure. Analysis of deposits seen on the ampoule walls and on the ingot surface after growth revealed the presence of Na, as well as various forms of the other starting elements; however, no Na was found within the crystals. Electrical measurements revealed trends in the thermoelectric power of the ingots to correspond with additions of Na, as well as the presence of excess Se. A sign conversion from p- to n-type was confirmed with addition of sodium to stoichiometric CuInSe_2 . A suggested mechanism used to explain the effects of Na on the material, based on these experimental observations, is presented.

RÉSUMÉ

Des lingots monocristallins ont été développés dans cette étude par la croissance en phase fondue de Cu, In et de Se soit en proportions stœchiométriques (CuInSe_2) ou avec un excès de Se ($\text{CuInSe}_{2,2}$). L'addition, soit du sodium sélénure (Na_2Se) ou du sodium élémentaire (Na^0), a été faite pour les deux types de compositions avec des concentrations de 0 à 3 at. %. Les éléments ont été placés dans des ampoules de quartz et ces dernières ont été évacuées et fermées hermétiquement avant d'être subis à la méthode de croissance verticale Bridgman. L'analyse des dépôts observés sur les parois des ampoules et sur la surface des lingots après la croissance démontre la présence de Na, ainsi que d'autres formes variées des éléments premièrement introduits dans les ampoules, tandis qu'une absence de Na a été observée dans les cristaux eux-mêmes. Les résultats des mesures électriques démontrent des tendances dans la puissance thermoélectrique des lingots qui correspondent avec l'addition de Na ainsi qu'avec la présence en excès de Se. Une conversion de type-p en type-n du CuInSe_2 avec l'addition de sodium a été confirmée. Une explication possible par rapport à l'effet de Na sur ce matériel basée sur ces résultats est présentée.

ACKNOWLEDGEMENTS

The author wishes to express his gratitude to his supervisors, Prof. C.H. Champness and Prof. I. Shih, for their continued guidance throughout the course of this work. It is because of them that this work was made possible.

Furthermore, there are several individuals who have given their time and effort for the advancement of this work: Jozsef Boka and Don Pavlasek, from the mechanical workshop, for their help in machining various mechanical components; Slovak Poplawski and Monique Riendeau, from the Department of Mining and Materials Engineering, for the XRD analysis of the samples, and to Yue Tan, for insightful discussions concerning these analyses; Glenna Keating, from the Department of Earth and Planetary Sciences, for further analysis of the XRD results; Dr. Farid Bensebaa, of the Institute for Chemical Process and Environmental Technology, National Research Council, Ottawa, for the XPS analysis of the white and red deposits; Hui Du, for valuable discussions concerning the nature of these experiments; Han Jen Yang, for SEM analysis of some of the samples presented this work; Jeanne-Louise Shih, for help with the translation of the abstract; and, finally, the graduate students at the Nano Electronic Devices and Materials laboratory, for their continuous encouragement. To all of these individuals, the author wishes to extend his thanks and appreciation.

In addition, the author would like to acknowledge the sources of financial support provided to him during the course of this work: McGill University, Natural Science and Engineering Research Council of Canada (NSERC), and Fond québécois de la recherche sur la nature et les technologies (FQRNT).

Finally, the author would like to thank his wife, Lisanne, for her patience and support as this thesis was being written.

TABLE OF CONTENTS

ABSTRACT	i
RÉSUMÉ	ii
ACKNOWLEDGEMENTS	iii
TABLE OF CONTENTS	iv
1 INTRODUCTION	1
2 THEORETICAL BACKGROUND FOR THE ELECTRICAL EVALUATION	9
2.1 INTRODUCTION	9
2.2 THERMOELECTRIC POWER	10
(a) Definition	10
(b) Simplifying Conditions	10
(c) Relationships to Carrier Concentration	11
2.3 ELECTRICAL RESISTIVITY	12
(a) Definition	13
(b) Four-Point-Probe	13
(c) Assumptions	14
2.4 CARRIER MOBILITY	15
3 HISTORICAL REVIEW OF CIS PHOTOVOLTAICS	17
3.1 HISTORY	17
(a) Monocrystalline Solar Cells	18
(b) Polycrystalline Solar Cells	18
(c) Discoveries of the Beneficial Effects of Sodium	21
3.2 EFFECTS OF SODIUM IN POLYCRYSTALLINE CuInSe ₂ FILMS AND SOLAR CELLS	23
3.3 SODIUM EFFECT MODELS	25
(a) The Oxygen Model	26
(b) The In _{Cu} Model	26
(c) The Na _{In} Model	27
(d) The Na ₂ Se _x Model	28
4 BRIDGMAN-GROWTH OF CuInSe₂ WITH Na₂Se AND Na⁰	29
4.1 INTRODUCTION	29

4.2	AMPOULE PREPARATION	30
	(a) Ampoule Formation	30
	(b) Ampoule Cleaning	31
	(c) Boron Nitride Coating	32
	(d) Ampoule Neck Formation	33
4.3	CHARGE PREPARATION	34
	(a) Etching	34
	(b) Weighing	36
	(c) Indium Foil Formation	37
	(d) Loading	38
	(e) Evacuation and Sealing	39
	(f) Pre-Reaction Heating	40
4.4	BRIDGMAN GROWTH PROCEDURE	43
	(a) Initial Heating, Temperature Soaking, and Agitation	43
	(b) Ampoule Lowering and Cooling	46
4.5	DISCUSSION	47
5	EXPERIMENTAL RESULTS	62
5.1	INTRODUCTION	62
5.2	VISUAL INSPECTION OF AMPOULES	63
	(a) White Deposit	63
	(b) Red Deposit	64
	(c) Ampoule Dots	66
	(d) Selenium Deposits	67
	(e) Copper Nodules	67
5.3	VISUAL INSPECTION OF INGOTS	68
	(a) Opening of Ampoule and removal of Ingot	68
	(b) Cohesiveness and Mini-Cracks	69
	(c) Surface Deposits	72
	(d) Wafer Cutting and Cleaning	73
5.4	MICROSTRUCTURAL ANALYSIS	74
	(a) X-ray Diffraction	74
	(b) X-ray Photoelectron Spectroscopy	76
	(c) Scanning Electron Microscopy – Energy Dispersive X-ray	77
5.5	ELECTRICAL MEASUREMENTS	79
	(a) Resistivity	79
	(b) Thermoelectric Power	81
5.6	DISCUSSION	84

6	DISCUSSION AND CONCLUSIONS	112
6.1	INTRODUCTION	112
6.2	DISCUSSION OF RESULTS	112
6.3	FUTURE WORK	119
	REFERENCES	121

Chapter 1

Introduction

Copper indium diselenide (CuInSe_2), is a member of a family of compounds known as chalcopyrites, having the same crystal structure and chemical formula, I III VI₂. Apart from the other members of this family, which includes CuFeS_2 (fool's gold) [1.1], CuInSe_2 , whose the crystal structure is shown in Fig. 1.1 [1.2], is a material of extreme interest in the photovoltaic industry. This interest is primarily due its remarkably high optical absorption coefficient, which, having a value of 10^5 cm^{-1} over a wavelength ranging from 300 to 1300 nm, is approximately 1000 times greater than that of crystalline silicon [1.1]. In addition, the material has a direct bandgap of 1.04 eV. The combination of these two characteristics makes CuInSe_2 (also known as CIS) a serious choice as an absorber material in thin-film solar cells. Research over the past three decades has finally led to the production of polycrystalline CIS-based cells with efficiencies approaching 20% [1.3], leading to speculation that the performance of such thin-film devices may eventually challenge that of Si. However, in order for this to be achieved, much information and knowledge must be acquired into the nature and characteristics of this exciting, yet somewhat enigmatic compound. For comparative purposes, a plot of the best research-cell efficiencies, for various technologies versus the year that research was conducted, is shown in Fig. 1.2 [1.4]. The efficiency of a cell is defined as the

percentage of the total energy of the photons from the sun impacting the surface of the cell that is transformed into electrical energy by the cell.

The growth and study of monocrystalline ingots of CuInSe_2 (CIS) has been carried out for some time in this laboratory [1.5-7]. The aim of these previous works was to shed some light on the nature and characteristics of the chalcopyrite, and provide information that would ultimately improve the performance of photovoltaic devices using polycrystalline forms of the material. Included in these investigations has been the study of the physical [1.8] and electrical [1.9] characteristics of the material, as well as the effects of non-stoichiometry [1.10]. It was reported by Du et al [1.11] that a deficiency of selenium results in a conversion from p to n-type material; stoichiometric CuInSe_2 grown in this laboratory is always p-type. In addition, the effects of incorporating additional elements other than Cu, In, and Se into CuInSe_2 growth-melts has been explored. Among these additional elements is sodium, in experiments conducted by Wang et al [1.12] in which elemental sodium, Na^0 , was added to melts containing Cu, In, and Se in the stoichiometric proportions of 1:1:2, respectively. It was discovered during the course of this previous work that CuInSe_2 becomes n-type when high concentrations of Na^0 , 0.25 at. % or above, are added.

It has been well established that polycrystalline CuInSe_2 solar devices benefit from the presence of sodium [1.13-15]; this is known as the “sodium effect” [1.16]. Despite many years of research, which has taken place at numerous laboratories and

institutions located on several continents, there has yet to be a consensus on the actual cause of this benefit. In addition to the work of Wang et al [1.12], there has been some research exploring this effect which was performed using monocrystalline materials, including epitaxial films [1.17,18]. As well, the effects of annealing solution-grown monocrystals in sodium vapour were investigated by Lyahovitskaya et al [1.19]. However, as thin-film polycrystalline cells are the intended application devices that motivate studies investigating the cause of this effect, much of the work performed elsewhere has been on polycrystalline CIS films. In these studies, the presence of grain boundaries, on which it has been suggested [1.19,20] sodium or sodium compounds congregate, might complicate the analysis or perhaps mask the true effects of Na on the material. Therefore, the present work seeks to determine the effects of Na on CIS containing essentially no grain boundaries, i.e., single crystals.

Following an experimental procedure previously developed in this laboratory over two decades and fine tuned for this study, the starting constituents of copper, indium and selenium were incorporated into quartz ampoules along with varying amounts of Na, ranging from 0 to 3 atomic percent. Ingots were then obtained from melts of these starting constituents by Bridgman-growth. While these ingots are not completely defect-free, they were found to contain several centimeter-sized monocrystals, so that there are fewer deposition sites as compared to polycrystalline films.

Initially, Na was incorporated in the form of Na_2Se to ampoules containing stoichiometric proportions of Cu, In, and Se. It was speculated that the type conversion observed in the ingots of Wang et al [1.12] might have been the result of the removal of Se from the material due to it bonding with the sodium. Therefore, in order to counter this, some extra Se was added, which accompanied the addition of Na. Following this, the experiment was repeated with a further addition of Se, so that the amounts of Cu, In, and Se added to the ampoules corresponded to CIS with a chemical formula of $\text{CuInSe}_{2.2}$ (excess Se). As will be seen in this thesis, analysis of the resulting ingots exposed several influences of sodium on the material, including an increase in hole concentration with corresponding increases of Na_2Se . These findings are consistent with work conducted elsewhere [1.21-23].

Upon completion of these runs, both sets (stoichiometric and excess Se) were repeated, except Na^0 was used as the source of sodium rather than Na_2Se . It was found, as reported here, that the use of Na^0 yielded spectacularly different results from those obtained using Na_2Se ; results that were consistent with those reported by Wang et al [1.12]. It was from these experimentally observed results, as well as the results of both experimental and theoretical work performed elsewhere, that a mechanism used to explain the cause of the effects of Na on CuInSe_2 was hypothesized. Several runs were also completed with an even greater excess of Se, corresponding to a chemical formula $\text{CuInSe}_{2.4}$, however, the results and subsequent analysis of these runs is not provided in this work.

At this point, it is perhaps helpful to provide a brief summary of what is included in this thesis, and specifically where this information can be found.

In order to understand the analysis of the growth runs, which is given in the later chapters of this thesis, it is necessary to possess some knowledge of theoretical semiconductor principles. These principles are provided in chapter 2.

Following this, a historical review of the use of CuInSe_2 as a solar cell material is presented in chapter 3. This review begins with a description of the earliest monocrystalline cells from the 1970s, and continues through to the fabrication and refinement of thin-film photovoltaics in the 1990s, and the subsequent discovery of the beneficial effects of sodium. A description of the effects of sodium on CIS, including the specific performance enhancements that occur in Na-containing CIS solar cells, is then provided. The chapter concludes with a brief explanation of several mechanisms proposed in the literature in order to explain these effects.

A thorough explanation of the procedure used to grow all of the ingots presented in this work is given in chapter 4. It was hoped, when writing this section, that it provide enough details to allow all parts of the experiments to be repeated exactly as was done here, should it one day be required. To this end, a strong effort was made to include every particular of the experimental procedure in this chapter, however seemingly insignificant.

The results of these experiments are given in chapter 5. These results include, aside from the physical and electrical characteristics of the ingots obtained throughout this work, descriptions of the deposits found within the ampoules, as well as the information yielded through analysis of these deposits and the attempts to identify them. Once again, an effort was made to include every minute detail observed. Following this is a discussion and interpretation of these results.

Further discussions and conclusions are presented in chapter 6, and a mechanism, which seeks to explain the chemistry behind the sodium-effect, is put forward. The chapter, as well as the thesis, concludes with some suggestions as to how this work could be expanded or improved.

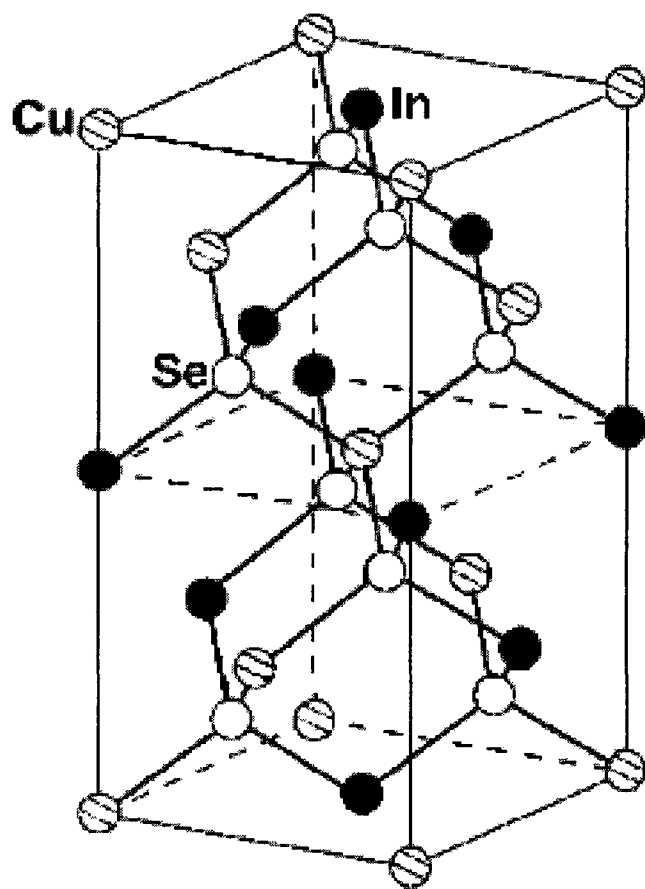


Figure 1.1 The crystal structure of CuInSe_2 [1.2].

Best Research-Cell Efficiencies

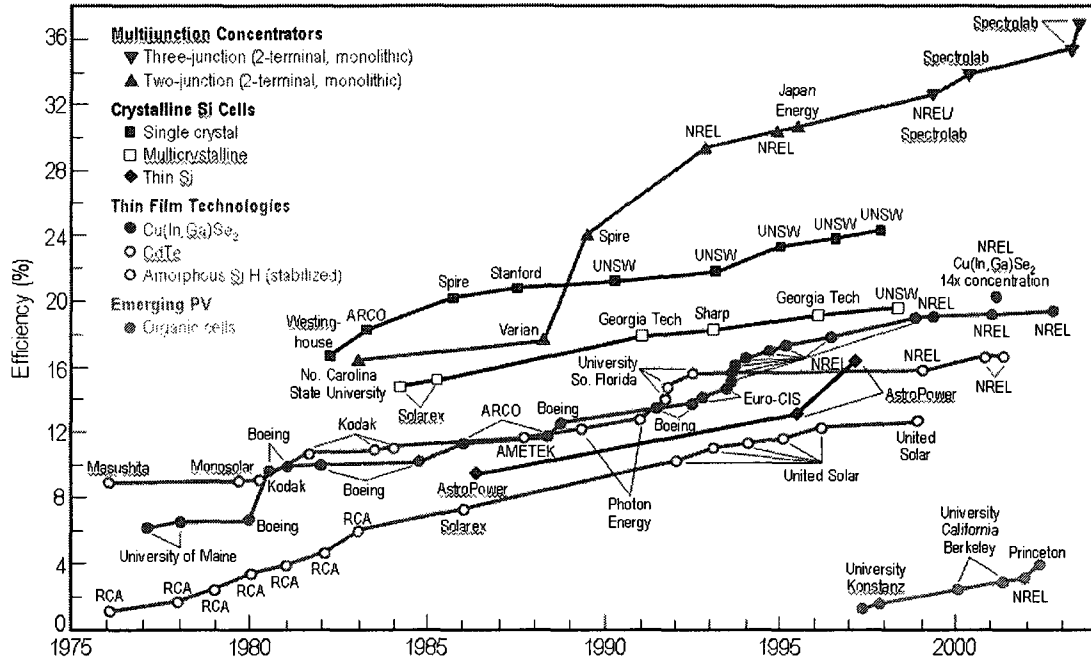


Figure 1.2 The best research-cell efficiencies for several solar cell technologies. The year of development of these cells is shown on the horizontal axis [1.4].

Chapter 2

Theoretical Background for the Electrical Evaluation

2.1. INTRODUCTION

While the main thrust of this thesis is the growth from the melt of CuInSe_2 with added sodium, it is convenient to present here, in this chapter, the basic relevant theoretical background of the quantities thermoelectric power and electrical resistivity. These two transport parameters were measured on the samples and used to evaluate the electrical changes in the material with increasing levels of sodium.

Copper indium diselenide has a higher electron-to-hole mobility ratio (μ) than most elemental semiconductors [2.1]. For this reason, the effect of the minority electrons when analyzing p-type materials cannot always be ignored. However, insight into the material can nonetheless be gained using single carrier analysis. As the objective of this work is to determine the effect that sodium (Na) has on CuInSe_2 , which is achieved through an examination of ingots grown with varying concentrations of Na, it is only necessary to recognize a general trend in the ingots. Thus, when analyzing the materials, only the majority carrier was considered. The expressions which govern this analysis are therefore presented in this chapter.

2.2. THERMOELECTRIC POWER

In chapter 5, thermoelectric power (α), or Seebeck coefficient, measurements are reported on the semiconductor samples, and this quantity was used to calculate mobile carrier concentrations. The following, therefore, is a simple treatment of how the thermoelectric effect was applied.

2.2 (a) Definition

Consider a sample of material in which there are two separate points with temperatures T_1 and T_2 , where $T_2 > T_1$, with a uniform temperature gradient existing between the points, as shown in Fig 2.1. If the measured thermoelectric voltage between these points is ΔV , then the thermoelectric power (α) is defined as:

$$\alpha = \frac{\Delta V}{T_2 - T_1} \quad \text{as } T_2 \rightarrow T_1 \quad . \quad (2.1)$$

2.2 (b) Simplifying Conditions

The equations governing the thermoelectric power of a semiconductor are greatly simplified when under the following conditions:

- 1) The free hole concentration (p) is very much greater than the free electron concentration (n), i.e. $p \gg n$;
- 2) The Fermi energy level E_F lies several kT above the valence band energy level E_V , i.e.,

$$E_F - E_V > 2kT \quad , \quad (2.2)$$

where T is absolute temperature and k is Boltzmann's constant. This corresponds to a nondegenerate distribution of holes, whereby, if the reduced Fermi energy for holes η_p^* is defined as

$$\eta_p^* = \frac{E_V - E_F}{kT} \quad , \quad (2.3)$$

then,

$$\eta_p^* < -2 \quad , \quad (2.4)$$

- 3) The hole mobility μ_p and effective mass m_p are isotropic and single-valued;
- 4) The scattering of the holes has a collision relaxation time τ , characterized by the relation

$$\tau = a\varepsilon_p^{-\frac{1}{2}} \quad , \quad (2.5)$$

where ε_p is the reduced kinetic energy of the holes in units of kT and a is a coefficient, independent of energy. The exponent of ε_p of $-1/2$ corresponds to ideal acoustic lattice scattering, which can apply to simple semiconductors often at and above room temperature.

2.2 (c) Relationships to Carrier Concentration

Under the conditions listed above, it can be shown in the literature [2.2] that α is given by

$$\alpha = \frac{k}{e} (2 - \eta_p^*) \quad , \quad (2.6)$$

and

$$p = N_V \exp[\eta_p^*] \quad , \quad (2.7)$$

where e is the electronic charge and N_V is defined as

$$N_V = 2 \left(\frac{2\pi m_p kT}{h^2} \right)^{3/2} \quad , \quad (2.8)$$

where h is Plank's constant. Therefore the thermoelectric power can be expressed as

$$\alpha = \frac{k}{e} \left[2 - \ln \left(\frac{ph^3}{2(2\pi m_p kT)^{3/2}} \right) \right] \quad . \quad (2.9)$$

Equation (2.9) can be used to calculate the carrier concentration (p) from the thermoelectric power. For example, if the experimentally measured thermoelectric power at room temperature is $500 \mu\text{V/K}$, with k/e taken as $86 \mu\text{V/K}$ and $m_p^*/m_0 = 1$ for simplicity [2.3], where m_0 is the free electron mass, then $p = 5.5 \times 10^{17} \text{ cm}^{-3}$. In this case, η_p^* would be -3.8 , thus satisfying Eq. (2.4).

2.3. ELECTRICAL RESISTIVITY

Chapter 5 also contains electrical resistivity (ρ) measurements on the semiconductor samples, which were then used in some cases to determine carrier

mobility. Like thermoelectric power, the basic equations for these measurements, carried out with a four-point-probe, are now set down.

2.3 (a) Definition

Consider a rectangular piece of semiconductor of length L and cross-sectional area A . If an electric field (ξ) is applied across the length of the semiconductor, producing a current per unit area (J), then the resistivity (ρ) can be defined as:

$$\xi = \rho \cdot J \quad , \quad (2.10)$$

or, rearranged,

$$\rho = \frac{AV}{LI} \quad , \quad (2.11)$$

where V is the voltage across the semiconductor and I is the current through the semiconductor.

2.3 (b) Four-Point-Probe

Consider a situation in which four co-linear probes are placed equidistant from each other on the surface of a material, as shown in Fig 2.2. If a current (I) passing from one outer-probe, through the material, to the other outer-probe produces a

voltage (V) between the two inner-probes, then it can be shown [2.4] that the electrical resistivity of the material can be expressed as:

$$\rho = 2\pi s \frac{V}{I} f \quad , \quad (2.12)$$

where s is the distance between the probes and f is the graphed correction factor, which is dependent on the spacings of the probes, the length of the probes to the edge of the sample surface, and whether the edge and the area underneath the sample is conducting.

In the case of a thin plate of material, however, the resistivity, neglecting the correction factor, is expressed considering the thickness t of the material rather than the distance between the probes as follows:

$$\rho = \frac{\pi}{\ln(2)} \frac{V}{I} t \quad . \quad (2.13)$$

2.3 (c) Assumptions

When using the four-point-probe method to measure resistivity of a semiconductor, it was necessary to make the following assumptions [2.5]:

- 1) The resistivity in the area of measurement is uniform;

- 2) The effect of minority carrier injection into the semiconductor on the conductivity is negligible;
- 3) The surface of measurement is flat, and there is no surface leakage;
- 4) The probes lie along the semiconductor surface in a straight line;
- 5) The area of contact between each of the four probes and the surface of the semiconductor is small compared to the spacing of the probes.

2.4. CARRIER MOBILITY

The carrier concentration, expressed in Sec. 2.2, can be combined with the resistivity, Sec. 2.3, to determine the mobility of the carriers according to the following relation:

$$\rho = \frac{1}{e(\mu_n n + \mu_p p)} \quad , \quad (2.14)$$

where μ_n and μ_p are the electron and hole mobilities, respectively, expressed in units of $\text{cm}^2/\text{V}\cdot\text{sec}$ if ρ is in ohm-cm and e is in coulombs. For a p-type semiconductor with $p \gg n$, Eq. (2.13), can be further simplified to:

$$\rho = \frac{1}{e\mu_p p} \quad . \quad (2.15)$$

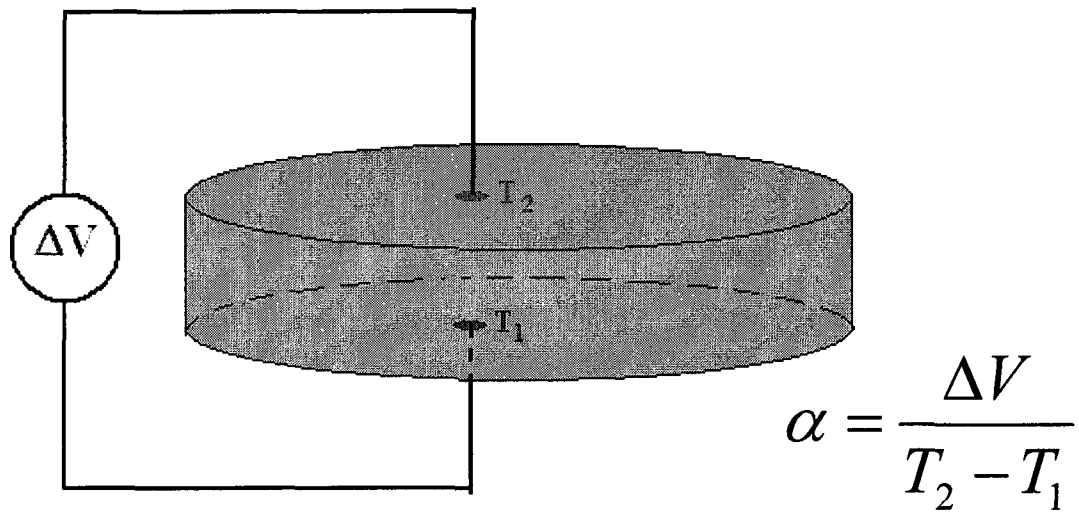


Figure 2.1 A piece of material in which there are two separate points with temperatures T_1 and T_2 , where $T_2 > T_1$, with a uniform temperature gradient existing between them. The thermoelectric power (α) is defined as the voltage produced between them divided by the temperature difference.

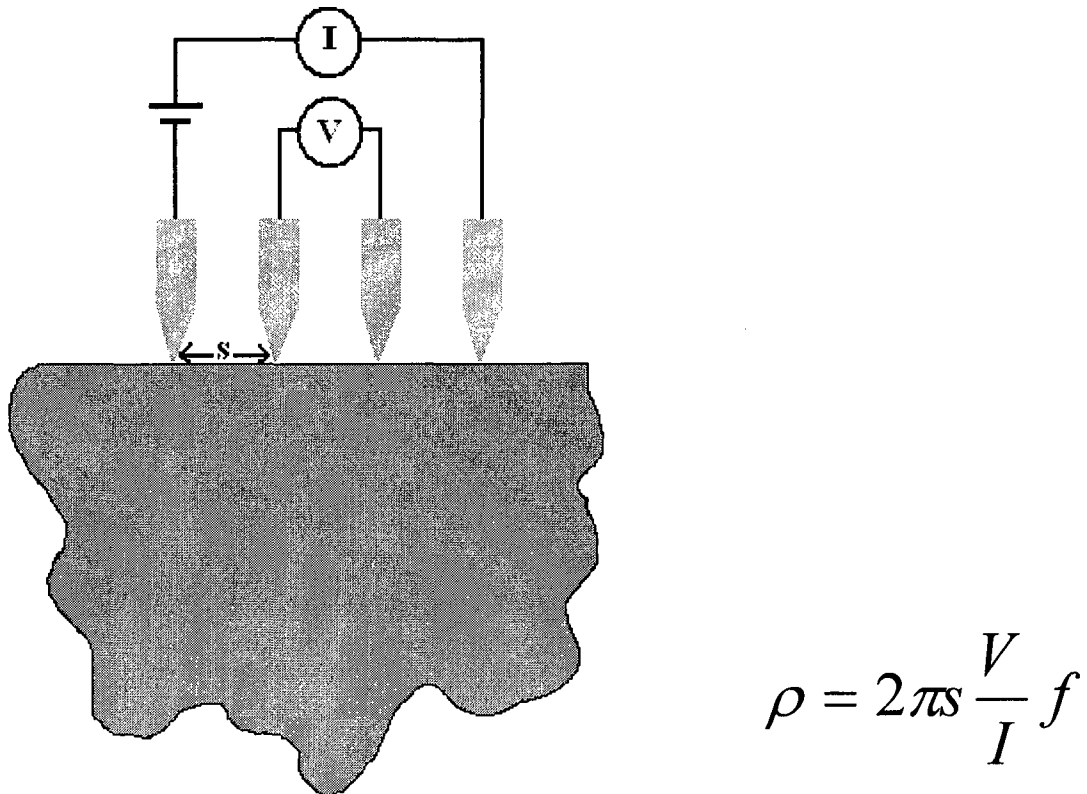


Figure 2.2 Graphical representation of a four-point-probe setup used to measure the resistivity (ρ) of a material. The equation used in calculating ρ is shown, where s is the spacing between the probes and f is a geometrical correction factor.

Chapter 3

Historical Review of CIS Photovoltaics

3.1. HISTORY

Before examining the effect of sodium on CIS and CIGS solar cells, it is helpful to understand the history of developments which eventually led to its use. While the synthesis of CuInSe_2 can be traced back to the early 1950s [3.1], the first photovoltaic cell employing this compound was fabricated about 20 years later, at Bell Telephone Laboratories in 1974, by Wagner, Shay, Migliorato and Kasper [3.2] using a monocrystalline absorber layer. Their cell had a solar conversion efficiency of 5%, which, by varying the construction, they more-than doubled the following year [3.3]. Shortly afterwards, studies into the fabrication of thin-film polycrystalline cells [3.4] had begun. As time went on and work progressed, changes were gradually made in the design structure of the cells, with the combined goal of reducing construction costs and improving efficiency. One of these changes was the substitution of alumina or glass substrates, on which the thin-film devices were previously made, for soda-lime glass. An important improvement in cell performance was eventually linked to the sodium content in the soda-lime glass, which led to the study of the effects of this element on CuInSe_2 and Cu(In,Ga)Se_2 .

3.1 (a) Monocrystalline Solar Cells

The single-crystal solar cell of Wagner *et al* [3.2] was constructed with melt-grown CuInSe_2 . The starting constituents were first loaded into a silica boat contained within a silica ampoule, which was then heated to 1050°C . Monocrystalline ingots were then obtained by directional freezing [3.5]. Substrates were cut from the ingots, and then polished and etched, followed by an anneal in selenium vapour to introduce p-type conductivity. A 5-10 μm thick layer of cadmium sulfide (CdS) was then evaporated on to the surface of the substrate. Indium contacts were then soldered on to the n-type CdS , while gold contacts were deposited from an aqueous AuCl_3 solution onto the p-type CuInSe_2 . The solar power conversion efficiency of this early device was recorded to be 5%. One year later, in 1975, the efficiency of the monocrystalline device was improved to 12% [3.3]. This was done by growing the CdS layer on the (112) face of the CuInSe_2 substrate. In addition, a layer of SiO was grown onto the CdS ; this layer serves as an antireflection coating. However, the effective area of the cell was only 0.79 mm^2 , which was too small for practical use.

3.1 (b) Polycrystalline Solar Cells

As single-crystal CuInSe_2 solar cells were being developed, work was simultaneously taking place regarding the preparation of thin films by researchers including L.L. Kazmerski *et al* [3.6], in which films of CuInS_2 , another I-III-VI₂ chalcopyrite, were grown using a two-source technique. In this technique, powdered single-phase CuInS_2 is evaporated from a crucible onto a substrate, while sulfur is

simultaneously evaporated from a second crucible. In this way, it was possible to control the amount of sulfur in the system and hence the carrier concentration. This method was later used to produce thin-films of CuInSe_2 by using selenium rather than sulfur in the second crucible [3.4]. By 1976, solar cells were fabricated by depositing this layer onto an Au-metallized glass substrate, followed by the growth of a CdS film directly onto the CuInSe_2 . Aluminum top contacts were then put on the CdS layer. In addition, a second configuration, whereby the CdS was grown onto the metallized surface, and the CuInSe_2 film was grown onto the CdS, was experimented with. With this inverted configuration, light is shone directly onto the CuInSe_2 . However, the former substrate configuration exhibited greater performance, achieving an efficiency of 5.7%, which, through refining, was improved two years later, in 1978, to 6.6% [3.7].

Shortly thereafter, in 1980, Michelsen and Chen, working at Boeing Aerospace Company, fabricated a thin-film CuInSe_2 solar cell using a simultaneous elemental evaporation process [3.8]. A layer of molybdenum and a layer of gold were first sputtered onto an alumina substrate, followed by the deposition of CuInSe_2 . This was done in two steps, first with a substrate temperature of 350 °C and second with 450 °C. The purpose of this was to create a thin polycrystalline layer of small grains and low resistivity on the gold surface, followed by a layer of larger grains. This was to avoid creating a non-Ohmic contact between the CuInSe_2 and the metal layers. Following this, the substrate was cooled to 150 °C for the deposition of the CdS. This as well was done in two steps. The first half of the CdS layer was deposited via CdS

evaporation, while the second half was co-evaporated with a small amount of indium, which serves to create a layer of reduced resistivity, thus reducing the series resistance of the device. An aluminum grid, placed on the CdS by vacuum deposition, served as the top electrode. The efficiency of this device was 5.7%.

However, four years later, the efficiency was improved dramatically to 11% [3.9]. In this cell configuration, gold had been left out of the construction; a layer of molybdenum 1.5 μm thick was sputtered onto the polycrystalline alumina substrates, which served as the back electrode. A 3-4 μm layer of CuInSe_2 was then deposited directly onto the molybdenum by elemental co-evaporation at a substrate temperature of between 350-450 $^\circ\text{C}$. Unlike the cell previously described, the grain size did not appear to be dependent on substrate temperature. After the CuInSe_2 deposition, the substrate was cooled to 200 $^\circ\text{C}$ for CdS deposition by compound evaporation. Additionally, cells were fabricated with CdZnS rather than CdS; the addition of zinc had been previously predicted theoretically to increase the open-circuit voltage of the cells [3.10], which was confirmed experimentally [3.9]. A thickness of 2-3 μm of CdS, or CdZnS, was deposited, with indium co-evaporation, once again near the final state of the deposition to reduce the resistivity. Following this, an aluminum film 2 μm thick was deposited by electron gun evaporation, and the entire cell was baked at 200-225 $^\circ\text{C}$ in oxygen for 20-60 minutes in order to grow a 95 nm thick layer of SiO_x , which served as an anti-reflection (AR) layer. The efficiency was subsequently increased to 12.4% due to refining of this AR layer, as well as reductions in resistive losses [3.11].

Over the next few years, several changes were made to the structure of CuInSe₂ thin-film cells. One such change involved the alloying of CuInSe₂ with CuGaSe₂ in order to obtain the material CuIn_{1-x}Ga_xSe₂, which has a larger bandgap than the ternary and is a better match to the solar spectrum [3.12]. As well, the CdS layer was reduced in thickness, and an additional thin layer of highly resistive ZnO was included above the CdS, followed by a thicker layer of lower resistivity ZnO:Al. The subsequent deposition of the top electrode on the highly resistive ZnO rather than directly on the CdS resulted in better performance of the cells [3.13].

3.1 (c) Discoveries of the Beneficial Effects of Sodium

One other change made to the structure of the cells involved the substrate material. Soda-lime glass (SLG) was originally chosen for its cost advantages [3.14], but it became apparent very quickly that the choice of this material over conventional substrates somehow contributed to a significant increase in device performance. This realization prompted research aimed at pinpointing the cause and nature of this performance enhancement.

In 1989, Margulis et al [3.15] saw a coarse “aggregate” structure in CuInSe₂ films deposited on 7059 corning glass or Si-single crystal substrates, but an absence of this aggregate structure on films deposited on SLG and Al₂O₃. This was attributed to a better match of thermal expansion coefficient between CIS and the latter substrates.

In 1992, Stolt et al [3.16] fabricated CuInSe_2 thin-film cells on substrates of SLG and sintered alumina. A higher open-circuit voltage and fill factor were observed for the SLG cells versus the alumina cells. In addition, a high conversion efficiency, 14.8%, was achieved for the SLG configuration. A close observation of the CIS films themselves revealed an increased grain size and $\langle 112 \rangle$ orientation as compared to the films deposited on alumina. These enhancements were as well attributed to the thermal expansion properties of the soda-lime glass.

Then, in 1994, Bodegård et al [3.17], at the European Photovoltaic Solar Energy Conference in Amsterdam, sought to isolate the influence of sodium, contained within the SLG, from the influence of thermal expansion properties of the soda-lime glass, focusing their work on film properties. They deposited films on substrates of borosilicate glass, sintered alumina, soda-lime glass, and soda-lime glass with a sodium diffusion barrier. XRD analysis of their samples indeed revealed an increase of $\langle 112 \rangle$ orientation for SLG without the diffusion barrier over the other substrates. They then put scratches in the diffusion barrier, and observed a corresponding increase in orientation around the scratches. XPS revealed sodium on the surface of these films. They also fabricated solar cells from these films and observed the highest efficiencies from the SLG cells without the diffusion barrier.

Holz et al [3.14], at the same conference, also sought to isolate the effects of sodium in SLG on CuInSe_2 thin-films. However, rather than only using a sodium diffusion barrier, they also used an alkali-free substrate (sapphire) in order to

guarantee that there was no sodium contamination from the substrate. They deposited CIS films on both bare and covered soda-lime glass, and both Na-implanted and Na-free sapphire. They chose to focus their study on the electrical properties of the films, and observed an increase in conductivity with sodium present, suggesting the Na-effect is not merely limited to structure and orientation of the films. This increase in conductivity was proposed to be attributed to an increase in p-type doping of the absorber by the sodium [3.18].

3.2. EFFECTS OF SODIUM IN POLYCRYSTALLINE CuInSe_2 FILMS AND SOLAR CELLS

It may be possible to categorize the study of the effects of sodium on CuInSe_2 into two distinct areas: the overall benefit in device performance, and the specific effects of the sodium on the properties and characteristics of CIS and CIGS films and crystals. There is a general consensus in the literature that the primary benefits of Na on photovoltaic cells are the increase of both the open-circuit voltage (V_{OC}) and the fill-factor (FF) [3.17, 19, 20], yielding an improvement in device efficiency [3.20]. This is true for devices constructed on alkali-containing substrates [3.17, 20] and for cases in which Na was added to the absorber elements during deposition [3.19, 21]. Additionally, V_{OC} and FF are observed to be dependent on deposition temperature when SLG is used as the substrate [3.22]; this is further evidence of the Na effect, as the rate of Na diffusion from the substrate into the absorber is a function of deposition temperature [3.23]. However, as a reduced deposition temperature is desirable in order to minimize internal stress in the substrate during fabrication, efforts have been

made to increase the quantity of Na in the film via other means, such the deposition of Na compounds onto the substrate in advance of CIGS deposition and Na co-evaporation during deposition. In addition, various methods aimed at facilitating the diffusion of Na through the molybdenum back electrode into the absorber have been suggested, including one method whereby the Mo deposition pressure was shifted to incorporate tensile and compressive stresses into the metal and thereby increase its alkali diffusivity [3.24].

Studies of the effects of Na on polycrystalline films have as well led to a consensus: a (112) preferred orientation was observed to correspond with increases of Na in both CIS [3.16, 17, 25, 26] and CIGS [3.27]. Furthermore, an increase in average grain size was also observed [3.13, 16, 20, 24, 26]. Evidence has been presented [3.17, 28-31] that Na inside films is primarily located on grain boundaries and crystal surfaces rather than within the grains themselves. Additional evidence has been put forward [3.32] that Na cannot enter into intact CIS crystals, except via defects. Be that as it may, it has been suggested [3.20, 27] that the incorporation of Na into intact grains might be achievable and, from there, the Na is quickly transported to grain boundaries and eventually resides on surfaces.

In addition to morphology and orientation, electrical characteristics appear to be affected by the presence of Na. As was mentioned in previous sections, conductivity was seen to increase with a corresponding increase of Na in films [3.14, 24, 26]. Na was also suggested to increase the net acceptor concentration [3.18, 19,

33-35], possibly through a reduction of compensating donors in polycrystalline films [3.26]. This was also observed for epitaxial films [3.36]. However, it is in apparent contradiction with work done on single-crystal CuInSe_2 for which a type conversion from p to n was seen for ingots grown with increased concentrations of Na [3.37]. Nevertheless, Na incorporation in CIGS films was found to result in the creation of a shallow acceptor state 75 meV above the valence band [3.38].

Another observation made regarding the incorporation of Na into CIS and CIGS films is linked to the formation of defect pairs within the materials. Various reiterations of an electrically neutral pair of two copper vacancies 2VCu^- coupled with a single indium-on-copper site $\text{In}_{\text{Cu}}^{2+}$ has been used to explain the formation of ordered defect compounds (ODC), such as CuIn_5Se_8 , CuIn_3Se_5 , CuIn_4Se_7 , etc. [3.39]. There is some controversy regarding the effects of Na on the ODC structure of the material. In some work, Na had been observed to suppress the formation of ODC [3.40]. However, this is in contrast to work in which it was suggested that the transition from chalcopyrite to ODC was stimulated by the presence of Na [3.41].

3.3. SODIUM EFFECT MODELS

Several models have been proposed to explain the effects of sodium on CIS and CIGS. While there has yet to be a clear consensus in the scientific community on which model or models to accept, it may nevertheless be beneficial for an explanation of some of the more popular ones to be given at this point.

3.3 (a) The Oxygen Model

With this model [3.42, 43], it is proposed that sodium is indirectly responsible for the passivation of selenium vacancies V_{Se}^+ on the surface of CIGS thin-films, which normally act as shallow donors [3.44], thus reducing the donor compensation in these films, resulting in an increase in majority hole concentration. It is suggested that these vacancy defects can be electrically neutralized by being occupied by an oxygen atom. Sodium acts as a catalyst in this reaction by inducing the O-O bond in the physisorbed O_2 molecule to become polarized while simultaneously enhancing tunneling from the substrate through a Na-induced lowering of the surface workfunction. The result is an increase in O_2^- , which can be more easily dissociated into atomic O than can O_2 . The oxygen atoms are then free to bond with the In at the surface of the material, and the reaction is complete. Some evidence for this model was put forward by Ruckh et al [3.35], in which a relationship was found between the amount of oxygen in thin-films and the amount of sodium.

3.3 (b) The In_{Cu} Model

It was first proposed by Contreras et al [3.45] that the role of Na involves the elimination of donor point defects, specifically the In_{Cu} antisite. It is suggested that Na, upon the creation of a Cu-vacancy, will rush to fill that vacancy, thereby robbing the In of the opportunity and, in doing so, eliminating the donor site before it is created. The final result, again, is a reduction in donor compensation and an increase in the net majority carrier concentration of the material. This effect would be masked

in Cu-poor materials, as the greater number of Cu-vacancies present more opportunities for occupation by In atoms; the amount of Na in the material is finite, and so the supply may become exhausted if too many V_{Cu} exist. This model can be used to explain several experimentally observed effects of Na in CIGS. Such effects include the increase in hole concentration when Na is present, but also the reduced effect of Na in increasing the conductivity of CIGS when the material is made to be Cu-poor. Furthermore, the increased $\langle 112 \rangle$ orientation of CIGS films when grown in the presence of Na is explained by the better ordering of the cations resulting from In_{Cu} annihilation, as the $\langle 112 \rangle$ planes contain only copper and indium, and are selenium free. Additionally, the accumulation of Na on grain boundaries may be a result of the increased probability of the formation of In_{Cu} on surfaces rather than within the crystals. It was further suggested by Granata and Sites [3.46] that, if a portion of sodium is present in the form of Na^0 , that the removal of Cu sites in bulk CIS by Na may result in the formation of $NaInSe_2$ and Cu^0 .

3.3 (c) The Na_{In} Model

This model, unlike the two previous models, suggests that Na is responsible for the increase in p-conductivity through a direct doping effect in CIGS thin-films. In an experiment performed by Niles et al [3.47], CIGS films deposited on soda-lime glass were analyzed using XPS and found to contain Na-Se bonds. It is their contention that these bonds are not the result of the formation of compounds such as Na_2Se , which would be electrically neutral. Rather, they propose that these bonds are

the result of Na replacing either In or Ga to create Na_{In} or Na_{Ga} , which act as acceptor states, thereby increasing the carrier concentration of the material.

3.3 (d) The Na_2Se_x Model

This model, proposed by D. Braunger et al [3.48], is based on the high affinity between Na and Se, and the preferential formation of Na_2Se_x during CIS film formation. They propose that Na^+ -ions are diffused along the grain boundaries to the surface during growth, where they subsequently bond with elemental Se, forming Na_2Se_x , where $x = 1 \sim 6 \neq 5$. These compounds act as a Se reservoir, supplying selenium to the surface of the films. Therefore, Na is segregated at the grain boundaries in the form of Na_2Se_x . These compounds also play a role in the oxidation of the material, as oxidation of Na-containing CIS implies oxidation of the Na_2Se_x as well. This results in the formation of Se^0 and other compounds such as Na_2SeO_3 . It is further proposed [3.48, 49] that at low Se partial pressures, the formation of Na_2Se is preferential. As the binding energy of Na_2Se is quite strong, it is not possible to remove the Se for use in the absorber, resulting in a film which is Se-deficient. However, at high Se partial pressures, the formation of Na_2Se_x , where $x > 1$, is preferential. This compound is easily broken apart, so as to supply the growing films with Se, thereby reducing the density of donor-like Se-vacancies.

Chapter 4

Bridgman-growth of CuInSe_2 with Na_2Se and Na^0

4.1. INTRODUCTION

This study involves the experimental analysis of monocrystalline CuInSe_2 ingots, grown with varying proportions of the starting constituents and sodium, with the objective of determining the effect of the sodium on the physical and electrical properties of the material. This chapter describes in detail the exact process by which these ingots were obtained. The method of crystal growth used here is known as the vertical-Bridgman method, whereby the material is heated above the melting point and then cooled gradually starting from the tip, known as the first-zone-to-freeze, to the end, the last-zone-to-freeze. The specific techniques used throughout this work were largely developed by Z.A. Shukri [4.1], G.I. Ahmad [4.2], and H.P. Wang [4.3], and can be used to obtain relatively void-free ingots containing several fairly large monocrystals. A major advantage of this method is that it is a one-ampoule method, meaning compound synthesis and growth takes place in the same ampoule, thereby minimizing the loss of selenium. When stoichiometric proportions are used, with no additives, the resulting ingots are always uniformly p-type. By contrast, the two-ampoule method, whereby the ampoule used for synthesis is cut open and the material transferred to a second ampoule for growth, results in n-type samples [4.4], possibly due to the loss of selenium during the transfer.

It may be helpful for a brief summary of this chapter to be provided at this point. Section 4.2 of this thesis describes the method of preparation of the ampoule, including the shaping and cleaning of the quartz, and the technique by which a boron nitride coating is applied. Following this, Sec. 4.3 describes the preparation of the charge, including the weighing and etching, and the loading and sealing of the ampoules, as well as an explanation of a method pioneered in this study known as the indium boat method, whereby the indium pellets are flattened into a foil, which is used to transport powdered material, in this case Na_2Se , into the ampoule. Furthermore, this section provides information on the pre-reaction heating, which allows the exothermic reaction between the indium and the selenium to take place in an enclosed environment as a precaution against a possible cracking or explosion of the ampoule. Finally, Sec. 4.4 describes the actual growth procedure, which is conducted inside a two-zone Bridgman furnace, the upper zone at a higher temperature than the lower zone. The ampoule is suspended in the middle of the hotter zone by a quartz rod and slowly lowered into the cooler zone, thus allowing the compound to gradually solidify and crystallize. Section 4.5 then provides a brief discussion on the experiences and concerns of using this method.

4.2. AMPOULE PREPARATION

4.2 (a) Ampoule Formation

The ampoules in which the ingots were grown were fabricated from fused quartz tubes having an outer diameter of 16 mm and an inner diameter of 12 mm. The 2 mm wall thickness was necessary in order to withstand the high vapour

pressure of selenium in subsequent growth steps. An oxygen-hydrogen flame was used in forming the tip of the ampoule, as well as in subsequent steps that require the quartz be heated. This tip was formed to allow the nucleation of crystals from the melt to occur over a narrow region, and thus enhance monocrystalline growth. A spare piece of quartz tubing was attached to the end of the ampoule, and then carefully pulled away while the ampoule was subjected to the heat from the flame, thus forming an increasingly narrowed region of quartz with a pointed tip. Care was taken to ensure that the walls of this narrowed region, leading to the tip, remained thick in order to withstand the internal pressures that the ampoule will eventually experience. It is necessary, when performing this procedure, to rotate the ampoule constantly above the flame in order to ensure that the circumference is heated uniformly. The quartz emits a bright white light when heated to the appropriate temperature, and becomes somewhat soft and malleable. Failure to heat the quartz sufficiently or rotate it consistently results in great difficulty in shaping the ampoule.

4.2 (b) Ampoule Cleaning

Once the tip has been formed and the ampoule given several minutes to cool in the fume-hood, an acid solution, comprising three parts HCl and one part HNO₃ by volume, was poured into the quartz tube up to a height of approximately 15 cm in order to remove impurities. The tube was then kept upright for about 24 hours, with a small piece of aluminum foil covering the open end to prevent dust from falling in. After the time period had elapsed, the aluminum foil was removed and the acid poured out. The ampoule was then rinsed twice with de-ionized water to wash away

any acid or impurity residue still left in the tube. This procedure was then repeated with acetone in order to remove organic contaminants, with the time modified to around five hours rather than 24.

4.2 (c) Boron Nitride Coating

The process of coating the inside of the ampoule with boron nitride (BN) was pioneered in this laboratory by Ziad Shukri [4.1], and has proven to be an integral part of the fabrication procedure. Attempts at creating CuInSe_2 by the Bridgman method prior to the development of this process had resulted in ingots which adhered to the sides of the quartz ampoule and were plagued with cracks and cavities [4.5]. The treatment of the inside of the ampoule with BN proved to be a solution to both these problems. Approximately five grams of Boron Nitride Coating Type A, manufactured by The Carborundum Company, were added to 20 ml of acetone. The mixture was agitated to create a suspension, and poured into the ampoule. The ampoule was then rotated at such an angle as to allow the BN to distribute evenly across the inside surface, while simultaneously pouring out the BN suspension. It was necessary to repeat this process several times until the desired uniformity and consistency was obtained. De-ionized water was used to rinse away carefully the BN from the sides of the tube, which would not be included in the ampoule, leaving the powder undisturbed up to a length of approximately 10 cm from the tip. The quartz tube was then placed in the fume hood and supported at an angle of roughly 30° from horizontal, with the open end being lower than the tip. After an air drying period lasting anywhere between 15 and 72 hours, the ampoule was subjected to an intense

flaming-in process, whereby the exterior surface of the quartz was subjected to an oxygen-hydrogen flame, causing it to become white hot. It could be observed that the powder would vaporize during this step, allowing the coating to spread out and adhere to the entire inside surface. It was judged that the flame-in process was complete when the sides of the quartz, before which the white powder was clearly visible, became totally transparent, except for some faint streaks of cloudiness, as indicated in Fig. 4.1. The flaming-in process occasionally resulted in the forming of a BN residue at the tip of the ampoule. Attempting to flame-in this residue would normally result in a misshapen tip, which was undesirable for crystal growth. In these instances, the tip would be reformed following the procedure detailed in Sec. 4.2 (a).

4.2 (d) Ampoule Neck Formation

This process involves creating a region of quartz 2 cm in length, approximately 12 cm from the tip, with an outer diameter roughly equivalent to one-third its starting diameter. The purpose of this was to facilitate the sealing of the ampoule, as explained in Sec. 4.3 (e) of this work. The neck was formed much the same way as the tip, by rotating a portion of the quartz continuously over an intense flame while simultaneously pulling both sides away from the flame. The notable exception, however, is that the pieces were not completely pulled apart but rather were left attached with an inner diameter large enough to allow the pellets of material to pass through. In the case of the ampoules used for runs without sodium selenide, the neck formation process was done immediately following the BN flaming-in step, after the spare piece of quartz was attached to the ampoule tip but before the tip was

reformed. However, for the runs involving sodium selenide, adding the Na_2Se prevented the neck region from being formed previously, making it necessary to perform neck formation once the sodium selenide had been loaded into the ampoule. It was necessary to protect this charge from reacting due to the heat from the neck formation step. To this end, a piece of paper towel was folded over three times and soaked in cold water before being wrapped around the ampoule up to a length of 10 cm, encompassing the tip and the charge. Furthermore, when forming the neck, the quartz tube was held at an angle not less than 15° from horizontal to ensure that the charge remained at the bottom, away from the heat.

4.3. CHARGE PREPARATION

4.3 (a) Etching

The materials used in these experiments which required etching were the copper (Cerac Coating Materials, 2-6 mm shot, 5N purity), the selenium (Noranda Mines Limited, 2-3 mm shot, 5N purity), the indium (Metal Specialties Inc, 2-5 mm shot, 5N purity), and the metallic sodium, Na^0 . The only other material that was included in several runs was sodium selenide, Na_2Se (Alfa Aesar, powder packed in Argon, 99.8% purity), which did not require etching. In the case of the copper, a solution comprising a 1:10 volume ratio of nitric acid to DI-water was used. A quantity of pellets weighing roughly 5 grams more than the final required amount was placed in a beaker, into which was added 30 ml of acid. A starting mass of copper well above the final mass plus the expected weight lost from etching was necessary for the weighing step, as explained in Sec. 4.3 (b). The pellets were allowed to soak

for 3 minutes, during which time the beaker was agitated to ensure uniform etching. The acid was then carefully poured out such that the pellets remained in the beaker, and DI-water was poured in to rinse off any excess acid or residue. The pellets were then placed between two laboratory wipes to allow them to dry. Upon etching the copper, the physical appearance of the pellets changed from somewhat dark to a bright, salmon colour. It was noticed that the former colour returned to the pellets within a few hours of drying, and that it would be increasingly dark each time an etching was performed. For this reason, the etching of the copper was done as close as possible to the time of evacuation of the ampoule, and after the etching and weighing of the other materials. The procedure used for etching the selenium was identical to that for the copper, with the notable exception that a solution of 1:10 hydrochloric acid to DI-water was used rather than 10% nitric acid, and that the quantity etched was approximately one gram greater than the final amount required. As for the indium, the 10% hydrochloric acid solution was again employed, but the pellets were allowed to soak for only 30 seconds. It had previously been observed that excessive etching of indium causes the pellets to stick together, resulting in complications and difficulty during the weighing process [4.6-7].

The metallic sodium was stored in mineral oil, and so it was necessary to remove this oil before loading the sodium into the ampoule. In order to accomplish this, the sodium was immersed in toluene for approximately 30 seconds, and then, to minimize oxidation, immediately loaded into the ampoule, which was subsequently

evacuated of air. This cleaning was done after the weighing of the sodium, unlike the other starting elements, for which etching was completed before weighing.

4.3 (b) Weighing

The quantities for ingots HM-B01 and HM-B02, shown in Table 4.1, were measured on a Nova Digital Pocket Scale with an accuracy of 0.01 grams. For all of the other growth runs presented in this work, a Mettler AE100 balance (readability 0.0001 g) was used. When weighing the indium, small bits were twisted off the pellets with tweezers in order to attain the desired final amount with as high an accuracy as possible. With the selenium, one pellet could be split in several pieces with the end of a spatula for the same purpose. Achieving a highly accurate measurement was more complicated with the copper, as the pellets could not be easily separated into smaller pieces. It was therefore necessary to etch a relatively large quantity of copper to allow pellets of different sizes to be tested until a combination with the desired weight and accuracy was found. While the package supplied by the manufacturer states that the copper pellets are between 2-6 mm in size, significantly smaller pieces were included at the bottom of the container and a quantity of them was intentionally included in the etching process. These smaller pieces facilitated the adjustment of the total final weight of the copper. Such measures were not necessary when weighing the sodium selenide, as the starting material was in powdered form. The copper, indium, and selenium were all weighed out on a piece of aluminum foil, while the sodium selenide was weighed either on aluminum foil or on indium foil made from the previously measured indium pellets, as explained in Sec. 4.3 (c). The

elemental sodium was cut from a larger piece stored in oil and was also weighed on indium foil. However, as the removal of the oil took place after weighing, in order to prevent the material from oxidizing from exposure to air, the mass of the weighed material was approximately 10% greater than the theoretically required value. This is to compensate for the mass of the oil. Therefore, the added quantity of metallic sodium could only be relatively compared for each run (i.e. a 2% run had approximately double the sodium used in a 1% run), but could not be said to be accurate to one ten-thousandth of a gram, as could be said for the other elements and the sodium selenide.

4.3 (c) Indium Foil Formation

The addition of sodium selenide to the starting constituents of copper indium diselenide, pioneered in this work, resulted in several unanticipated problems. It was noticed, as the sodium selenide was poured into the top of the ampoule, that some of it adhered to the sides of the quartz before descending into the bottom of the ampoule. Attempts to dislodge this material by tapping on the ampoule were not entirely successful and only managed to free some of it. Aside from the raising uncertainties of the quantity of sodium selenide within the completed ingots starting constituents, it was believed that the presence of sodium selenide on the walls of the quartz weakened its structural integrity and caused it to crack during the ampoule sealing process, described in Sec. 4.3 (e). Two separate methods were therefore devised to ensure that the entire weighed quantity of sodium selenide was present in the bottom of the ampoule during sealing. The first method involved forming a long, thin spoon

out of aluminum foil, and using this spoon to pass the material down the quartz tube to the bottom of the ampoule. To prevent the powder from sticking to the sides of the tube due to static charges, the end of the spoon was shaped to form a cylinder, so that upon reaching the ampoule, the tube could be lifted upright and the powder shaken out before the spoon was retracted. This method was used only for runs HM-B09, HM-B16, and HM-B17 (Table 4.1), and was experimented with as an alternative to the second method, which is more time consuming and labour intensive. After the etching and weighing of the indium pellets, they were placed one-by-one on a small piece of aluminum foil, which had been polished with a laboratory wipe, and rolled thin with a hard cylindrical piece of plastic. Subsequent pellets were pressed into the previously thinned mass of indium until all pellets were included, resulting in a circular piece of indium of approximately 2 cm in diameter and 1.5 mm in thickness. The sodium selenide could then be weighed directly on this piece of indium, after which it was delicately folded and squeezed into a shape resembling a boat, with the complete quantity of powder inside. This boat was placed just inside the open end of the quartz tube, and carefully pushed to the closed end with a thin quartz rod, as can be seen in Fig. 4.2. This method was used for all growth runs which included Na_2Se , with the exception of the three runs previously mentioned.

4.3 (d) Loading

Once the neck region had been given adequate time to cool to room temperature in the fume hood, approximately 10 minutes, the remainder of the starting constituents could be added. For the runs which included Na_2Se , the order in

which they were added was first the indium boat with Na_2Se , then selenium, and then copper. In the cases where an indium boat was not used, the Na_2Se was added first, followed by selenium, indium and copper. For all other ingots, the charge was added in the order of Se, In, Cu, and, if applicable, Na^0 . The first three elements could simply be poured down the quartz tube and into the ampoule. However, the metallic sodium pieces were inserted immediately after cleaning to prevent oxidation and, still being wet with toluene, stuck to the sides of the tube. A straightened wire hanger was therefore used. Here, the sodium piece was stuck to one end of the hanger and carefully fed into the tube, whereupon it was pushed off the hanger and onto the metal pellets in the ampoule.

4.3 (e) Evacuation and Sealing

After loading of the charge, it was necessary to create a vacuum inside the ampoule. This was done using a Difstak 50/60 110V 60W diffusion pump system, manufactured by BOC Edwards. The open end of the ampoule was positioned in the narrow opening of the pump, between which was placed an O-ring to ensure a proper seal. After securing the O-ring in place with a metal guide and attaching a rubber stopper just after the guide to prevent the ampoule from being sucked into the pump, the diffusion pump was activated. After a preliminary procedure lasting 30 minutes, during which the roughing pump was used to remove air from the tube, the baffle was opened; the evacuation time, shown for each run in Table 4.1, was counted from this point. For the first four growth runs, the evacuation was performed without the use of gauges to monitor the level of vacuum. Later, with the use of a BOC Edwards AIM-

S-NW25 Active Inverted Magnitron Gauge, it was determined that about two hours of evacuation time was sufficient to reach a pressure of approximately 5×10^{-6} torr, while five hours resulted in a pressure of 1×10^{-6} torr. The procedure for sealing the ampoule was started by wrapping a sheet of paper towel, that had been soaked in cold water, around the lower three quarters of the ampoule; this was to inhibit a reaction taking place from heat during the sealing process. Following this, an intense oxygen-hydrogen flame was passed evenly over the thinned region of the quartz. Care must be taken during this part of the sealing, as the quartz can crack quite easily if the heating is uneven. As well, it is preferable to have a long region of quartz above the open cavity of the ampoule; this will facilitate the joining of the ampoule to the quartz rod in the subsequent growth stage. With this in mind, the initial sealing of the cavity occurred at approximately one third the length of the narrowed neck region from the main ampoule region, while the remaining two thirds of the neck region were then progressively sealed. The baffle was closed during this process for safety concerns, as the quartz could easily crack during the sealing; the evacuation time was stopped at the closure of the baffle. Finally, the ampoule was detached from the remainder of the quartz tube by delicately applying downward pressure on the ampoule while simultaneously concentrating the heat from the flame on the top portion of the neck.

4.3 (f) Pre-Reaction Heating

Before Bridgman growth can take place, it is necessary for the ampoule contents to undergo a preliminary heating in order to allow the exothermic reaction between the selenium and the indium to take place. During the heating, the two

elements reacted at a temperature between 220°C and 240°C, above the melting point of selenium at 221°C. The heat generated by this reaction caused the selenium to vaporize, resulting in excessive pressures which could cause the quartz ampoule to crack. Accordingly, this pre-reaction heating was allowed to take place, in the present work, in a Thermolyne type 10500 brick furnace for the reason that, should the ampoule crack, the result would be contained, as opposed to the Bridgman furnace, in which the explosion would be more hazardous.

For runs HM-B01 and HM-B02, the ampoules were placed at approximately 15° to the horizontal in the brick furnace. The pre-reaction heating of these ampoules followed the temperature-ramp scheme depicted in Fig. 4.3 (a). The temperature was adjusted to 150°C, where it was given ten minutes to stabilize, and then raised at a rate of 10°C every ten minutes up until 250°C. From here, it was raised quickly to 300°C and kept at this temperature for a length of time before the furnace was shut off and the ampoules allowed to cool naturally to room temperature.

In the case of run HM-B03, the temperature was initially raised to 100°C before being increased 10°C every ten minutes, and this rate continued up until 300°C as depicted in Fig. 4.3 (b). The reason for the added caution during the pre-reaction was that it was unknown what effect the sodium selenide would have on the sample. Prior to this successful run, three ampoules in a row cracked during the pre-reaction heating, forcing their runs to be abandoned. A fourth, later called HM-B08, was temporarily abandoned when it was noticed, after the pre-reaction heating had taken

place, that the tip of the ampoule had been damaged. It was decided to heat the sample to 1100°C in the brick furnace to ensure the ampoule did not break or that the molten material did not leak from the damaged spot at such high temperatures. Having observed no such leak, the ampoule was then put through the Bridgman growth procedure, as detailed in Sec. 4.4.

While the pre-reaction scheme depicted in Fig. 4.3 (b) was employed for HM-B04, it was nonetheless decided to alter the procedure slightly in order to minimize the chance of future ampoules cracking. For all subsequent runs, the charge was positioned in the center of the ampoule, away from the thinned tip and neck region, and the ampoule was placed horizontally in the furnace. Furthermore, the time kept at 300°C was increased for all subsequent growth runs. This is in response to run HM-B05 cracking at a temperature of 350°C in the Bridgman furnace, for which it was suspected that the reaction time of 1 hour and 5 minutes had not been sufficient for the pre-reaction between the selenium and the indium to be completed. As well, for run HM-B10 and all subsequent runs, the temperature before the slow ramp-up was increased from 100°C to 150°C, as depicted in Fig. 4.3 (c), as it was realized that the added sodium did not have any effect on the ampoule cracking below the pre-reaction temperature.

4.4. BRIDGMAN GROWTH PROCEDURE

4.4 (a) Initial Heating, Temperature Soaking, and Agitation

After the pre-reaction heating had taken place and the ampoule had returned to room temperature, it was attached to one end of a quartz rod in order for it to be placed inside the Bridgman furnace. Before attaching the ampoule to the rod, it was once again necessary to wrap the ampoule with a sheet of paper towel that had been soaked in cold water to prevent a reaction from taking place, leaving the end that had been sealed after evacuation exposed. An oxygen-hydrogen flame was once again employed to heat the quartz during the attachment process. It was necessary to ensure that the ampoule was attached securely to the rod so that it did not break off during manual agitations. The rod was then introduced into the furnace, and positioned such that the tip of the ampoule was just beside the end of the upper furnace thermocouple.

The furnace itself is comprised of two heating elements separated by an insulating baffle. With the upper heating element set to a temperature above the melting point of the sample, and the lower heating element below that temperature, the sample was initially positioned in the upper zone and then lowered mechanically to the lower zone. Ideally, solidification of the sample would initially occur at the lowest point of the ampoule, and then gradually progress upwards along the sample, resulting in a monocrystalline ingot. A representation of the furnace used for these runs can be seen in Fig. 4.4, and the temperature profile of the furnace for soaking temperatures of 1100°C and 1050°C, measured using a type K thermocouple, is shown in Fig. 4.5. The furnace used for this experiment was a model 23/238-24-

2ZV-ST manufactured by Thermcraft, while the controller used to operate it was a Honeywell UDC 5000 unit.

For runs HM-B01 through HM-B03, the initial heating inside the Bridgman furnace was done at a rate of 5°C/min up to the maximum soaking temperature of 1100°C, as depicted in Fig. 4.6 (a).

During the heat soak phase of crystal growth in run HM-B04, an interruption occurred when the upper elements of the Bridgman furnace overheated and burned-out. An attempt was made to include a third thermocouple to the furnace setup, which would have been placed very close to the upper element itself. This would have been used to trigger an emergency shutdown if the temperature exceeded a critical value, thus preventing another burn-out. With a replacement element installed and the temperature again raised to 1100°C with the ampoule inside, the temperature as measured by the third thermocouple drifted downwards to a point, where the reading could not be trusted and the power was shut off a second time. The third-thermocouple method of protection was then abandoned. It was decided to lower the maximum temperature of the furnace to 1050°C (Fig. 4.6 (b)) and, for all subsequent runs, to lower the power supplied to the heating element, as controlled by the UDC 5000, from 100% to 60.5% of maximum once the soaking temperature had stabilized. The third attempt at Bridgman growth for HM-B04 was successful. The percentage of supplied power had to be gradually increased as the quality of the heating element deteriorated with use. Eventually the open end of the furnace was covered with

aluminum foil to minimize heat loss (HM-B31), thereby further stretching the lifetime of the heating element before it was finally replaced. The effects of this covering on the temperature profile of the furnace and, by extension, the crystal, have yet to be investigated.

After run HM-B05 cracked in the furnace during the ramp-up phase of the heating, the heating procedure was altered again for runs HM-B06 and HM-B07. The heating for these runs was done initially at a rate of $1^{\circ}\text{C}/\text{min}$ up to 300°C , whereupon the temperature was maintained for 1 hour before being raised at a rate of $5^{\circ}\text{C}/\text{min}$ to the maximum soaking temperature, as shown in Fig. 4.6 (c). This scheme was then changed again for run HM-B08 through to run HM-B17 to speed up the initial soaking by increasing the heating rate from room temperature to 150°C to $5^{\circ}\text{C}/\text{min}$ (Fig. 4.6 (d)). Nevertheless, the cracking of the next two unnamed ampoules (one at a temperature of 160°C and the next at a temperature of 360°C), caused the heating scheme to be altered yet again to the one depicted in Fig. 4.6 (e). Although a few more ampoules cracked at different times during the heating process, this is the scheme used for all runs after and including HM-B18.

The ampoules were kept at their maximum soaking temperature in the upper furnace for between 18 and 26 hours. Within this period of time, the ampoules were carefully but quickly removed from the furnace and gently rocked back and forth to ensure the melt was homogeneous before being returned to the furnace. This manual rocking comprised one agitation. Although it had not happened over the course of

this work, there is a risk that the ampoule could break when removed from the furnace. As such, it is important that safety precautions be taken when performing the agitations, including wearing protective goggles and gloves.

4.4 (b) Ampoule Lowering and Cooling

During the heating of the ampoule in the upper furnace, the temperature of the lower furnace was gradually raised to 700°C, which is below the melting point of CuInSe₂ of 986°C [4.8-9]. Once the ampoule had completed the heat soak, the lowering mechanism was activated, allowing the ampoule to move into the lower furnace at a rate of approximately 5 mm/hr. However, for run HM-B10 and subsequent runs, the ampoules were manually lowered in the upper furnace, such that the tips of the ampoules were about 5 cm above the insulating baffle before the mechanism was turned on, thus saving one day of lowering time. As the material is still liquid at this position, runs HM-B01 to HM-B09 might be considered to have soaked for longer than the 24 hours that is stated in Table 1. Once it was ascertained that the tip of the ampoule had reached the location of the lower thermocouple, the temperature of the upper zone was reduced to 700°C. Following this, the temperature of both the upper and lower heating elements was cooled at a rate between 15 and 30°C/hr; it is believed that a slow cooling rate will minimize internal stresses within the ingot and result in minimal ingot cracking. Once the ampoule had cooled to room temperature, the quartz was cut open and the ingot obtained. The appearance of the ampoule used to grow ingot HM-B32 at three preparation stages (after sealing, after

the pre-reaction, and after growth) can be seen in Fig. 4.7 (a), 4.7 (b), and 4.7 (c), respectively.

4.5. DISCUSSION

This Bridgman growth method, as developed in this laboratory, has several major advantages to other growth methods, including the ease of varying the proportions of starting constituents for different runs and allowing synthesis and growth to occur in the same ampoule, and it results in favorable ingots containing, in some cases, large monocrystals about a centimeter in diameter. However, there are some difficulties as well. Quartz, having a softening point of 1665°C [4.9], is a difficult compound to work with, and the skills required to form satisfactory ampoules, which are the core of this entire process, take some time and patience to develop. 32 growth runs are presented in this work, including runs HM-B16, HM-B17 and HM-B30, for which the ampoules were found, after the cooling phase, to have cracked near the first-zone-to-freeze, and run HM-B05, for which the ampoule cracked well below the temperature required for compound synthesis. However, there in fact were many more attempted runs which were abandoned before completion and are not mentioned elsewhere in this work. Of these runs, five were abandoned after it was noticed that a hole in the quartz had developed during the sealing process after evacuation, thus destroying the vacuum inside the ampoules and providing a means for the escape of selenium vapour during subsequent heating processes. Several more runs were interrupted after the pre-reaction heating due to the ampoules cracking. In addition, several ampoules cracked during the initial

heating in the Bridgman furnace after having survived the pre-reaction heating in the brick furnace. This cracking was a persistent problem during the early part of this research, but appeared to have subsided somewhat after run HM-B05, although not completely. It was initially believed that this problem was caused by the addition of sodium into the ampoules. Sodium, either as Na_2Se or as Na^0 with additional elemental selenium, had never been added to quartz ampoules containing copper, indium and selenium before the start of compound synthesis in a vertical-Bridgman furnace. Haiping Wang [4.3] experimented with Na^0 and stoichiometric proportions of Cu, In and Se, and varying proportions of Ga, using a horizontal-Bridgman furnace, and as well, reported the potential of quartz ampoules to break during heating, which she attributed to a violent reaction of the melt. Indeed, sodium has been shown to diffuse into quartz at elevated temperatures [4.10]. It was thought that this may have led to the breakdown of the quartz, and may have been the cause of the cracking. The runs which contained no sodium did not crack, but many runs containing sodium did. It was with this in mind that the indium foil method, which serves the dual purpose of transporting the Na_2Se entirely into the ampoule and keeping it away from the inner quartz walls, was conceived. In addition, other slight variations in procedure, described in this section, were developed with the objective of minimizing the risk of cracking. However, the exact cause of the cracking was never completely determined, nor could a definitive pattern of steps which would lead to cracking be identified. It is entirely possible that improper forming of the ampoules is the cause, and while not positively identified, the problem was intuitively avoided as experience working with the quartz was acquired.

One other point worth mentioning is the quality of the Na_2Se used in these experiments. The quantities, used for all runs containing this material, came from the same 5g bottle batch, which was initially packed in argon. Initially, the material was a rust-coloured powder, as can be seen in Fig. 4.2 (b), but over a period of several months it became increasingly gray. It is suspected that this could be due to oxygen contamination, and therefore raises questions as to the exact chemical composition of the melts for the samples involving Na_2Se , primarily the later ones.

Table 4.1
Ingot Growth Conditions

	HM-B01*	HM-B02	HM-B03	HM-B04	HM-B05	HM-B06	HM-B07	HM-B08
Composition (g)	2g In; 2.75g Se; 1.11g Cu	2.5g In; 3.44g Se; 1.38g Cu	5g In; 6.88g Se; 2.77g Cu; 0.17g Na ₂ Se	2.5g In; 3.4385g Se; 1.3836g Cu; 0.0027g Na ₂ Se	2.5g In; 3.438g Se; 1.384g Cu; 0.0137g Na ₂ Se	2.5g In; 3.438g Se; 1.384g Cu; 0.0137g Na ₂ Se	2.5g In; 3.438g Se; 1.384g Cu; 0.02747g Na ₂ Se	5g In; 6.877g Se; 2.767g Cu; 0.0054g Na ₂ Se.
Composition (mol)	CuInSe ₂	CuInSe ₂	(CuInSe ₂) _{0.97} + (Na ₂ Se) _{0.03}	(CuInSe ₂) _{0.999} + (Na ₂ Se) _{0.001}	(CuInSe ₂) _{0.995} + (Na ₂ Se) _{0.005}	(CuInSe ₂) _{0.995} + (Na ₂ Se) _{0.005}	(CuInSe ₂) _{0.99} + (Na ₂ Se) _{0.01}	(CuInSe ₂) _{0.999} + (Na ₂ Se) _{0.001}
Evacuation Time (h:m)	2:20	2:15	5:50	6:15	3:15	5:45	4:45	5:30
Pre-reaction time (h:m)	3:25	12:25	1:15	1:15	1:05	6:15	8:45	1:15
Peak Upper Furnace Temperature (°C)	1100	1100	1100	1050	400	1050	1050	1050
Reaction Time (h)	24	24	24	24	N/A	19:45	24:45	24
Number of Agitations	0	1	2	1	N/A	1	0	1
Lowering Rate (mm/h)	5.44	4.77	4.87	5.21	N/A	5.19	N/A	4.81
Peak Lower Furnace Temperature (°C)	700	700	700	700	N/A	700	700	700
Pre-reaction scheme	Fig. 4.3 a	Fig. 4.3 a	Fig. 4.3 b	Fig. 4.3 b	Fig. 4.3 b	Fig. 4.3 b	Fig. 4.3 b	Fig. 4.3 b
Heating scheme	Fig. 4.6 a	Fig. 4.6 a	Fig. 4.6 a	Fig. 4.6 b	Fig. 4.6 b	Fig. 4.6 c	Fig. 4.6 c	Fig. 4.6 d
Cooling Rate (°C/h)	30	25	20.45	20.45	N/A	19.29	N/A	22.66
Comments [†]	Ingot erroneously n-type; considered a practice run.			Run interrupted at 1100°C after about 15 hours, and later at 1050°C; ingot erroneously n-type.	Ampoule cracked at 400°C, run interrupted.		Cooling interrupted when sample crashed through furnace; growth most likely complete by this time.	Went up to 1100°C in the brick furnace.

* Ingot numbering: HM-B01 Hadley Myers – Bridgman run number 1

† All ingots p-type unless otherwise stated.

Table 4.1 (continued)
Ingot Growth Conditions

	HM-B09	HM-B10	HM-B11	HM-B12	HM-B13	HM-B14	HM-B15	HM-B16
Composition (g)	5g In; 2.767g Cu; 7.565g Se; 0.1683g Na ₂ Se	5g In; 2.767g Cu; 7.565g Se; 0.0550g Na ₂ Se.	5g In; 2.767g Cu; 7.565g Se; 0.0054g Na ₂ Se	5g In; 2.767g Cu; 7.565g Se; 0.0237g Na ₂ Se	5g In; 7.565g Se; 2.767g Cu;	5g In; 7.565g Se; 2.767g Cu; 0.0054g Na ₂ Se.	5g In; 2.7672g Cu; 6.8770g Se;	5g In; 2.767g Cu; 7.565g Se; 0.1110g Na ₂ Se
Composition (mol)	(CuInSe _{2.2}) _{0.97} + (Na ₂ Se) _{0.03}	(CuInSe _{2.2}) _{0.99} + (Na ₂ Se) _{0.01}	(CuInSe _{2.2}) _{0.999} + (Na ₂ Se) _{0.001}	(CuInSe _{2.2}) _{0.995} + (Na ₂ Se) _{0.005}	CuInSe _{2.2}	(CuInSe _{2.2}) _{0.999} + (Na ₂ Se) _{0.001}	CuInSe ₂	(CuInSe _{2.2}) _{0.98} + (Na ₂ Se) _{0.02}
Evacuation Time (h:m)	2:48	5:40	5:15	5:35	5:37	6:58	6:20	5:50
Pre-reaction time (h:m)	6:00	6:07	4:35	5:10	5:00	5:45	5:15	4:35
Peak Upper Furnace Temperature (°C)	1050	1050	1050	1050	1050	1050	1050	1050
Reaction Time (h)	24	17:53	24	24:20	24	24:05	24	24
Number of Agitations	2	1	1	1	1	1	1	1
Lowering Rate (mm/h)	5.15	6.46	4.36	4.32	4.35	4.49	4.40	4.41
Peak Lower Furnace Temperature (°C)	700	700	700	700	700	700	700	700
Pre-reaction scheme	Fig. 4.3 b	Fig. 4.3 c	Fig. 4.3 c	Fig. 4.3 c	Fig. 4.3 c	Fig. 4.3 c	Fig. 4.3 c	Fig. 4.3 c
Heating scheme	Fig. 4.6 d	Fig. 4.6 d	Fig. 4.6 d	Fig. 4.6 d	Fig. 4.6 d	Fig. 4.6 d	Fig. 4.6 d	Fig. 4.6 d
Cooling Rate (°C/h)	22.66	29.43	22.63	17.89	22.33	16.19	22	17.63
Comments			Uncertainty over indium content.					Ampoule cracked sometime during Bridgman growth.

Table 4.1 (continued)
Ingot Growth Conditions

	HM-B17	HM-B18	HM-B19	HM-B20	HM-B21	HM-B22	HM-B23	HM-B24
Composition (g)	5g In; 2.767g Cu; 6.8770g Se; 0.1110g Na ₂ Se	5g In; 7.565g Se; 2.767g Cu; 0.1110g Na ₂ Se	5g In; 7.565g Se; 2.767g Cu; ~0.024g Na.	5g In; 7.565g Se; 2.767g Cu; ~0.0011g Na	5g In; 7.565g Se; 2.767g Cu; ~0.0055g Na	5g In; 7.565g Se; 2.767g Cu; ~0.031g Na	5g In; 7.565g Se; 2.767g Cu; ~0.0117g Na	5g In; 6.8770g Se; 2.767g Cu; ~0.0011g Na
Composition (mol)	(CuInSe _{2.2}) _{0.98} + (Na ₂ Se) _{0.02}	(CuInSe _{2.2}) _{0.98} + (Na ₂ Se) _{0.02}	(CuInSe _{2.2}) _{0.98} + Na _{0.02}	(CuInSe _{2.2}) _{0.999} + Na _{0.001}	(CuInSe _{2.2}) _{0.995} + Na _{0.005}	(CuInSe _{2.2}) _{0.97} + Na _{0.03}	(CuInSe _{2.2}) _{0.99} + Na _{0.01}	(CuInSe ₂) _{0.999} + Na _{0.001}
Evacuation Time (h:m)	3:15	3:55	4:15	4:48	3:30	4:50	4:00	3:50
Pre-reaction time (h:m)	5:05	5:20	5:10	6:20	4:32	4:30	5:40	6:40
Peak Upper Furnace Temperature (°C)	1050	1050	1050	1050	1050	1050	1050	1050
Reaction Time (h)	24:15	24:04	24	24:04	24	24:22	25:10	24:00
Number of Agitations	1	2	2	2	2	4	1	3
Lowering Rate (mm/h)	3.80	4.14	4.19	4.10	3.94	3.92	4.12	4.10
Peak Lower Furnace Temperature (°C)	700	700	700	700	700	700	700	700
Pre-reaction scheme	Fig. 4.3 c	Fig. 4.3 c	Fig. 4.3 c	Fig. 4.3 c	Fig. 4.3 c	Fig. 4.3 c	Fig. 4.3 c	Fig. 4.3 c
Heating scheme	Fig. 4.6 d	Fig. 4.6 e	Fig. 4.6 e	Fig. 4.6 e	Fig. 4.6 e	Fig. 4.6 e	Fig. 4.6 e	Fig. 4.6 e
Cooling Rate (°C/h)	15.95	15.71	15.71	15.71	15.71	15.71	15.71	15.71
Comments	Ampoule cracked sometime during Bridgman growth.							

Table 4.1 (continued)
Ingot Growth Conditions

	HM-B25	HM-B26	HM-B27	HM-B28	HM-B29	HM-B30	HM-B31	HM-B32
Composition (g)	5g In; 8.2524g Se; 2.767g Cu; ~0.033g Na	5g In; 6.8770g Se; 2.767g Cu; ~0.03g Na	5g In; 6.8770g Se; 2.767g Cu; ~0.0055g Na	5g In; 6.8770g Se; 2.767g Cu; ~0.011g Na	5g In; 6.8770g Se; 2.767g Cu; ~0.022g Na	5g In; 8.2524g Se; 2.767g Cu; ~0.12g Na	5g In; 8.2524g Se; 2.767g Cu; ~0.12g Na	5g In; 8.2524g Se; 2.767g Cu.
Composition (mol)	(CuInSe _{2.4}) _{0.97} + Na _{0.03}	(CuInSe ₂) _{0.97} + Na _{0.03}	(CuInSe ₂) _{0.995} + Na _{0.005}	(CuInSe ₂) _{0.99} + Na _{0.01}	(CuInSe ₂) _{0.98} + Na _{0.02}	(CuInSe _{2.4}) _{0.9} + Na _{0.1}	(CuInSe _{2.4}) _{0.9} + Na _{0.1}	CuInSe _{2.4}
Evacuation Time (h:m)	3:22	3:35	3:07	3:25	4:48	3:20	3:35	3:15
Pre-reaction time (h:m) [*]	3:00	5:00	3:45	5:00	5:55	6:00	6:20	4:45
Peak Upper Furnace Temperature (°C)	1050	1050	1050	1050	1050	1050	1035	1050
Reaction Time (h)	24	24	24	24	24	1	6	22
Number of Agitations	3	2	2	2	2	N/A	1	1
Lowering Rate (mm/h)	3.93	4.35	4.32	4.56	4.15	N/A	4.44	4.15
Peak Lower Furnace Temperature (°C)	700	700	700	700	700	N/A	700	700
Pre-reaction scheme	Fig. 4.3 c	Fig. 4.3 c	Fig. 4.3 c	Fig. 4.3 c	Fig. 4.3 c	Fig. 4.3 c	Fig. 4.3 c	Fig. 4.3 c
Heating scheme	Fig. 4.6 e	Fig. 4.6 e	Fig. 4.6 e	Fig. 4.6 e	Fig. 4.6 e	N/A	Fig. 4.6 e	Fig. 4.6 e
Cooling Rate (°C/h)	15.71	15.71	15.71	15.71	15.71	N/A	15.71	15.71
Comments		Ampoule heated to 1050°C before being interrupted when the furnace shutdown; resumed 4 days later; n-type sample.	n-type sample.	n-type sample.	n-type sample.	Was heated up to 1050°C in the brick furnace, forming polycrystalline ingot; ampoule subsequently cracked in Bridgman furnace at 105°C.	Furnace was initially not able to reach the desired temperature; the ampoule soaked for 15 hours at 975°C before aluminum foil was placed over the opening for better insulation.	

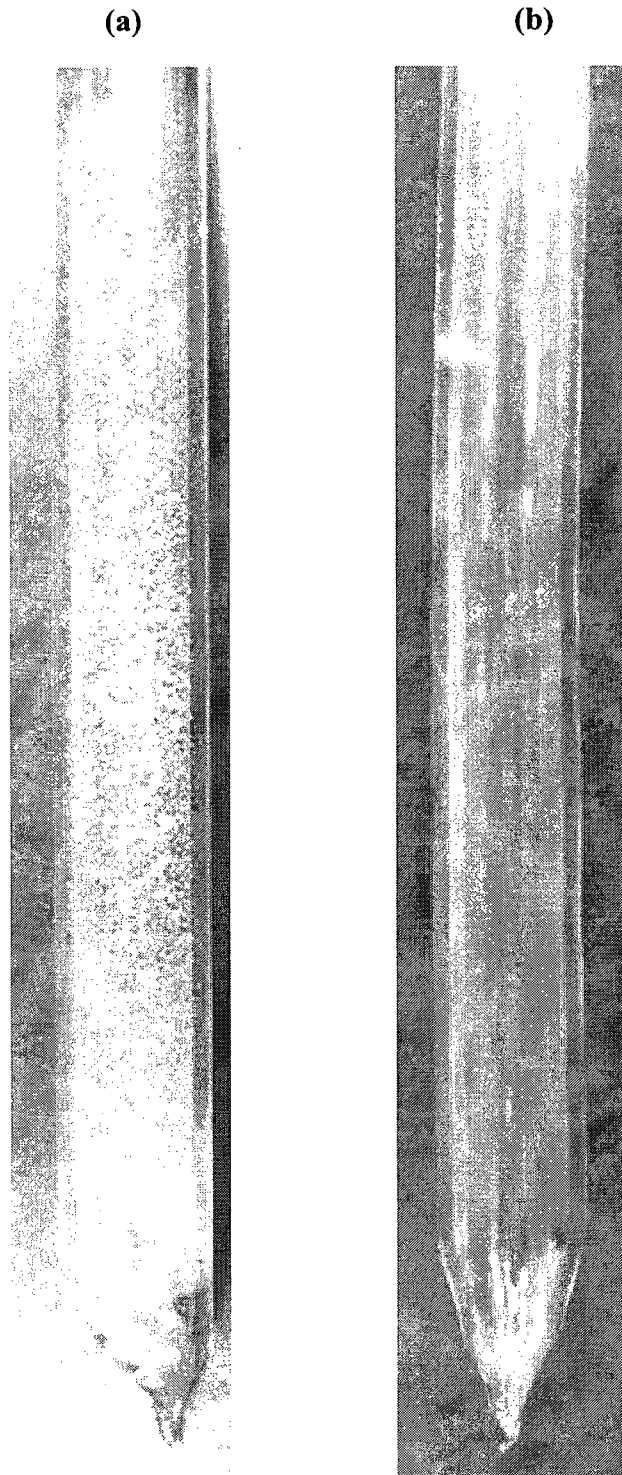
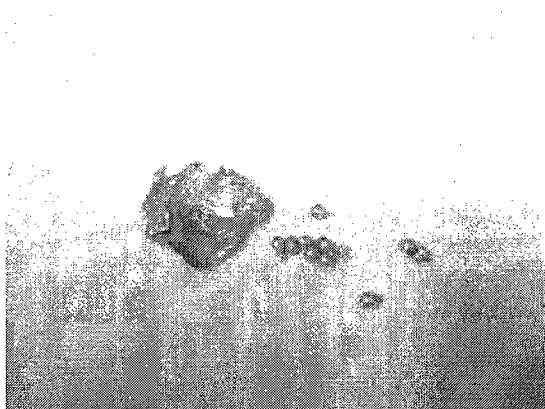
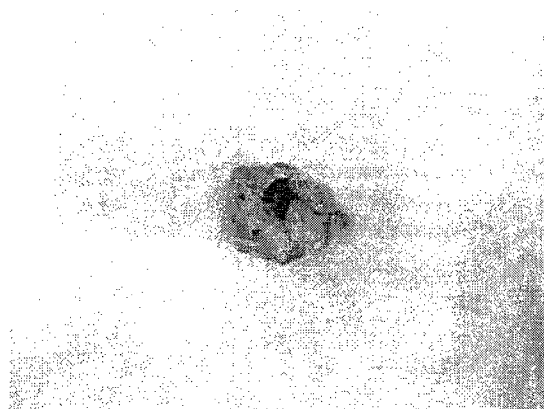


Figure 4.1 A section of quartz shown with a coating of boron nitride powder (a) after the powder had been applied, and (a) after the flaming-in process.



(a)



(b)



(c)



(d)

Figure 4.2 Photographs showing the stages of the indium “boat”, used to transport a weighed quantity of Na₂Se into the ampoule; (a) indium after being flattened into a foil, shown beside indium pellets; (b) indium foil with Na₂Se; (c) indium foil after being formed into a boat with Na₂Se inside; (d) indium boat containing Na₂Se after being pushed into the quartz ampoule.

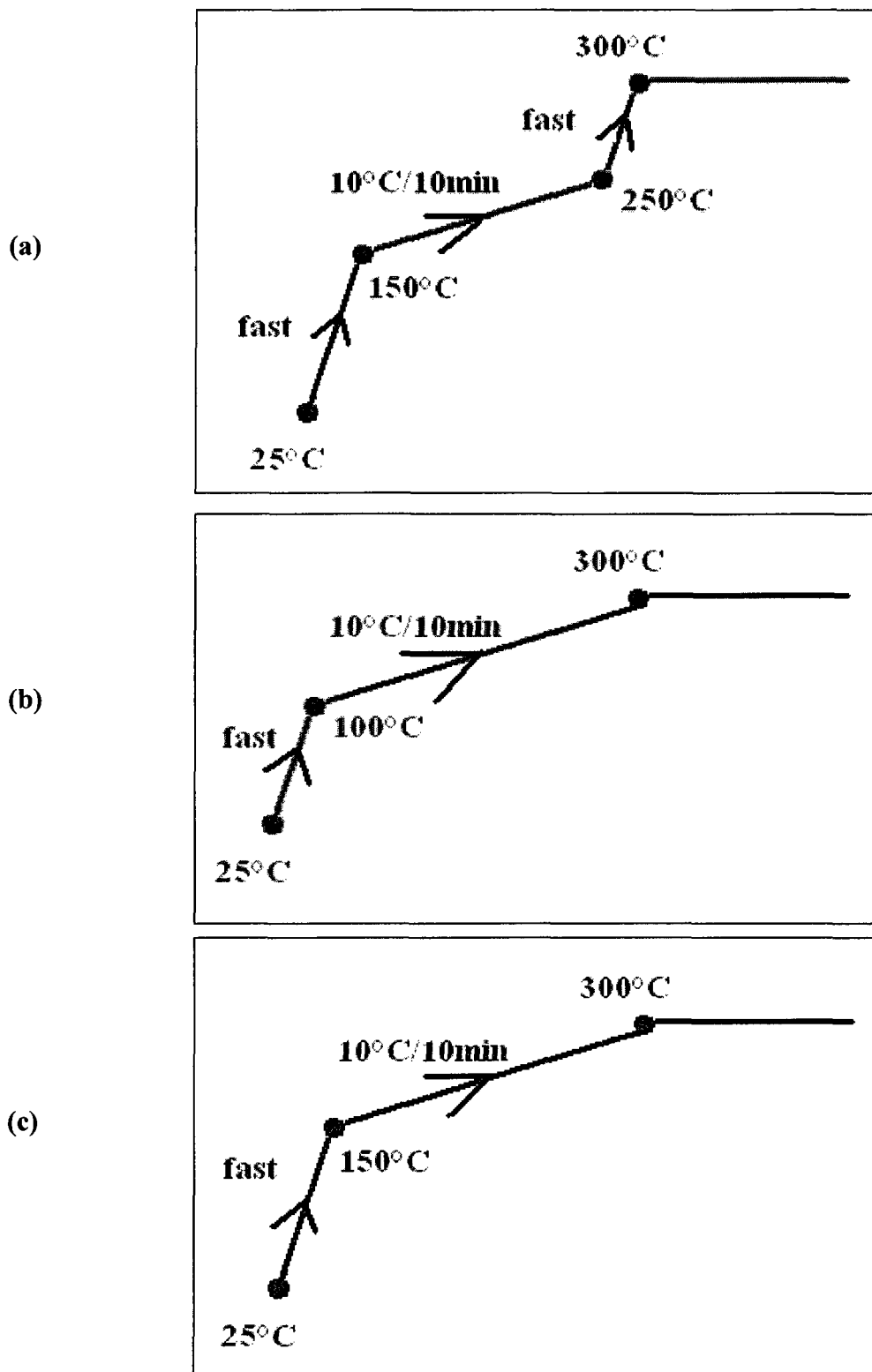


Figure 4.3 Pre-reaction heating schemes used for HM-B01 and HM-B02 (a), used for HM-B03 to HM-B09 (b), and used for HM-B10 and subsequent runs (c). The fast ramp rate was measured to be approximately 30-40°C/min.

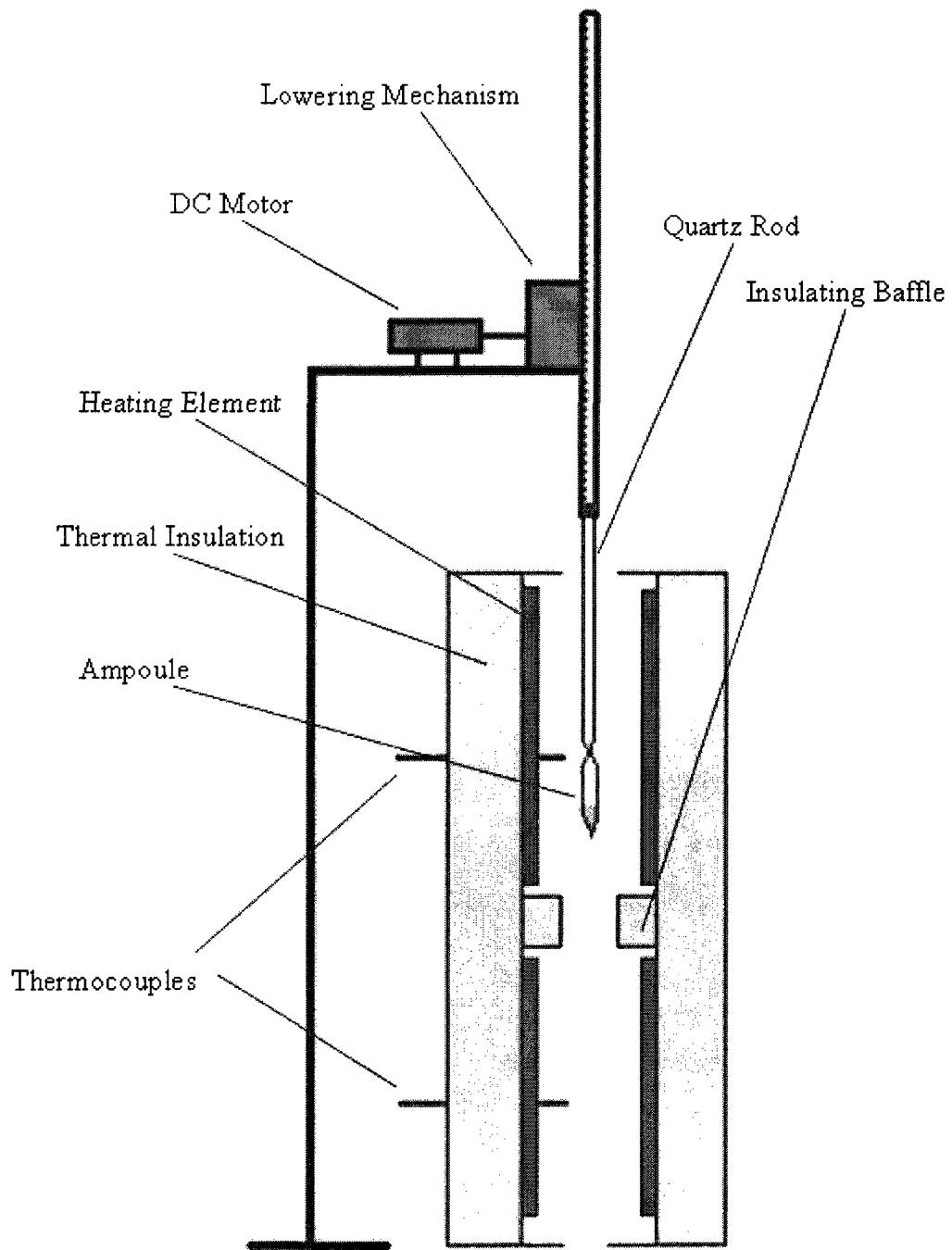


Figure 4.4 Vertical Bridgman-growth apparatus used in the fabrication of all ingots reported in this work.

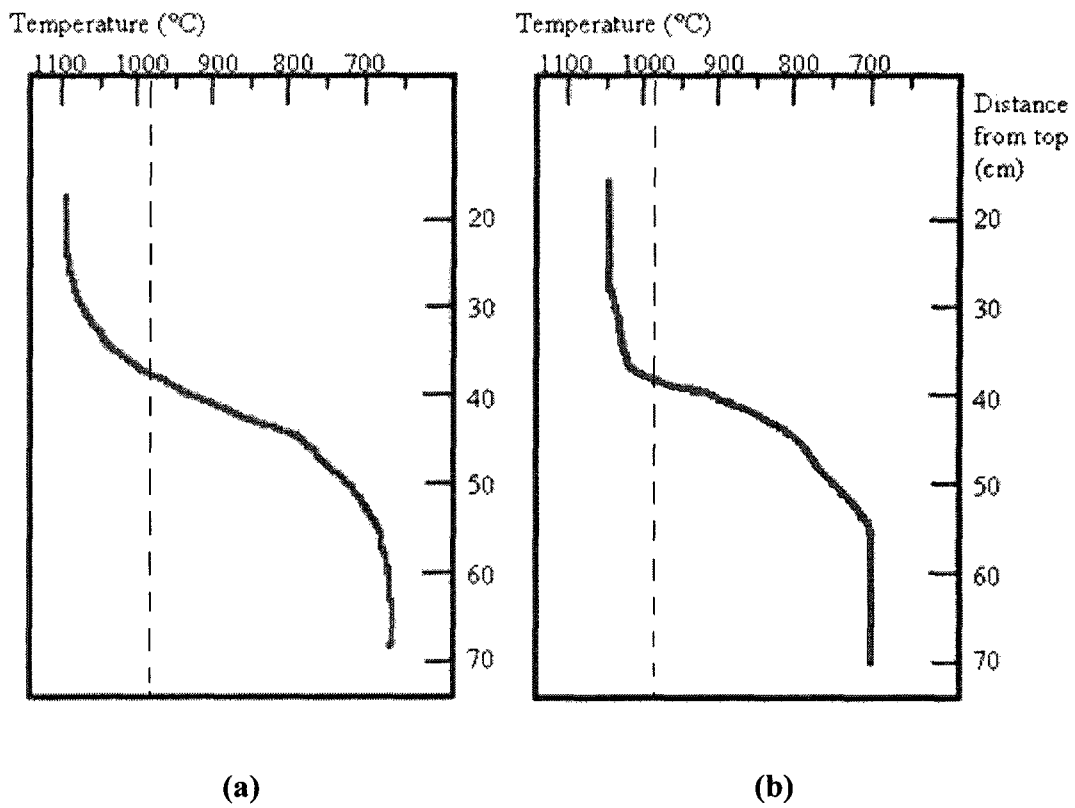


Figure 4.5 Temperature profile of the Bridgman-furnace with the bottom zone set to 700°C and the top zone set to (a) 1100°C and (b) 1050°C. The vertical dotted lines indicate the melting point of CuInSe_2 , 986°C.

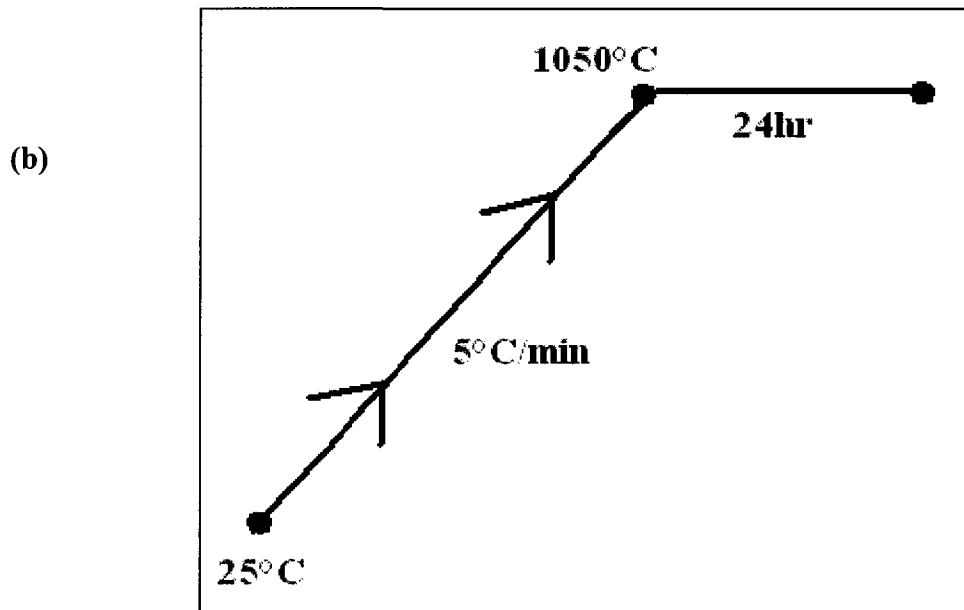
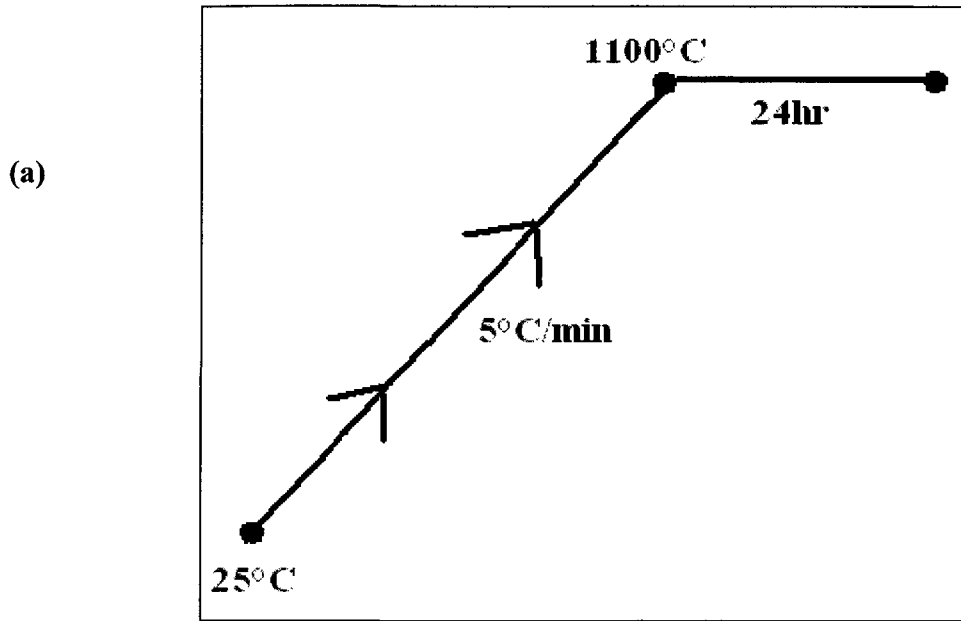


Figure 4.6 Bridgman heating schemes; (a) used for HM-B01 to HM-B03; (b) used for HM-B04 and HM-B05.

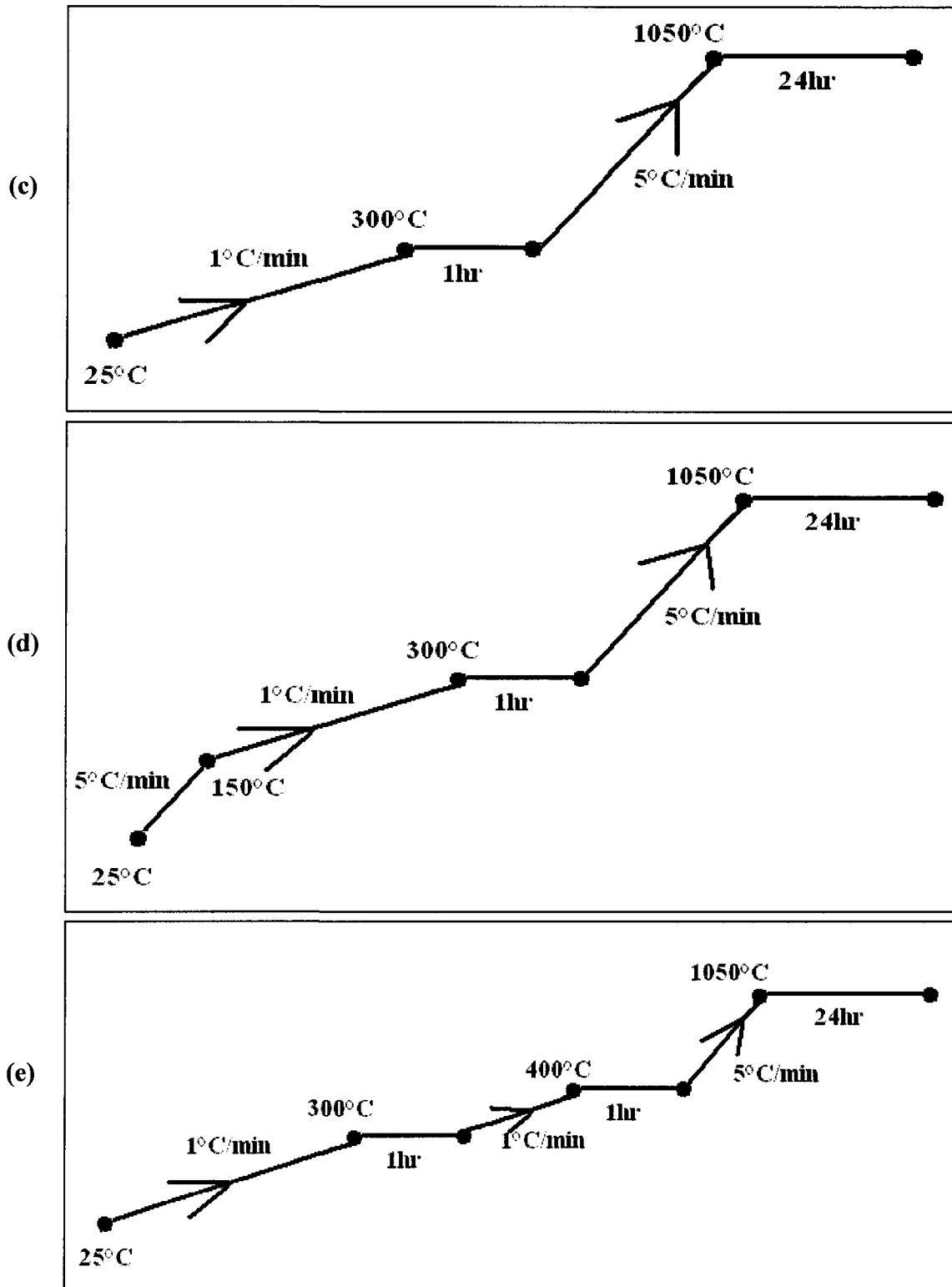
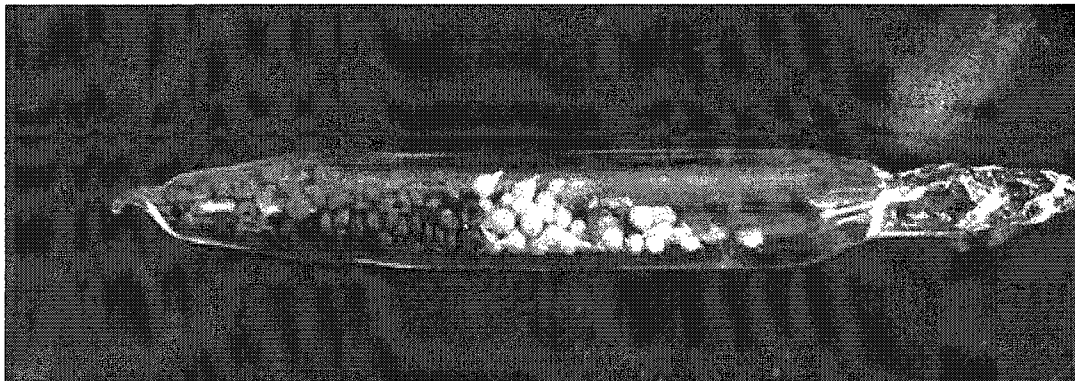
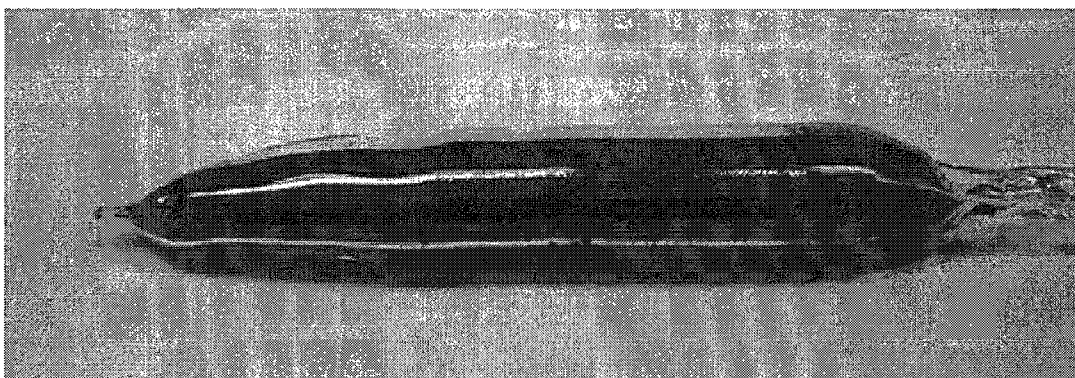


Figure 4.6 (continued) Bridgman heating schemes (cont); (c) used for HM-B06 and HM-B07; (d) used for HM-B08 to HM-B17; (e) used for HM-B18 and subsequent runs.

(a)



(b)



(c)

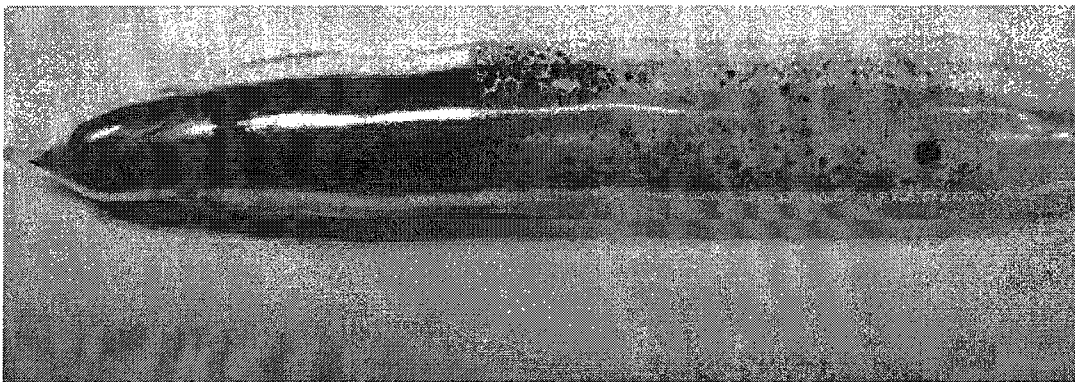


Figure 4.7 Ampoule from run HM-B32 ($\text{CuInSe}_{2.4}$), grown with much excess Se, at three different stages of fabrication: (a) after sealing, (b) after the pre-reaction, and (c) after crystal growth.

Chapter 5

Experimental Results

5.1. INTRODUCTION

This chapter contains all of the experimental results, obtained through various techniques of analysis, of the growth runs described in Chapter 4. Of all the techniques used, the one that was used first, almost immediately after the ampoules were cooled upon the completion of growth, was visual inspection. This was necessary in order to document any change in the appearance of the ampoules which may have been a result of a change in the composition of the melts. Among the changes observed was the appearance of a white deposit on the inner walls of some the ampoules, as well as a red deposit. The presence of crystalline metallic-like dots, known as ampoule dots, was also observed to be affected by the presence of sodium, as well as selenium deposits and nodules resembling elemental copper.

Following the visual inspection of the ampoules, the ingots were removed and subject to a second visual inspection. During this inspection, two distinctive films, one red and the other black, were noticed and documented. The ingots were then cut into wafers and cleaned, and the presence or absence of cracks, as well as the relative cohesiveness of the ingots, was recorded. Microstructural analysis, including XRD, XPS, and SEM-EDX, was also performed on some of the deposits in order to aid in the compositional analysis of them. Finally, electrical measurements were taken in

order to determine what effects the sodium may have had on these characteristics. The results were then used in order to estimate trends in the carrier concentrations of the ingots.

These results are compiled in Table 5.1 and 5.2 for the runs grown in the presence of Na_2Se and Na^0 , respectively. As well, a summary of the results, in which the stoichiometric ingots are compared with those grown with excess Se, for both forms of sodium addition is given in Table 5.3 and 5.4. A discussion and interpretation of these results is presented in Chapter 6.

5.2. VISUAL INSPECTION OF AMPOULES

5.2 (a) White Deposit

It was immediately apparent, upon the removal of some of the ampoules from the furnace after growth, that a white substance had adhered to the inner walls of the quartz. It was initially noticed that the quantity of this deposit increased with additions of Na_2Se , so that at 3 at. % the ampoule was completely opaque (see Fig. 5.1). It was also noticed that slightly less appeared in the excess Se runs containing Na_2Se than in the stoichiometric runs grown with this compound (Table 5.1). The same is true for the more recent runs grown with additions of Na^0 , in which considerably more white deposit was found for stoichiometric than excess Se runs, as can be seen in Fig. 5.2. Furthermore, comparing the runs grown with Na_2Se with those grown with Na^0 by considering an equivalent number of sodium atoms for each set (there are twice as many sodium atoms for the same atomic percent with Na_2Se

than with Na⁰), it was also apparent that more white deposit appeared in the latter set, being with Na⁰, than in the former. Therefore, it could be concluded that quantity of white deposit present in the ampoules was roughly proportional to the amount of sodium added to the melt, but at the same time inversely proportional to the amount of selenium.

An initial attempt at identifying this deposit was made by scraping a portion from the sides of the ampoule from run HM-B03 and pulverizing it into a powder in order to perform XRD. However, this proved fruitless, as large amounts of quartz contaminated the sample and resulted in meaningless readings. However, a further attempt, this time using XPS, proved more successful. The deposit was found to contain, aside from Si and O (most likely from the quartz) and C, more Na than Cu, In, or Se. Specifically, the composition was found to be, in atomic percent, 25.0 Si, 50.3 O, 20.0 C, 2.2 Na, 0.6 Cu, 1.3 In, and 0.74 Se. As well, compositional analysis done with SEM/EDX showed portions of the white deposit to contain Si, O, C, and Na, but found none of the other starting elements. Therefore, it seems clear that this white deposit is principally sodium.

5.2 (b) Red Deposit

The second type of deposit which had appeared on the inside quartz walls appeared in the form of a rust-coloured layer, also seen in Fig. 5.1, and was present in all ampoules containing high added concentrations of sodium, although significantly less was found in the stoichiometric samples containing Na⁰ than in all other cases.

This is shown in Fig. 5.2. It is perhaps significant that, with moderate concentrations of sodium in the melt, the red deposit formed on the part of the ampoule just above the ingot and between the last-zone-to-freeze and the ampoule wall. As the concentration increased, the deposit eventually covered the full length of the ingot.

As is the case with the white deposit, various attempts were made at identifying the red deposits, including XRD, XPS, and SEM-EDX. The first such attempts by XRD were unsuccessful. The deposit, after being scraped off the quartz and ground into a powder, was subject to XRD, but the resulting peaks revealed only CuInSe_2 , with no other identifiable compounds. However, XRD of the ampoule dots from HM-B03, described in Sec. 5.2 (c), revealed the presence of Cu_3Se_2 . It is possible that this reading was from the red deposit.

XPS analysis of the red deposit from the ampoule of run HM-B09 ($\text{CuInSe}_{2.2} + 3\% \text{Na}_2\text{Se}$) exposed various components, including Se^0 , Cu^0 , CuSe , and In^0 , as well as CuO , InO_x , and SeO . Sodium was also identified. Further analysis using SEM-EDX, this time of run HM-B19 ($\text{CuInSe}_{2.2} + 2\% \text{Na}^0$), as well revealed various inhomogeneities among the red deposit, but showed large portions to consist of copper and selenium, with no other elements present. With this in mind, it was suggested that, for simplicity, the red deposit be described as primarily selenium, with some copper and sodium phases.

5.2 (c) Ampoule Dots

Grey, metallic-like spots approximately one millimeter in diameter, called ampoule dots, were found on the inside walls of the ampoules for runs which contained either Na_2Se , or Na^0 with excess selenium, with a general increase in the number and size of the spots with increase of sodium. Very few spots were found for the stoichiometric runs which contained Na^0 , and virtually none were noticed for the stoichiometric runs without sodium, HM-B01, HM-B02, and HM-B15 (Table 4.1).

A collection of these dots, taken from the ampoule of run HM-B03 ($\text{CuInSe}_2 + 3\% \text{Na}_2\text{Se}$), was powdered for XRD analysis. As mentioned above, this analysis showed them to be comprised of primarily CuInSe_2 , with Cu_3Se_2 , known as umagite, also identified. Red deposit, described above, was sometimes observed on the quartz in the immediate vicinity of the ampoule dots (see Fig. 5.3). It is entirely possible that the quantity of dots seen from run to run may be connected to the presence of the red deposit. As is previously described, the appearance of red deposit between the ingot surface and the quartz signaled the adherence of the ingot to the sides of the ampoule, complicating its removal. It is possible that the presence of red deposit on the ampoule dots resulted in their sticking to the ampoule walls as well. Thus, there may be a direct correlation between the amount of red deposit and the number of ampoule dots found within the same ampoule.

5.2 (d) Selenium Deposits

Another type of deposit was what appeared to be elemental Se, whether in the form of small amorphous hemispheres (Fig. 5.4 a) or as very small crystalline dendritic needles (Fig. 5.4 b). It is presumed that the former were originally condensed as a liquid and the latter as a solid from Se vapour. These deposits were present on all ampoules prepared with excess Se, including those which contained no Na, and hence have no direct connection to sodium. As well, very little was observed for the stoichiometric runs grown with Na₂Se, and even less was seen for the stoichiometric runs with Na⁰.

A few dots were collected from the ampoule of run HM-B14 (0.1 at. % Na₂Se in CuInSe_{2.2}), placed in close proximity on a glass slide and carefully warmed by means of a hotplate. Also warmed at the same time were fragments of what was known to be selenium. It was observed that both the known selenium and the deposits from HM-B14 melted at exactly the same temperature (see Fig. 5.4 c). Therefore, it was confirmed that the deposits in question were elemental selenium which had not combined with any other element and therefore solidified in its elemental form on the sides of the ampoule during cooling.

5.2 (e) Copper Nodules

A final type of deposit, found only in the 2 and 3 % Na⁰ runs with stoichiometric CuInSe₂, HM-B29 and HM-B26 respectively, was tiny precipitates, or nodules, of what appeared to be metallic copper on the outer surfaces of the ampoule

dots, as is shown in Fig. 5.5. That these nodules are metallic copper has yet to be confirmed. If in fact they are Cu^0 , considering a ratio of copper to indium and to selenium of 1:1:2 were added to the ampoules, a deficiency of copper within the bulk ingot would be deduced. Furthermore, as they appeared only in stoichiometric samples, and not in the samples grown with excess Se, and that amongst those they consistently appeared only for high added concentrations of elemental sodium, rather than Na_2Se , it is suggested that their presence is connected to both the amount of Na and Se within the melt.

5.3. VISUAL INSPECTION OF INGOTS

5.3 (a) Opening of Ampoule and removal of Ingot

Once the appearance of the ampoule had been carefully documented and all identifying characteristics were noted, it was necessary for it to be cut open in order to retrieve the ingot inside. This was done by first scoring the outer surface with a diamond-scriber so as to weaken the quartz. The ampoule was then wrapped in aluminum foil and squeezed with pliers at a point away from the ingot to minimize the chances of it being damaged during this process. A small wire-cutter was used to remove the remaining quartz and free the ingot. It was observed, when no sodium was used, that the quartz was easily broken away, and the ingot showed no signs of sticking. However, as sodium was added in the form of Na_2Se for both the stoichiometric and excess Se cases, the ingot became increasingly difficult to free, so that with large additions, it had adhered tenaciously to the sides of the quartz and required some effort in order to be removed. This was also true for the ingots grown

with Na⁰ and excess Se, but was not true for the stoichiometric ingots, in which the ingots exhibited no signs of sticking, except perhaps at the last-zone-to-freeze.

5.3 (b) Cohesiveness and Mini-Cracks

The Bridgman-growth method, previously described in Chap. 4, was used to obtain all of the ingots presented in this work. As it was the aim of this research to study the effects of sodium on monocrystalline ingots, the growth method chosen was the one which had been continuously refined over more than a decade of study [5.1-3] and had produced ingots the largest and highest quality CIS crystals of any other method experimented with in this laboratory. One such ingot, HM-B15 (stoichiometric CuInSe₂ with no added sodium) is shown immediately after having been removed from the ampoule, as well as after having been sliced into wafers, in Fig. 5.6. As can be seen, the ingot resulting from this particular growth run did not consist of perfect single crystals and was far from being completely defect free. Nevertheless, good quality ingots containing several centimeter-sized monocrystals can be obtained.

One indication of the size of a crystal is the presence of twinning, which can be easily detected visually by rotating a sample under strong lighting. If a twin is present, it will appear as a dark band, while the main part of the crystal around the twin will appear light. Normally, the presence of twins is considered a detriment [5.4]; however, in this study, twins signal the existence of monocrystalline segments within the ingot, and therefore confirm the presence of single crystals. One such twin

could be seen on the surface of ingot HM-B06 ($\text{CuInSe}_2 + 0.1\% \text{Na}_2\text{Se}$), shown in Fig. 5.7, and is indicative of large, high-quality monocrystals within the ingot.

Another indication of monocrystallinity is the presence triangular growth facets, shown in Fig. 5.8, which are a distinctive feature of the $\{112\}$ plane. They are sometimes seen at the bottom of voids, which can appear on the outer surface of the ingots and represent areas in which free-growth was allowed to occur, as opposed to where growth was interrupted and the resulting shape of the ingot was dictated by the walls of the ampoule.

Wafers sliced from ingots grown in this work without sodium showed few cracks on their surfaces, and were reasonably solid. This is also true in the case of ingots grown with 0.1% added Na_2Se , which were at least as good as those prepared with no Na additive. However, there occurred a general increase in brittleness and cracking which corresponded to increases of sodium, either in the form of Na_2Se or Na. Indeed, ingot HM-B03, grown with 3 at. % Na_2Se , was extremely brittle and easily broke into smaller fragments. This observed increase in brittleness was the true for ingots prepared both with stoichiometric and with excess Se proportions. However, a notable exception was the n-type ingot HM-B26 (stoichiometric plus 3 at. % Na^0), which appeared quite solid with few cracks as compared to ingot HM-B24 (0.1 at. % Na^0). However, the last-zone-to-freeze of HM-B26 was p^+ -type and quite brittle, and disintegrated into a powder, as did the last-zones-to-freeze of the stoichiometric ingots grown with the 1 and 2 % Na^0 . This particularly specific

phenomenon was also observed by Wang et al [5.5] when a high concentration of sodium was incorporated into the melts of stoichiometric ingots.

The presence of large cracks on the surface of wafers is perhaps indicative of degradation in crystal quality within the ingot, as is a lack of cohesiveness. As this was generally observed to occur with increases in sodium addition, it is easily assumed that the sodium is directly responsible for this crystal degradation. Indeed, Wang et al [5.5] observed an increase in brittleness in ingots grown with large quantities of sodium. This is consistent with a deterioration of quality in polycrystalline films observed by Granata and Sites [5.6] at high sodium levels. However, it is also possible that the cracking and lack of cohesiveness observed in this work is an indirect effect, which occurs as a result of the ingots adhering to the sides of the ampoule in the presence of the red deposit. Ingots grown before the discovery of the effects of boron nitride on the growth process were plagued with cracks and internal voids which hampered crystal growth [5.7]. It is speculated here that the cracks occurred during the cooling phase of crystal growth as the ingot stuck to the quartz, creating internal stresses which resulting in cracking. The same phenomenon is perhaps responsible for the cracking and brittleness seen in this work. It could be that the presence of mini-cracks and a general decrease in cohesiveness is due to the sticking of the ingots caused by the red deposit. Crystal degradation and a significant increase in defect densities was observed by Lyahovitskaya et al [5.8] to occur as CIS ingots were annealed in the presence of metallic Na vapour, yet this activity was tempered with the introduction of Se^0 , via Na_2Se formation. However,

the general increase in crystal degradation observed in this work corresponded with additions of Na_2Se , as well as Na^0 with excess Se, but was not seen as clearly when Na^0 was added to stoichiometric CuInSe_2 , in which there was no sticking.

5.3 (c) Surface Deposits

Two identifiable deposits were observed on the surface of some of the ingots after their removal from the ampoules. These were a red film and a black film. The latter, shown in Fig. 5.9, appeared in the $\text{CuInSe}_{2.2}$ runs and is assumed to be elemental Se. Notice in Fig. 5.9 (b) ($\text{CuInSe}_{2.2}$ without Na) that the film has a slight cherry-red tint that resembles the appearance of amorphous selenium thin-films, which also exhibit a red tint. The presence of this film is indicative of some Se remaining unbound as the melt was slowly solidified, and eventually depositing in a elemental form on the solid surface. That this occurred more with excess Se was expected.

The red film is most probably the same as that was described in Sec. 5.2 (b). Some of the film was deposited on the ampoule just above the ingot, and some was deposited between the ingot itself and the quartz, so that, upon removal of the ingot, part remained on the outside surface of the ingot and the rest remained on the ampoule wall. This film was found in large quantities for the samples containing Na_2Se , but less was seen on the ingots containing $\text{CuInSe}_{2.2} + \text{Na}^0$ and practically none with $\text{CuInSe}_2 + \text{Na}^0$, with the exception of the last-zone-to-freeze, on which some did appear (see Fig. 5.10).

5.3 (d) Wafer Cutting and Cleaning

Once inspection of the ingot had been completed, the process of cutting it into wafers was initiated. For the first few ingots prepared in this work, HM-B01, B02, and B03, the slices were made radially, so as to produce circular-shaped wafers, but all subsequent ingots were cut longitudinally. This was to better examine the differences, if any existed, between the first- and last-zones-to-freeze. The wafers were cut using a water-cooled diamond-blade circular saw, with a slab of metal underneath the ingots for support. Candle wax was dripped over the entire surface of the ingots in order to secure it to the metal. Once the one or two wafers had been cut, a heat-gun was used to melt away the wax.

The process of cleaning the wafers was performed immediately after the cutting was complete. First, they were submerged in approximately 20 ml of toluene for 20 minutes, followed by a rinse with DIW. This was repeated another two times, after which the wafers were submerged in acetone for 5 minutes. They were rinsed with DIW a final time, and then left to dry in between two clean laboratory wipes. Once the wafers were completely dry, after approximately 45 minutes, it was possible to proceed with the electrical measurements. However, before the results of these measurements are given, a discussion of the results of the microstructural analyses, used in identifying some of the deposits previously described, is provided.

5.4. MICROSTRUCTURAL ANALYSIS

5.4 (a) X-ray Diffraction

Powder X-ray diffraction (XRD) was performed using a Rigaku Rotaflex RU200B X-ray Diffractometer with a rotating anode generator, with $\text{CuK}\alpha$ radiation. Attempts to determine the components of the white and red deposit, taken from sample HM-B03, were met with very limited success. However, XRD analysis of the first-zone-to-freeze of this ingot proved more successful. In addition, a collection of ampoule dots, also taken from HM-B03, were analyzed, the results of which are shown along with the results from the analysis of the first-zone-to-freeze in Fig. 5.11. As can be seen, the usual peaks of CuInSe_2 are present in both samples. However, as explained previously, some additional peaks detected in the ampoule dots have been identified as Cu_3Se_2 , known as umangite. It was speculated above that perhaps this latter compound may represent a crystallized portion of red deposit from the surface of the dots rather than an extra phase from within the dots. No sodium or sodium compounds have been identified within the samples by XRD.

The location of the experimentally determined peaks of the first-zone-to-freeze of HM-B03 are shown tabulated in Table 5.5, along with the resulting d_{hkl} spacing, calculated according to Bragg's formula:

$$d_{hkl} = \frac{\lambda}{2 \sin \theta} \quad , \quad (5.1)$$

where θ corresponds to half the diffraction angle, and λ corresponds the wavelength of $\text{CuK}\alpha$ radiation (1.54 Å). The result was then used to determine the a-parameter of the lattice according to the following formula for tetragonal crystals:

$$a = d_{hkl} \sqrt{h^2 + k^2 + \left(l \frac{a}{c}\right)^2}, \quad (5.2)$$

where a/c was taken to be 0.5 and $h k l$ are the Miller indices of the planes associated with each peak, and are also shown in Table 5.5. While the first several calculated values of the a-parameter appear to deviate considerably from each other, they seem to eventually stabilize at a value of 5.78 or 5.79 Å, which is consistent with the accepted value of 5.784 Å [5.9], indicating that the presence of Na_2Se (3 at. %) had no noticeable effect on the crystal size and contributing to evidence suggesting that sodium did not penetrate the crystal of CuInSe_2 .

Analysis was also performed on the first-zone-to-freeze of HM-B26 (n-type), the results of which are shown in Fig. 5.12. As can be seen from this figure, the diffraction lines appear very clear, with little noise or distortion. The peaks from this sample match all the usual peaks of the chalcopyrite with no change of lattice parameters, and there is no evidence of any extra phases present, such as CuIn_3Se_5 [5.10] or NaInSe_2 [5.11].

5.4 (b) X-ray Photoelectron Spectroscopy

X-ray Photoelectron Spectroscopy (XPS) was used in the compositional analysis of the white and red ampoule deposits. This analysis was performed at the National Research Council Canada, Ottawa, on the white deposit from HM-B03, and on the red deposits from HM-B09 and HM-B11. The results of the analysis for the white deposit, which described the composition, in atomic percent, of each element, are detailed in Sec. 5.2 (a). Therefore, these results will not be repeated here except to state that more Na was found in the deposit using this method than Cu, In, or Se.

Analysis of the red deposits from HM-B09 and HM-B11 revealed them to be comprised of many phases, including Se^0 , Cu^0 , and In^0 , as well as CuO , and possibly InO_x and SeO . Sodium was also seen in both samples. Analysis also revealed that there may be differences in the relative compositions of both samples. For example, more copper was found in the deposit of HM-B11 ($\text{CuInSe}_{2.2} + 0.1\% \text{Na}_2\text{Se}$) than that of HM-B09 ($\text{CuInSe}_{2.2} + 3\% \text{Na}_2\text{Se}$). However, the reverse is true for indium, as more was found in HM-B09 than in HM-B11. Equivalent concentrations of selenium, however, were present in both samples. The results of the XPS analysis are shown for HM-B09 in Fig. 5.13.

It may be valuable to note that, while HM-B11 was used in the analysis of the red deposit, it was not included in the other electrical results as there was some uncertainty as to the amount of indium which went into the ampoule. Sample HM-B14, of equivalent composition, was grown as a replacement for HM-B11, and is

included in the study of the electrical properties of the material. Furthermore, the small difference in binding energy between In^0 and InO_x makes distinguishing between the two very difficult. It is for these uncertainties that further analysis using SEM-EDX was carried out.

5.4 (c) Scanning Electron Microscopy – Energy Dispersive X-ray

The analysis of the white and red ampoule deposits with Scanning Electron Microscopy – Energy Dispersive X-ray (SEM-EDX) was performed using a Philips XL30 FEG SEM with Orientation Imaging Microscope (OIM) and EDS/X-ray Microanalysis capabilities. The resolution of this device is 2.0 nm at 30 kV. Sample HM-B29 (stoichiometric + 2% Na^0) was used for the analysis of the white deposit. Several different locations within this deposit, each comprising various shapes and patterns, were investigated, revealing the presence of minute amounts of Na and Cu, along with large relative quantities of Si, O, and C. One such area, shown in Fig. 5.14 and taken at 8000x magnification, contained, aside from Si and O (likely from the quartz), and C (contamination), only Na. Specifically, the composition of this area, in atomic percent, was found to be approximately 16.1 Si, 49.7 O, 32.5 C, and 1.7 Na, with 0.0 Cu, In, or Se. It is believed that this area is representative of the entire composition of the white deposit, and that the defining component of this deposit is essentially Na (see Discussion, Sec. 5.6).

Samples HM-B03 (stoichiometric + 3% Na_2Se) and HM-B19 (excess Se + 2% Na^0) were used for the analysis of the red ampoule deposit. Once again, this analysis

proved complicated, as different areas containing different structural properties were found to be composed of different proportions of elements. For example, the area of HM-B03 shown in Fig. 5.15, taken at 5000x magnification, was found by SEM-EDX to contain mostly selenium, indium, and oxygen, with little copper and silicon, and no sodium. However, visual inspection of the crystal facets, possible chalcopyrite CuInSe_2 , suggests that more copper is present in the material than was revealed in the scan. The area of HM-B19 seen in Fig. 5.16, taken at 10000x magnification, by contrast, was found to be comprised only of Se and Cu, in the atomic ratio of approximately 70:30, respectively. Note that the SEM images (Fig. 5.14, 5.15 and 5.16) were each taken at 20 kV acceleration voltage and 7.8 μA probe current, with an Everhart-Thornley detector. No traces of other elements were found by SEM-EDX at all. As this region is relatively free of inhomogeneous structures, it is believed to be the best representative sample of the red deposit. Taken together with the information obtained by XRD (Fig. 5.11) of the ampoule dots from ampoule HM-B03, the implication is that copper and selenium play a role in the formation of the red deposit which is not shared by the other elements contained within the ampoule. Therefore, upon completing this analysis, it was decided that the red deposit be considered as comprised primarily of selenium with some copper, and perhaps with phases that include the other starting elements, principally sodium, also present, to a smaller degree.

5.5. ELECTRICAL MEASUREMENTS

5.5 (a) Resistivity

The resistivity measurements for all the samples presented in this work were taken using a four-point-probe, with a probe spacing of 2.5 mm. The resistivity (ρ) was calculated according to Eq. 2.13 by considering $\frac{\pi}{\ln(2)}$ to be exactly equal to 4.5324. Furthermore, as the wafers were of finite width and non-negligible thickness, it was necessary that the calculated resistivity be multiplied by two correction factors in order to obtain the final value; these correction factors were determined in accordance with Smits' treatment [5.12].

The following describes the experimental procedure used to determine the resistivity of the samples: the four-point-probe, having brass probe tips, was first lowered onto the surface of a wafer and current was applied across the outer probes, while the corresponding voltage across the inner probes was recorded. The readings were taken under room light conditions but in fact no sensitivity to illumination was apparent. The current was varied so as to allow eight separate readings to be gathered. The resistivity value was calculated for each one of these readings, and the final resistivity was taken as the average of these values. This constituted the resistivity in the forward direction for one point. The current was then reversed, and the procedure was repeated in order to determine the resistivity with a reversed current polarity. The average of the resistivity in the forward and reverse directions was considered as the final resistivity for that point. This entire process was repeated a total of eight times, with eight different regions of each ingot investigated. The

average of the resistivity values of all eight points was taken as the resistivity of the ingot. The results are given in Tables 5.1 and 5.2 (row 4) for both the Na₂Se and Na⁰ runs, respectively. Each of the ρ values given was determined using the procedure described except for that of HM-B03. As was previously explained, this ingot was extremely brittle and broke up into tiny fragments on which resistivity values could not be measured by the four-point-probe method. It was only possible to obtain one measurement before this occurred. While this value is given in Table 5.1, it should therefore be viewed with reserve.

In some instances, the ρ values obtained for the eight different points of the same sample are in close agreement. However, this is not true for all samples; it is perhaps best exemplified by considering HM-B26 (3 at. % Na⁰) and HM-B27 (0.5 at. % Na⁰), both stoichiometric. The final values of ρ for HM-B26 and HM-B27 were determined to be 2.5 and 61 $\Omega\cdot\text{cm}$, respectively. In the former case, the values for the eight points considered in this analysis are within reasonably close proximity to each other, resulting in a very small experimental error. The actual current and voltage values recorded for each of these points are shown plotted in Fig. 5.17. Conversely, as can be seen in Fig. 5.18 for HM-B27, the values are widely divergent; in some cases, even the forward and reverse values for the same point are in disagreement. It is believed that these discrepancies are due to the presence of mini-cracks, which may divert the flow of current from the probes and thus severely complicate the analysis. It should also be noted that the wafers had been cut several months before the resistivity measurements were made, and had been stored during this time in an

ambient-air environment, which may have caused the surface to oxidize. However, any surface effects would have been completely overshadowed by the effect of the mini-cracks on the measurements.

The final ρ values determined for all p-type samples are shown plotted versus the percent addition of Na in Fig. 5.19. The resistivity values for the stoichiometric samples grown with additions of Na⁰, for which a type change from p to n was seen above a certain percent of added Na⁰ (see Sec. 5.5 (b)), are shown in Fig. 5.20. Previous investigations [5.13-15] have determined that the resistivity of CIS and CIGS films decreases in the presence of small amounts of sodium. This observation could not be unequivocally confirmed in this part of the study. As can be seen from Fig. 5.19, the resistivity values obtained for the p-type samples in this study show no discernable pattern and are considered unreliable indicators of true bulk resistivity. However, for the n-type samples in Fig. 5.20, there appears to be an overall decrease in resistivity with increased sodium content. It is possible that a four-point probe with much smaller pin separations could produce more regular results.

5.5 (b) Thermoelectric Power

Thermoelectric power (α) was measured with a simple apparatus that consisted of a soldering iron, which served as the hot probe, with a Type J thermocouple attached very near to the tip. The soldering iron was powered through a Variac, which was kept at around 30 V AC in order to maintain a temperature averaging approximately 20 °C above room temperature; a grounded brass slab at

room temperature served as the cold probe. The wafers were placed on the brass slab, and their exposed sides were probed with the tip of the soldering iron. Simultaneously, the resulting voltage between the probes was measured and recorded, along with the voltage generated by the thermocouple. This was used to interpret the temperature across the wafer when calculating the thermoelectric power of the sample. For each growth run, a total of 60 points was measured near and around the middle of the ingot. The final value of α , recorded in Table 5.1 and 5.2 (row 3) for the runs containing Na_2Se and Na^0 , respectively, was taken to be the average values of these points. Unlike the resistivity values previously described, a pattern did eventually emerge linking thermoelectric power with the amount of Na which was added to the melt. As well, the form of the sodium, either Na_2Se or Na^0 , was seen to play an important role on the resulting α -values. The presence or absence of excess Se in the melt was also seen to influence the thermoelectric power. In this work, the conductivity type of the sample is denoted by the sign of the thermoelectric power, so that positive α -values denote p-type material and negative α -values denote n-type material.

A plot of the α -values for both the stoichiometric and excess Se ingots against the percent of added Na_2Se is shown in Fig. 5.21. Also included in this plot are the ingots grown with Na^0 . Note that the Na_2Se concentration is denoted in the top scale, while the middle scale, with values twice those of the top scale, denotes at. % of added Na^0 , either as elemental sodium or Na_2Se . As can be seen, the stoichiometric samples grown with additions of Na_2Se were all p-type. Furthermore, there is a

general decrease in thermoelectric power with increase of Na_2Se , with α reducing from $373 \mu\text{V/K}$ with 0% to $156 \mu\text{V/K}$ at 3%. The same phenomenon was also noticed for the excess Se ingots grown with Na_2Se , for which the samples were all p-type and α decreased from 441 to $130 \mu\text{V/K}$ with increase of added Na_2Se from 0 to 3%. Note that with no added sodium, the thermoelectric power was increased slightly with the addition of excess selenium. This is consistent with what was found through analysis of ingots grown with excess Se by Champness et al [5.16].

The excess Se ingots grown with additions Na^0 were also observed to be p-type. However, as can be seen, no significant change in thermoelectric power was observed to correspond with increases of Na^0 , with α deviating only slightly from its initial value. By contrast, the stoichiometric ingots grown with elemental sodium were seen, when a high enough concentration of Na^0 was added, to change from p- to n-type, as expressed by α exhibiting a change in sign from positive to negative; the amount of Na^0 required in order for the stoichiometric samples to undergo this transition, by examination of Fig. 5.21, is somewhere between 0.1 and 0.5 at. %. Wang et al [5.5] also reported a p- to n-type conversion with additions above 0.25% Na^0 to melts containing stoichiometric CuInSe_2 . This present work is thus consistent with those findings.

Further, while the main parts of the ingots of the present work were uniformly n-type, the last-zones-to-freeze, located towards the end of the ingots, were p^+ -type with extremely low α -values, as was the case with HM-B26, shown in Fig. 5.22. This

p^+ region was also observed for all the other ingots presented in this work, irrespective of composition, and is consistent with ingots grown using the same growth procedure in other studies [5.17].

5.6. DISCUSSION

It should be noted that initially, in the case of the stoichiometric ingots grown with Na_2Se , that an obvious decrease in thermoelectric power with increase of Na was not quite apparent. It was only after these measurements were repeated some months later that a clear trend emerged. The reason for this re-measurement was to ensure that the procedure used in obtaining the results was kept consistent for all samples; this particular set of ingots was grown and analyzed early in this work, and it was thought that the method of conducting the thermoelectric power measurements may have unknowingly and unintentionally evolved over time. Therefore, it was decided that the measurements be performed again using a standardized procedure, which was kept constant for all the samples presented in this work. It is possible that the change in result may be due to the measurements being conducted more consistently and reliably. However, it is equally possible that, during the months between when the thermoelectric power was first measured and when the re-measurements took place, that the samples underwent a change that impacted the α -values. Perhaps being kept in air led to the passivation of selenium vacancies through oxidation, as described in Sec. 3.3 (a) [5.18], which could result in a decrease in thermoelectric power. This possibility has yet to be further investigated.

In addition, while it was stated here, as well as in the previous chapter, that all of the ingots, apart from the stoichiometric ingots grown with large concentrations of Na^0 , were p-type. Ingots HM-B01 and HM-B04 (Table 4.1), in actuality, were found by hot-probe to be n-type. However, these ingots, as their numbers would suggest, were fabricated early in this study, and therefore at a time of when the author was inexperienced in crystal growth. It was discovered that the pellets of Cu, In and Se, used in the melt of HM-B01, had been weighed *before* being etched, and so the exact proportions of these constituents could not be guaranteed. The cause of the conductivity of HM-B04 was never completely identified, but it is believed that a similar oversight, as happened during the fabrication of HM-B01, had occurred. Different ingots grown with the same theoretical proportions of starting constituents as HM-B01 and HM-B04 were seen to be p-type, thus confirming the anomalous natures of these two early ingots. Furthermore, several principally p-type ingots were seen to contain small n-type regions. It is believed that these regions result from insufficient mixing of the melts.

It is possible to estimate the carrier concentration of the ingots from the thermoelectric power values, using the methods described in Sec. 2.2 (c), by considering simple idealistic conditions for the samples of isotropic and unity values of effective mass ratios, non-degeneracy and acoustic lattice scattering. While not all of these conditions may apply, particularly those of non-degeneracy for some of the smaller thermoelectric values, this exercise is nonetheless useful in estimating trends in the materials. Therefore, the conditions, including the decision to consider unity

effective mass ratios, were made only for the purpose of simplicity. The exact values of the carrier concentrations given in this work are not meant to be accurate, but to serve as a tool of comparison of the samples.

For the ingots grown with additions of Na_2Se , the thus calculated carrier concentration plotted against the atomic percent of added sodium is shown in Fig. 5.23. As can be seen from this plot, the presence of Na_2Se , within the range of 0 to 3 at. %, in the melt of CuInSe_2 has the effect of increasing the net hole concentration an amount equivalent to more than an order of magnitude over this range. The same is true for the ingots grown with excess Se, in which the net hole concentration of the material was also increased more than an order of magnitude as Na_2Se was increased from 0 to 3 at. %. This is in agreement with the numerous studies conducted elsewhere that found the majority carrier concentration in p-type material to increase in the presence of Na [5.19-20]. These works contributed to the now widely held belief that sodium, whether directly or indirectly, acts as an apparent acceptor in CuInSe_2 .

The clear trends observed in the electrical properties of the ingots grown with the additions of Na_2Se was not seen when Na^0 was used instead. Rather, differing but equally clear trends were seen to emerge. In the case of Na^0 added to ingots grown with excess Se, the thermoelectric power was seen to change little as Na was increased from 0 to 3 at. %. Therefore, it is apparent that the carrier concentration was not very affected by the increasing presence of Na^0 in these ingots. By contrast,

the presence of Na⁰ seemed to affect greatly the carrier concentration in the stoichiometric ingots. Note that, as the concentration of added Na⁰ is increased from 1 to 3%, the thermoelectric power was seen to decrease in magnitude from -465 to -401 $\mu\text{V}/\text{K}$. While this change is subtle, it is suggestive of a two-fold increase in the electron concentration of the material over this range. Therefore, the presence of Na⁰ in stoichiometric CuInSe₂ may have an apparent donor effect on the material, rather than an acceptor effect, as is commonly believed.

Concerning the mobility of the samples presented in this work, and considering that the objective of this work was to determine trends in the characteristics of the materials grown with increasing amounts of sodium, the room-temperature hole mobility was calculated for the samples grown with additions of Na₂Se in accordance with Sec. 2.4. However, as the resistivity measurements are quite erratic, as previously described, the mobility results, based on these resistivity measurements, are equally erratic. Nevertheless, some of the values are reasonably close to values from the literature. For example, the hole mobility value HM-B14 (CuInSe_{2.2} + 0.1% Na₂Se) was 3.2 $\text{cm}^2/\text{V}\cdot\text{s}$, respectively, at a carrier concentration of approximately $1.1 \times 10^{18} \text{ cm}^{-3}$. This value is similar to the value of 5 $\text{cm}^2/\text{V}\cdot\text{s}$, measured by H. Neumann et al [5.21] for a p-type sample at room temperature with a carrier concentration of 10^{17} cm^{-3} . By contrast, the hole mobilities for the other samples in this series of ingots differ considerably from this accepted value. Similar results were obtained for the stoichiometric ingots grown with Na₂Se. A hole mobility of 3.2 $\text{cm}^2/\text{V}\cdot\text{s}$, calculated for sample HM-B08 at a carrier concentration of

$1.15 \times 10^{18} \text{ cm}^{-3}$, is within range of the value from the literature. However, the other values of this series, like the previously described series, deviate considerably. It is possible that the dramatic differences in the mobility values from sample to sample are due to changes in the carrier concentration of the materials resulting from high concentrations of Na_2Se in the melt. However, it is far likelier that they are due to erroneous resistivity values, resulting from microcracks and inhomogeneities in the materials, which, when plugged in to Eq. 2.15, produce doubtful mobility results.

Finally, concerning the results from analysis of the white and red deposit described in Sec. 5.4 (c), the belief that the SEM-EDX result taken from analysis of the area shown in Fig. 5.14 is a representative sample of the white deposit is based on the appearance of the area in question. It could be seen, using a simple microscope with 20x magnification, that the white deposits from various samples were littered with inhomogeneous bits of material, which were quite distinctive from the deposits themselves. It was presumed that these bits may have complicated many of the SEM-EDX measurements taken at various locations of the deposits. However, the scan shown in Fig. 5.14 revealed a relatively uniform area. Therefore, the results from the analysis of this area were taken to represent the actual, untainted white deposit. However, it is acknowledged by the author that this is subjective, and the actual constituents of the deposits may be more complex than can be revealed by analysis of these two areas alone.

Table 5.1
Results for the growth runs containing Na₂Se

Melt Composition	CuInSe ₂ (stoichiometric) +Na ₂ Se							CuInSe _{2.2} (excess Se) +Na ₂ Se						
	2	8	6	7	17*	3	13	14	12	10	18	9		
Growth run No.	0	0.1	0.5	1	2	3	0	0.1	0.5	1	2	3		
at. % Na ₂ Se	373	437	326	312	307	156	441	439	395	272	361	130		
avg. α (μV/°C)	4.8	1.7	353	37	2.2	1050	5.9	1.8	48	55	9.7	5.5		
White deposit	None	Little	Some	Little	Much	Much	None	None	Little	Some	Much	Much		
Reddish-brown deposit	None	None	None	Some	Much	Much	None	None	Little	Some	Much	Much		
Grey dots	None	Some	Some	Many	Many	Many	None	Several	Many	Many	Many	Many		
Se-like deposits	None	Little	Little	Some	None	Little	Much	Much	Much	Much	Much	Much		
Conductivity	p	p	p	p	p	p	p	p	p	p	p	p		
Cohesiveness	Solid	Solid	Mostly solid	Increased brittleness	Solid	Very brittle	Solid	Solid	Mostly solid	Increased brittleness	Brittle	Brittle		
Mini-cracks	Some	Few	Some	Many	Few	Ingot broke up	Few	Few	Some	Some	Many	Many		
Surface deposits	None	Little	Very Little	Some	None	None	Much	Some	Some	Some	Some	Much		
	None	None	None	Some	Much [†]	Much	None	None	Little	Much	Much	Much		

* Ampoule cracked near end of run #17.

† Some discernable red, but also a greenish deposit presumed to be oxide contamination from the cracking.

Table 5.2
Results for the growth runs containing Na⁰

Melt Composition		CuInSe ₂ (stoichiometric) +Na							CuInSe _{2.2} (excess Se) +Na						
Growth run No.		2	24	27	28	29	26	13	20	21	23	19	22		
at. % Na ₂ Se		0	0.1	0.5	1	2	3	0	0.1	0.5	1	2	3		
avg. α (μV/°C)		373	412	-373	-465	-455	-401	441	506	473	463	437	470		
avg. ρ (Ω·cm)		4.8	779	61	26	38	4.5	5.9	4.8	18	25	8.5	148		
White deposit		None	Some	Some	Some	Some	Some	None	None	None	None	Little	Some		
Reddish-brown deposit		None	None	Little Near Ingot End	Little Near Ingot End	Little Near Ingot End	Little Near Ingot End	None	Little	Some	Much	Much	Some		
Grey dots		None	None	Some	Few	Some*	Some*	None	Some	Some	Many	Many	Many		
Se-like deposits		None	Very Little	Very Little	Very Little	Little	Very Little	Much	Much	Much	Much	Much	Much		
Type	Main	p	p	n	n	n	n	p	p	p	p	p	p		
	LZTF	p ⁺	p ⁺	p ⁺	p ⁺	p ⁺	p ⁺	p ⁺	p ⁺	p ⁺	p ⁺	p ⁺	p ⁺		
Cohesiveness		Solid	Solid	Mostly Solid	Increased Brittleness	Increased Brittleness [†]	Solid [†]	Solid	Mostly Solid	Mostly Solid	Increased Brittleness	Mostly Solid	Brittle		
Mini-cracks		Some	Many	Some	Some	Some [‡]	None [‡]	Few	Few	Few	Some	Few	Many		
Surface deposits	Black	None	Very Little	Very Little	Very Little	None	None	Much	Much	None	Much	Much	Much		
	Red	None	None	Very little only at p-type LZTF	Very little only at p-type LZTF	Very little only at p-type LZTF	Very little only at p-type LZTF	None	None	Much	Much	Much	Some		

*Grey dots showed copper-coloured fibrous deposits on the surface.

[†]Part of the last zone to freeze disintegrated into a powder.

[‡]Increased brittleness, and cracking, in the p-type region of the last-zone-to-freeze (LZTF).

Table 5.3

Summary of results for growth runs containing Na₂Se

		CuInSe ₂	CuInSe _{2.2}	Comments
Ampoule	White Deposit	Some	Less	} Less white deposit and more red deposit with excess Se
	Reddish-Brown Deposit	Little	More	
	Grey Dots	Some	Some	No significant difference
	Selenium-like Deposits	Very Little	Much	As expected, more deposited Se with excess Se
Ingot	Cohesiveness	Brittleness increases with Na ₂ Se	Brittleness increases with Na ₂ Se	} No significant difference
	Mini-cracks	Some	Some	
	Surface Deposits	Some	More	More black film and red deposit with excess Se
	α (μV/K) change with Na ₂ Se	Decrease 373 to 156	Decrease 441 to 130	Acceptor action from Na ₂ Se observed in both sets

Table 5.4

Summary of results for growth runs containing Na⁰

		CuInSe ₂	CuInSe _{2.2}	Comments
Ampoule	White Deposit	Some	Less	Less white deposit, but more red deposit and grey dots with excess Se
	Reddish-Brown Deposit	Little	More	
	Grey Dots	Some	More	
	Selenium-like Deposits	Very Little	Much	As expected, more deposited Se with excess Se
Ingot	Cohesiveness	General decrease with increasing Na	General decrease with increasing Na	No significant difference
	Mini-cracks	Some	Some	
	Surface Deposits	Only on p-type end of ingots	On entire surface of ingots	Much more black film and red deposit with excess Se
	α (μ V/K) change with Na	Decrease 373 to -401	No decrease 441 to 470	p-type conductivity requires excess Se

Table 5.5

Lattice constant calculations based on the XRD results from the first-zone-to-freeze
of HM-B03

2 θ	θ	$d_{hkl} = \lambda/2\sin\theta$	{hkl}	$a = d_{hkl}(h^2+k^2+l^2(a/c)^2)^{1/2}$ *
17.4	8.7	5.09	1 0 1	5.69
26.8	13.4	3.32	1 1 2	5.75
27.9	13.95	3.19	1 0 3	5.75
31.1	15.55	2.87	2 0 0	5.74
35.8	17.9	2.51	2 1 1	5.75
42.0	21	2.15	1 0 5	5.79
44.3	22.15	2.04	2 2 0	5.77
48.0	24	1.89	3 0 1	5.75
52.6	26.3	1.74	3 1 2	5.77
62.9	31.45	1.48	3 0 5	5.78
64.3	32.15	1.45	4 0 0	5.80
67.2	33.6	1.39	2 1 7	5.77
70.9	35.45	1.33	3 3 2	5.80
71.6	35.8	1.32	3 2 5	5.79
79.9	39.95	1.20	4 1 5	5.79
81.5	40.75	1.18	4 2 4	5.78
84.1	42.05	1.15	5 0 1	5.78
87.2	43.6	1.12	1 1 10	5.82
87.8	43.9	1.11	5 1 2	5.77
92.2	46.1	1.07	4 1 7	5.79
96.3	48.15	1.03	5 0 5	5.76
97.5	48.75	1.02	4 0 8	5.77
97.9	48.95	1.02	4 4 0	5.77
104.0	52	0.977	3 1 10	5.78
104.1	52.05	0.976	5 1 6	5.77
104.2	52.1	0.976	5 3 2	5.77
108.8	54.4	0.947	6 1 1	5.78
114.1	57.05	0.918	2 0 12	5.81
114.7	57.35	0.915	6 0 4	5.79
121.4	60.7	0.883	3 3 10	5.79
121.8	60.9	0.881	5 3 6	5.78
122.0	61	0.880	3 2 11	5.79

*a/c is assumed to be 0.5.

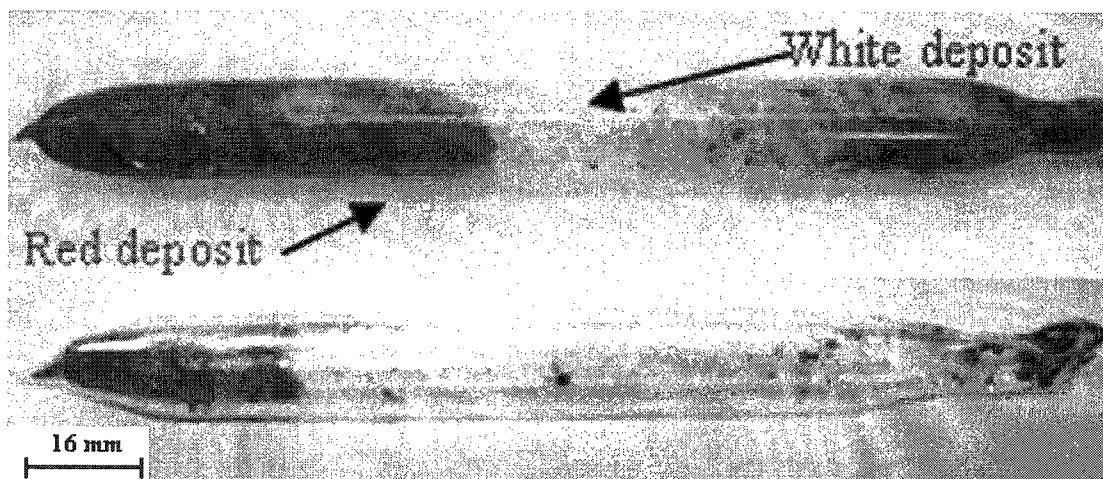


Figure 5.1 Ampoule from run HM-B09 (top), containing excess Se and 3 at. % Na_2Se , showed a large amount of white deposit, as well as red deposit, and thus appeared completely opaque as compared with HM-B13 (bottom), which contained no Na_2Se .

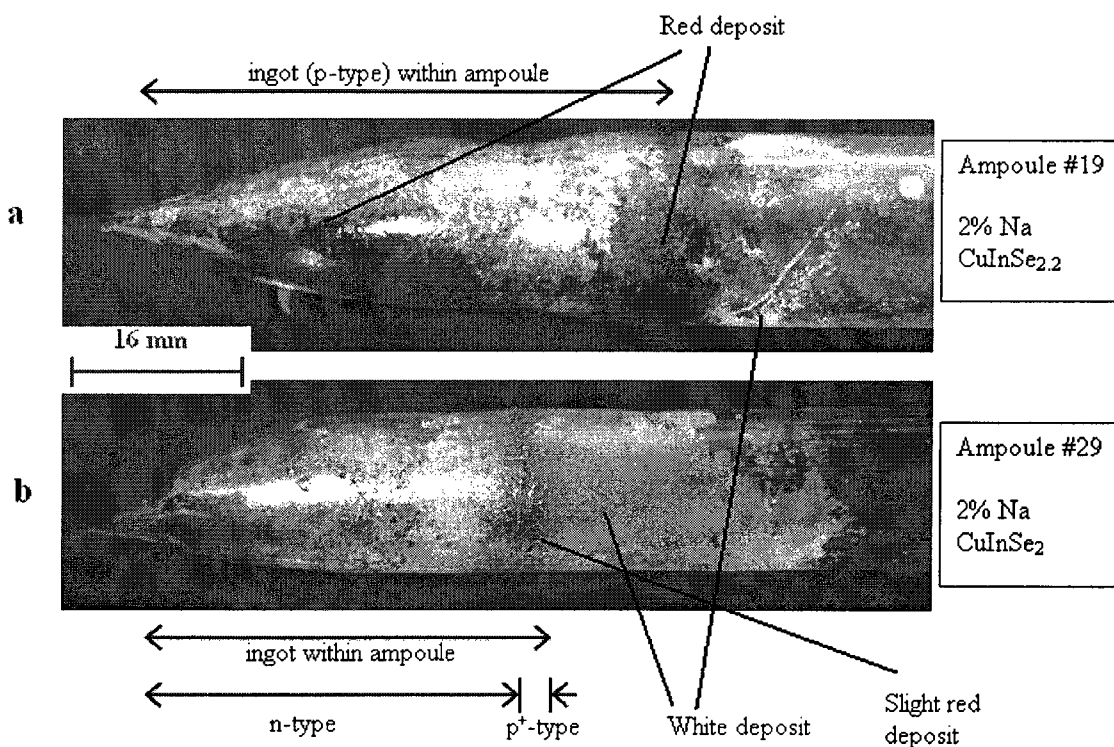


Figure 5.2 Red and white deposits observed in ampoules containing excess Se (a) and stoichiometric (b) proportions of Cu, In and Se, plus 2 at. % Na^0 . As can be seen, excess Se results in an increase of red deposit but a decrease of white deposit.

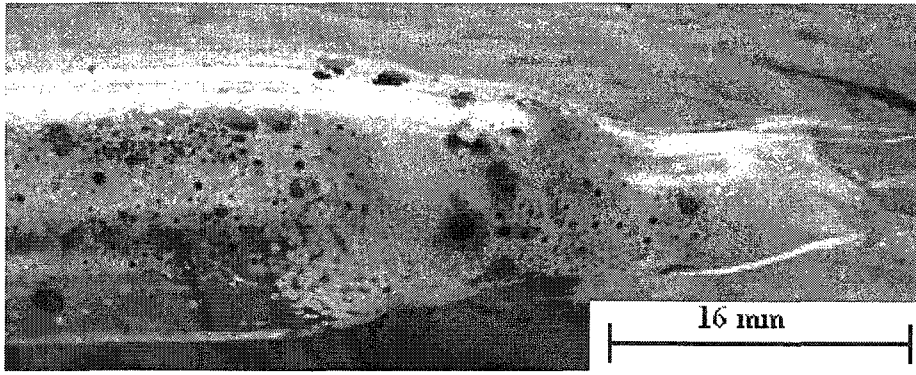


Figure 5.3 Red deposit seen on the ampoule dots of HM-B22 (excess Se with 3 at. % Na⁰).

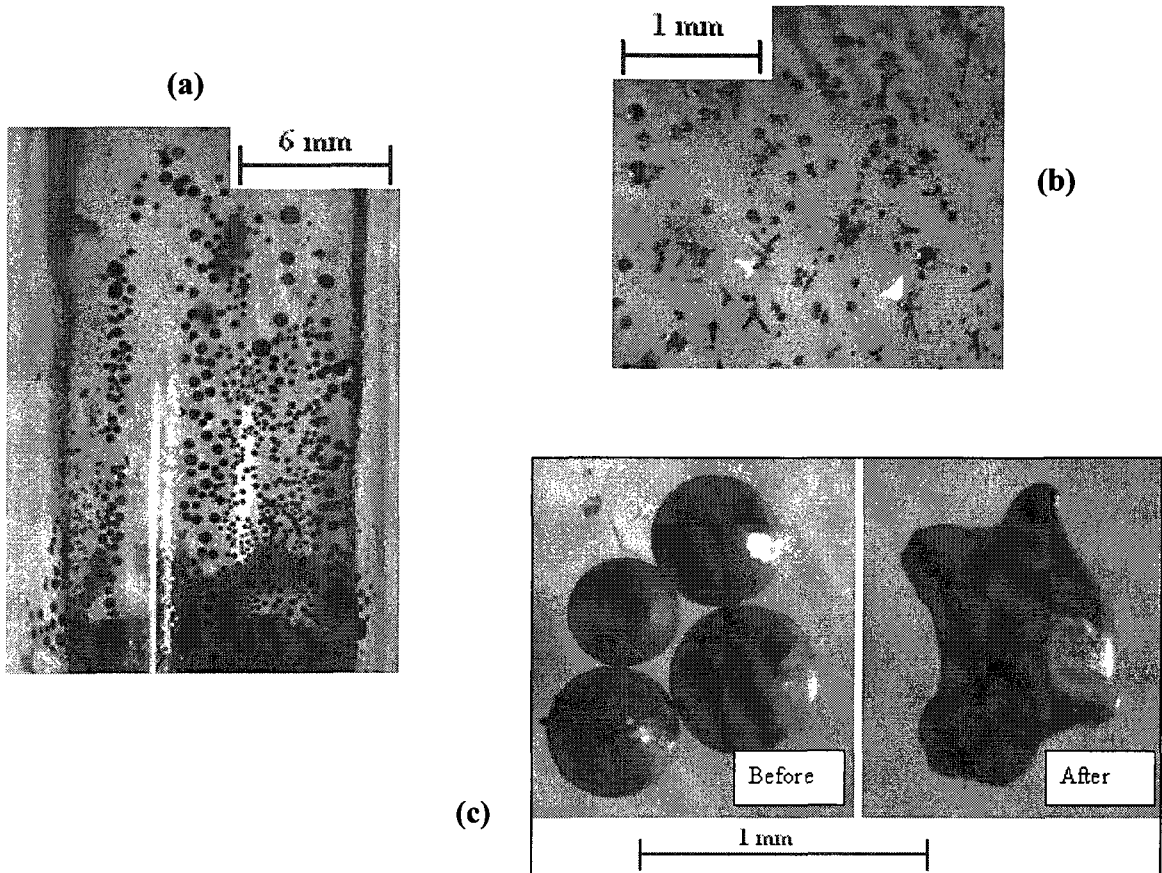


Figure 5.4 Selenium in the form of (a) hemispherical spots (HM-B13), and (b) dendritic needles (HM-B16). A collection of spots taken from ampoule HM-B14 (c) was heated on a hotplate, and seen to melt at the same temperature as that of Se, thus confirming them to be essentially this element.

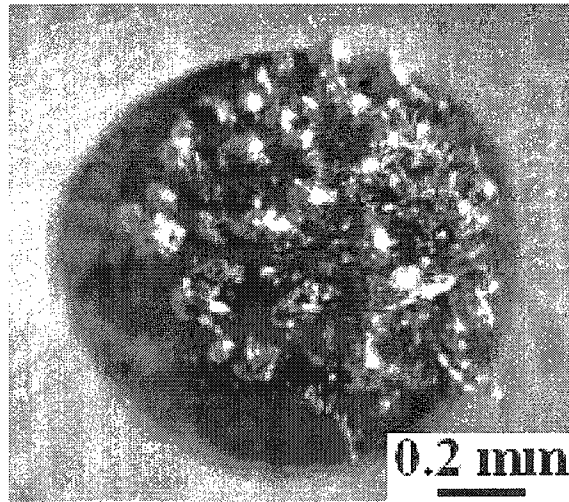


Figure 5.5 Copper-like nodules, seen on the ampoule dots from sample HM-B26.

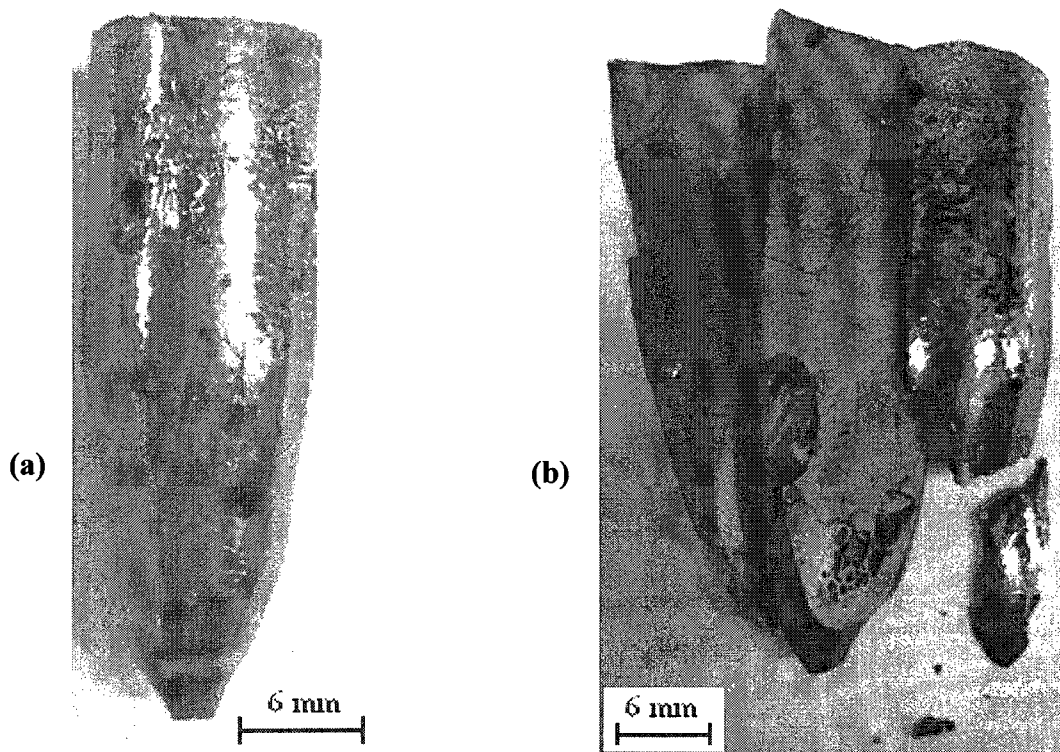


Figure 5.6 Ingot HM-B15, (a) immediately after having been removed from the ampoule, and (b) after having gone through the cutting process.

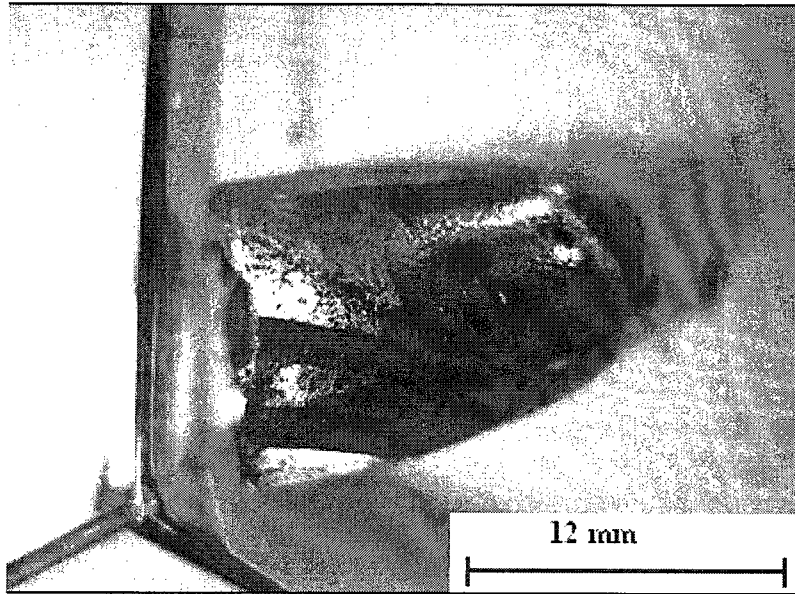
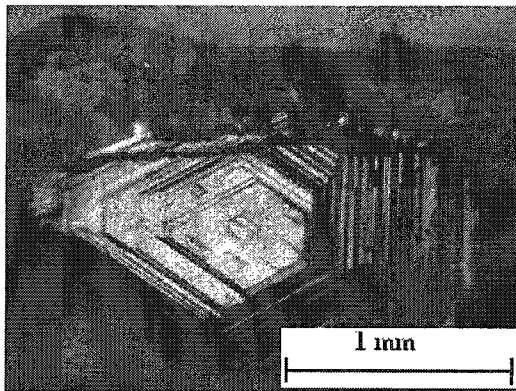
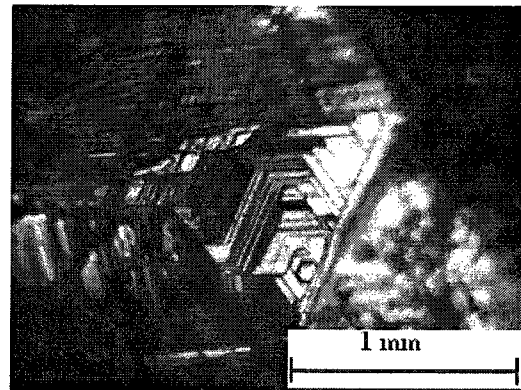


Figure 5.7 A twin, seen on ingot HM-B06, is an indication of monocrystalline regions within the ingot.



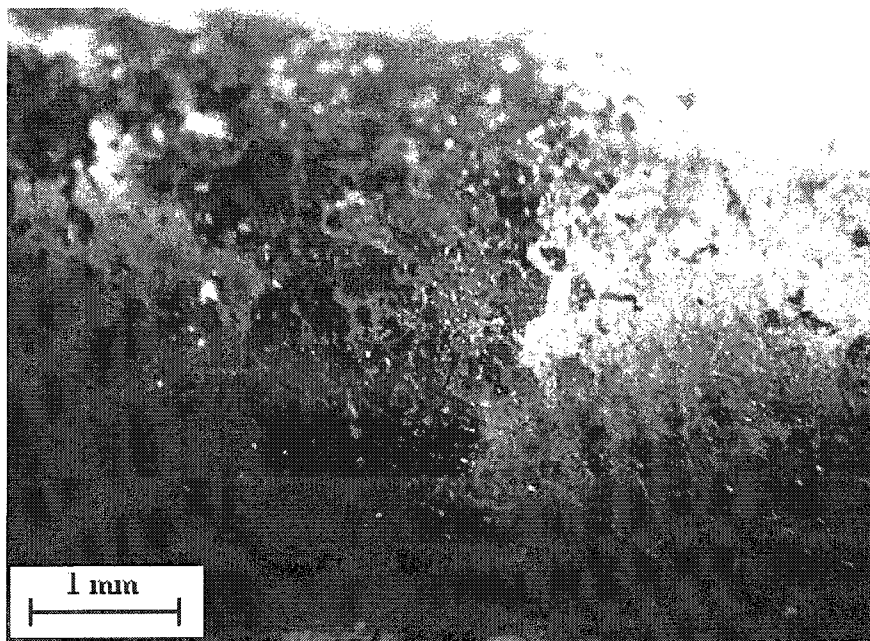
(a)



(b)

Figure 5.8 Angular growth facets, seen at the bottom of growth cavities of ingots (a) HM-B24 and (b) HM-B15. These facets are also indicators of monocrystals within the ingot.

(a)



(b)

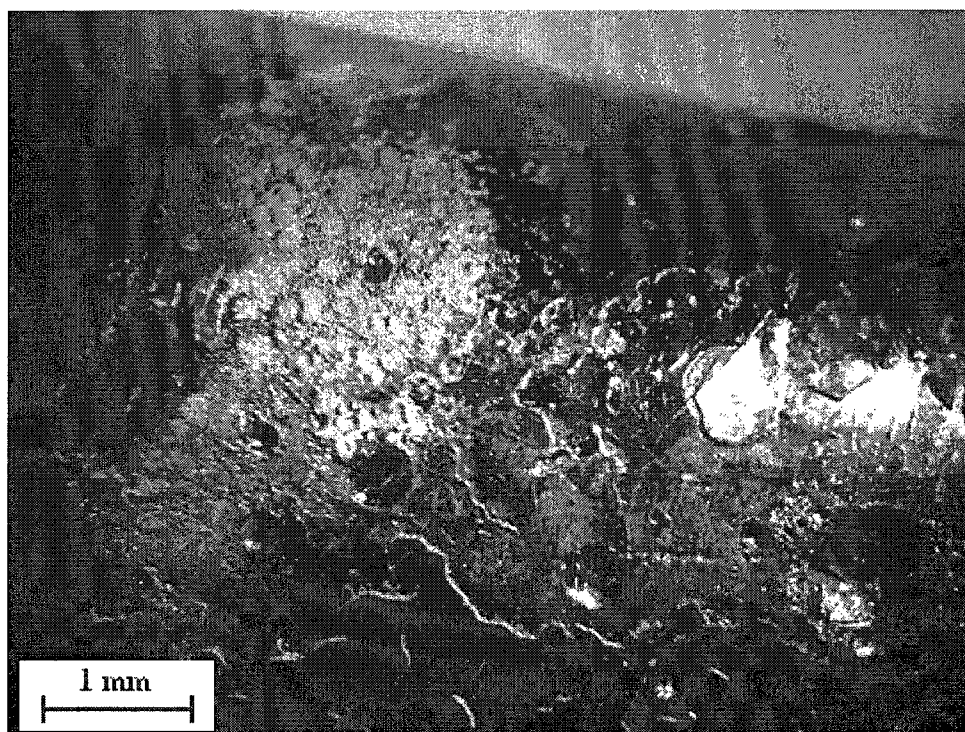


Figure 5.9 (a) Red and black film on the surface of ingot HM-B12 ($\text{CuInSe}_{2.2} + 0.5\% \text{Na}_2\text{Se}$), shown through the quartz ampoule, and (b) black film on the surface of HM-B13 ($\text{CuInSe}_{2.2}$). Notice that the film has a slight red colour, indicative of a thin layer of amorphous selenium.

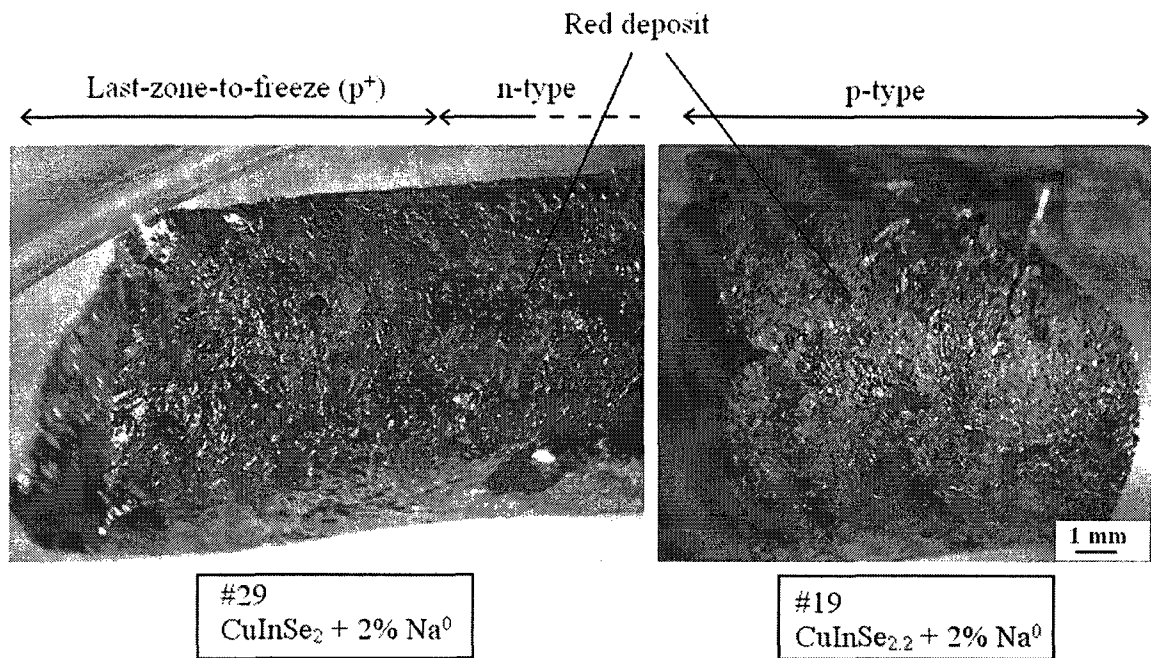


Figure 5.10 The last-zone-to-freeze of a ingot HM-B29 (left) and a portion of ingot HM-B19 (right), both grown with 2 at. % Na^0 , showing much more red deposit in the $\text{CuInSe}_{2.2}$ material.

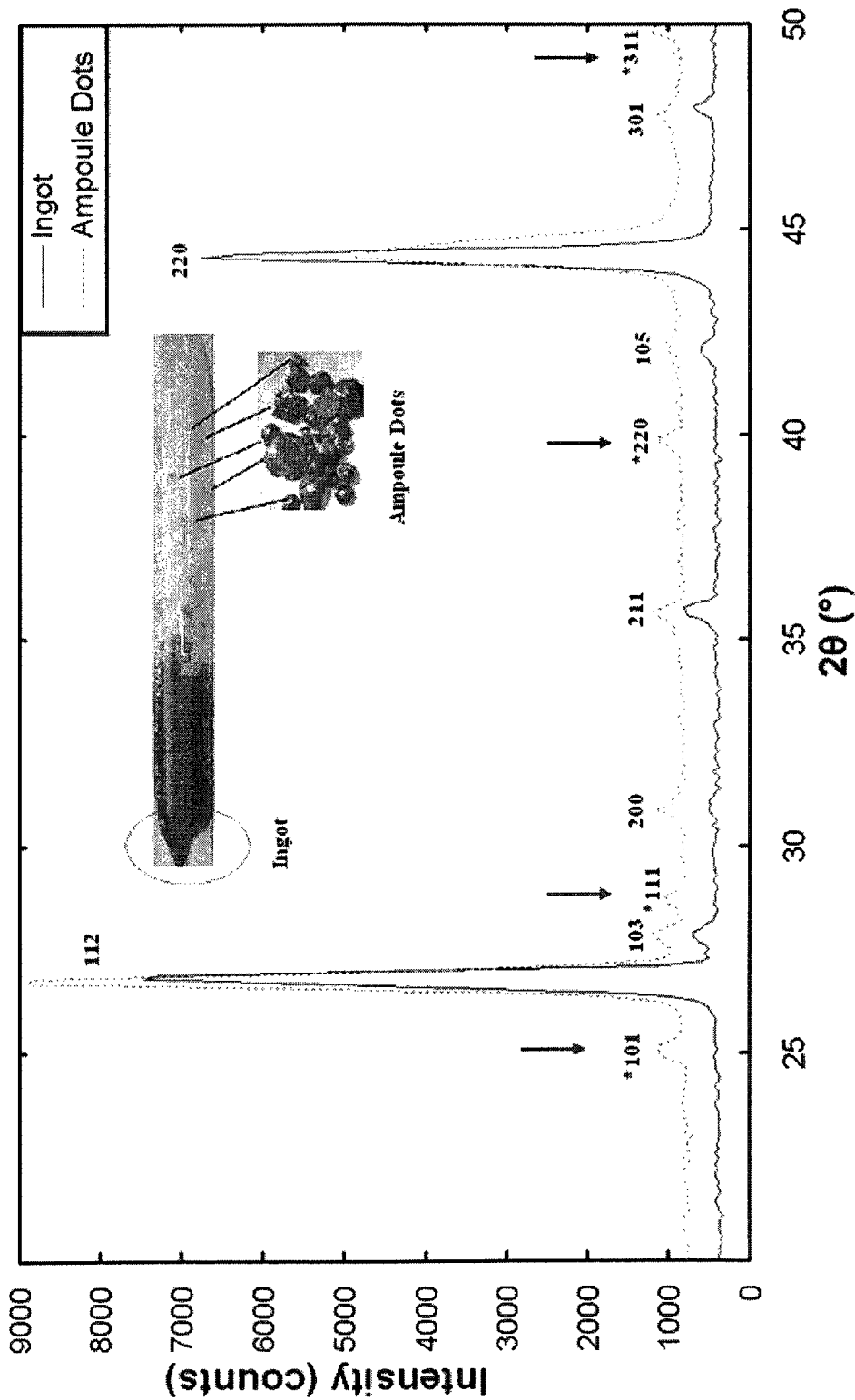


Figure 5.11 X-ray Diffraction pattern of the first-zone-to-freeze (black line) and a collection of the ampoule dots (red dotted line) from sample HM-B03. The usual peaks of Cu_3Se_2 (JCPDS 40-1487) appear in the both lines, however the ampoule dots have some additional peaks, identified as Cu_3Se_2 (JCPDS 47-1745), shown with red arrows. The Miller indices of each peak are also given, with an asterisk (*) indicating the Cu_3Se_2 planes.

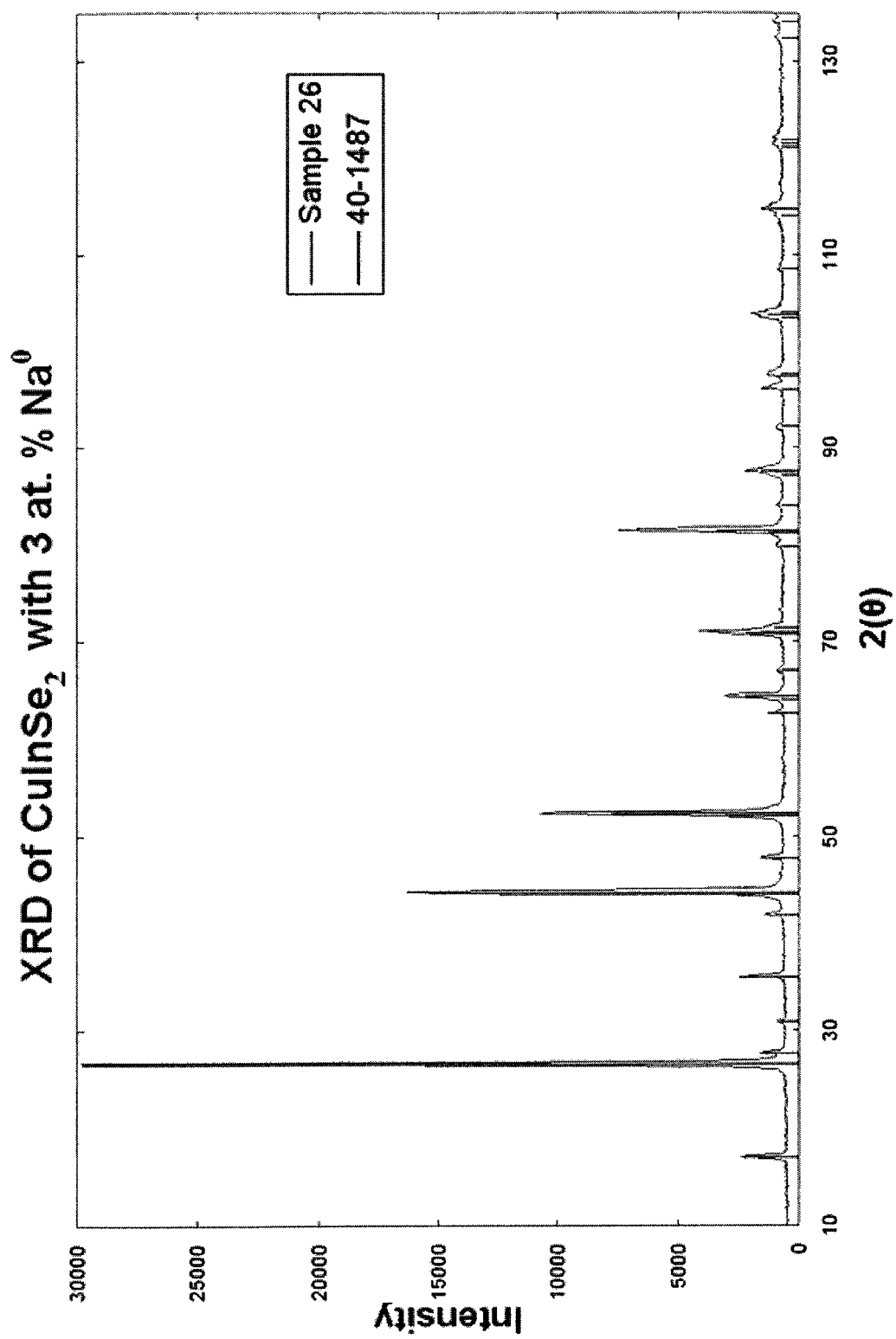


Figure 5.12 Powder X-ray diffraction from the 3 at. % Na stoichiometric n-type ingot HM-B26, showing the usual peaks (JCPDS 40-1487) for CuInSe_2 .

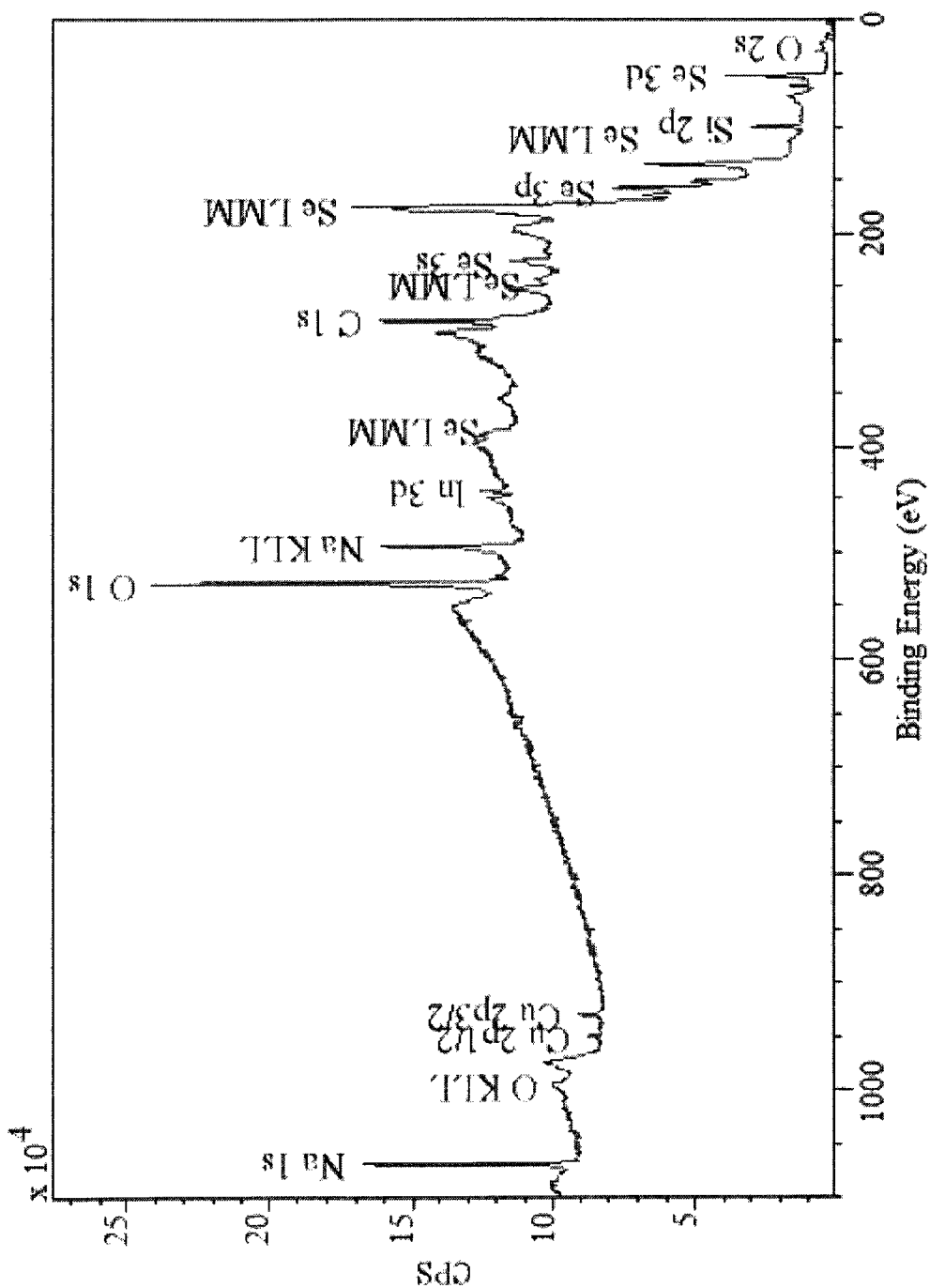


Figure 5.13 X-ray photoelectron spectroscopy results of the red deposit from the ampoule of HM-B09, showing it to be comprised of many phases, including Se^0 , Cu^0 , and In^0 , as well as CuO , and possibly InO_x and SeO . Sodium is also seen in this sample.



Figure 5.14 SEM image of the white deposit from the ampoule of HM-B29. The area within the marked square was found to contain, aside from Si, O (likely from the quartz), and C, only Na.

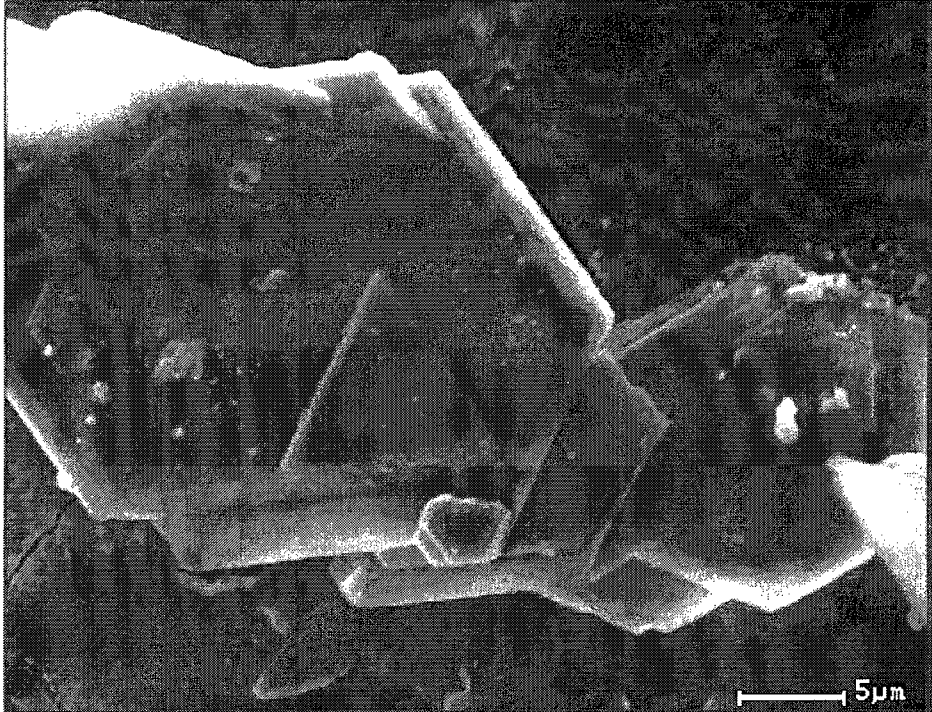


Figure 5.15 SEM image of a crystalline structure on the ampoule of HM-B03.

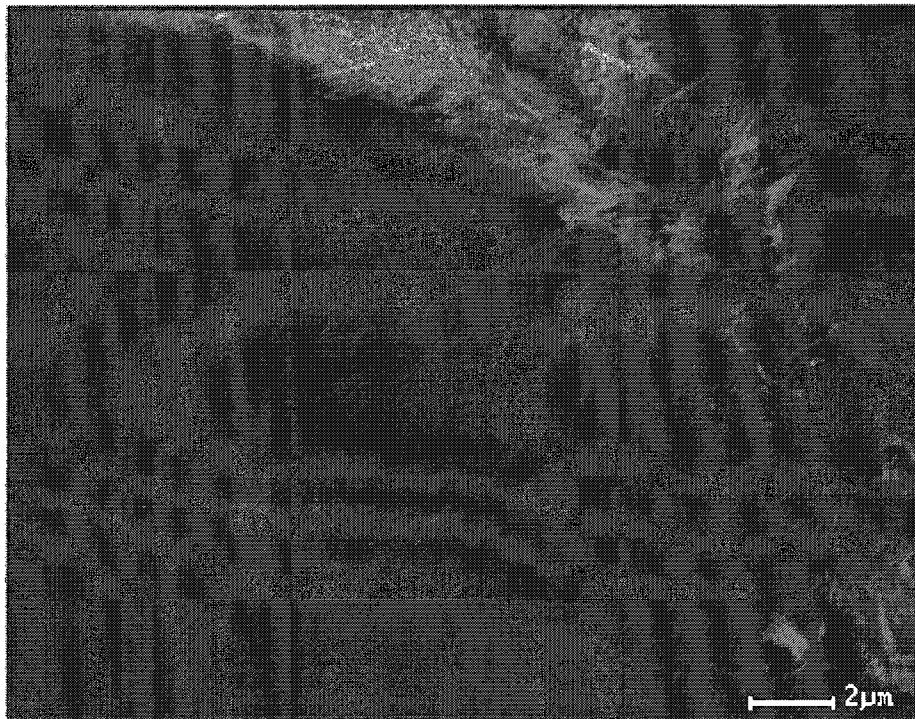


Figure 5.16 SEM image of the red deposit from ampoule HM-B19, which was found to contain only Cu and Se in the ratio of roughly 3:7.

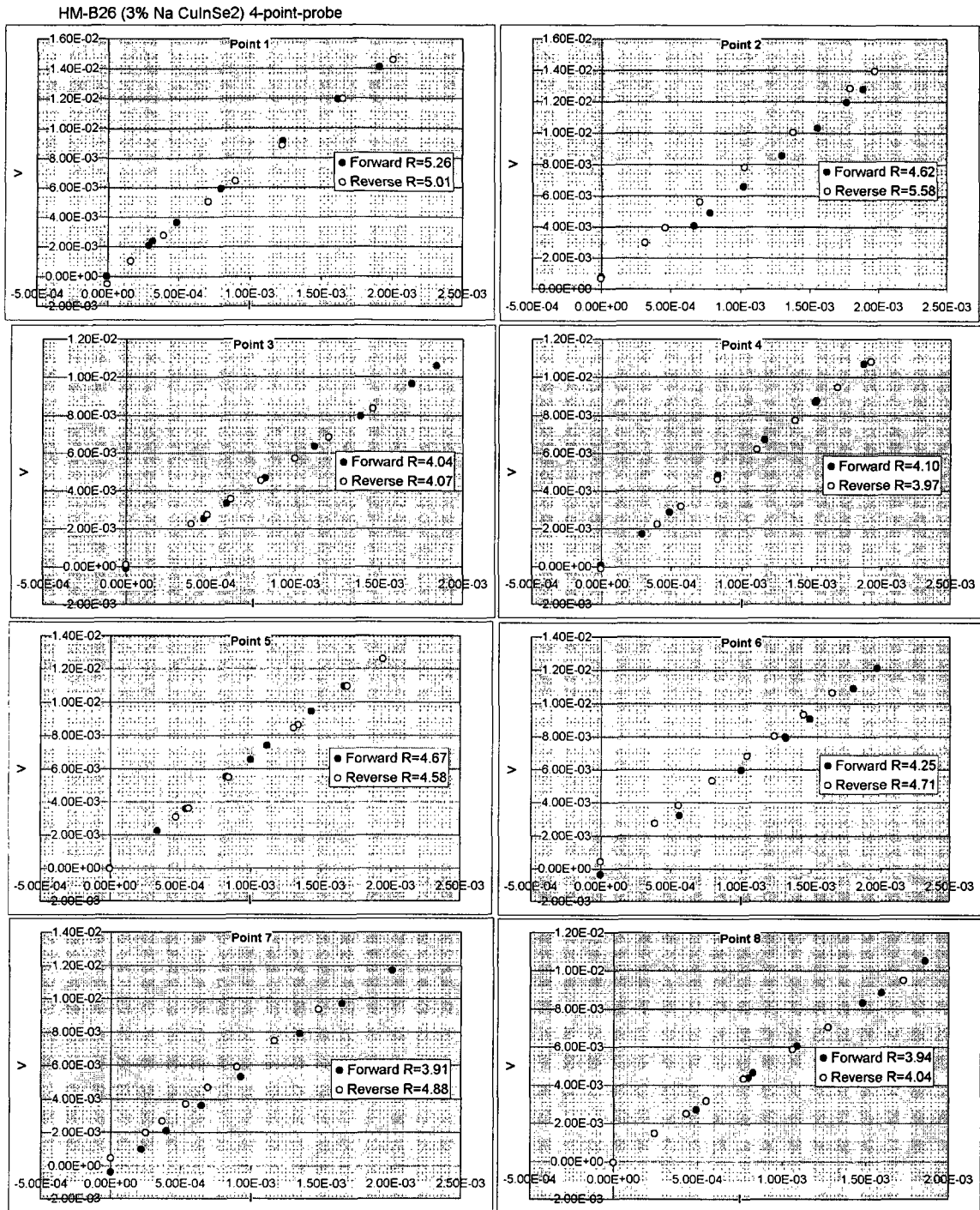


Fig. 5.17 Voltage versus current plots for all the points taken by 4-point-probe on wafers from sample HM-B26. As can be seen, there is little deviation between the values, thus resulting in an average value of resistivity with a small experimental error.

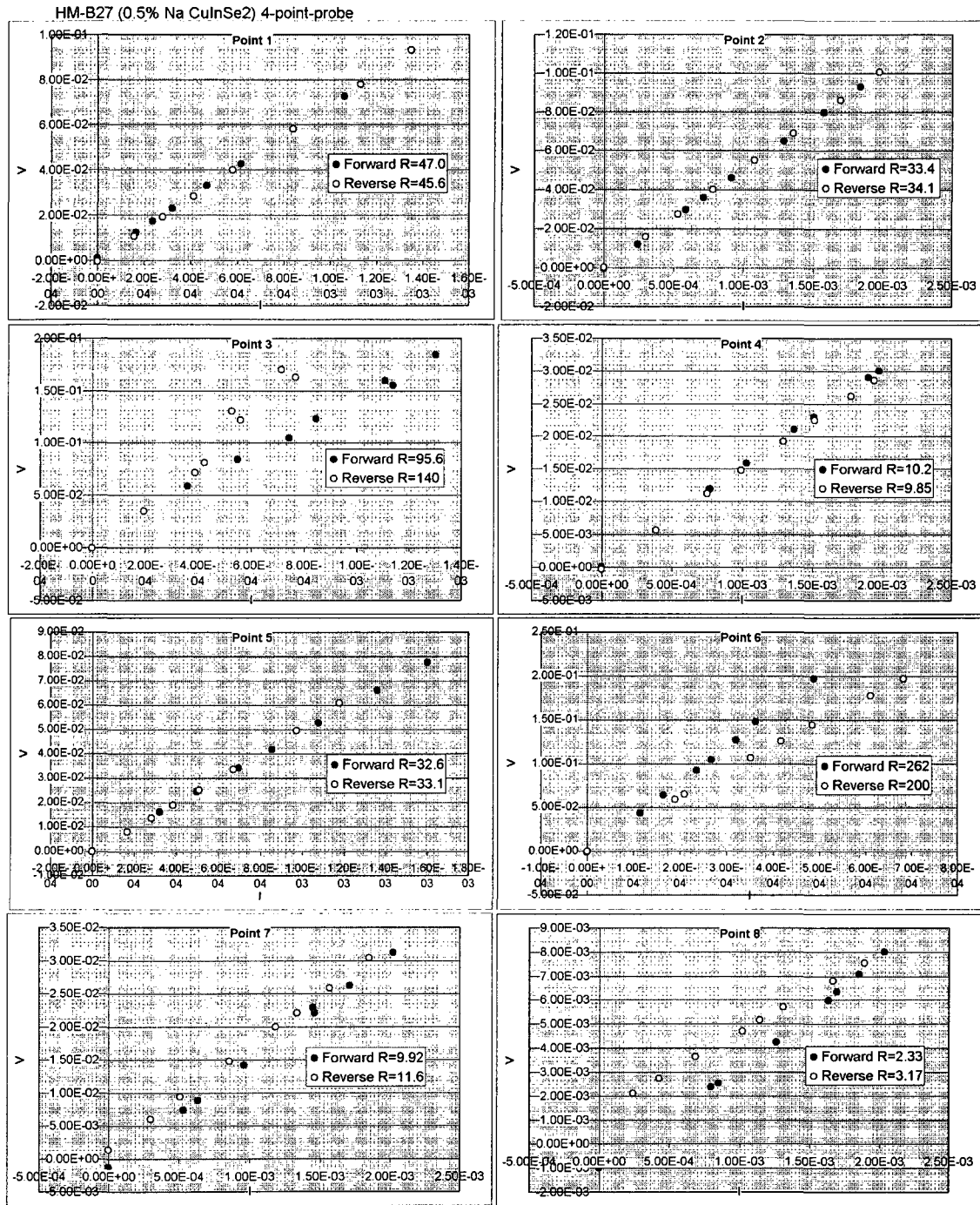


Fig. 5.18 Voltage versus current plots for all the points taken by 4-point-probe on wafers from sample HM-B27. By contrast to the results from HM-B26, there is much deviation between the values, thus resulting in an average value of resistivity with a high experimental error. The values are thus considered unreliable.

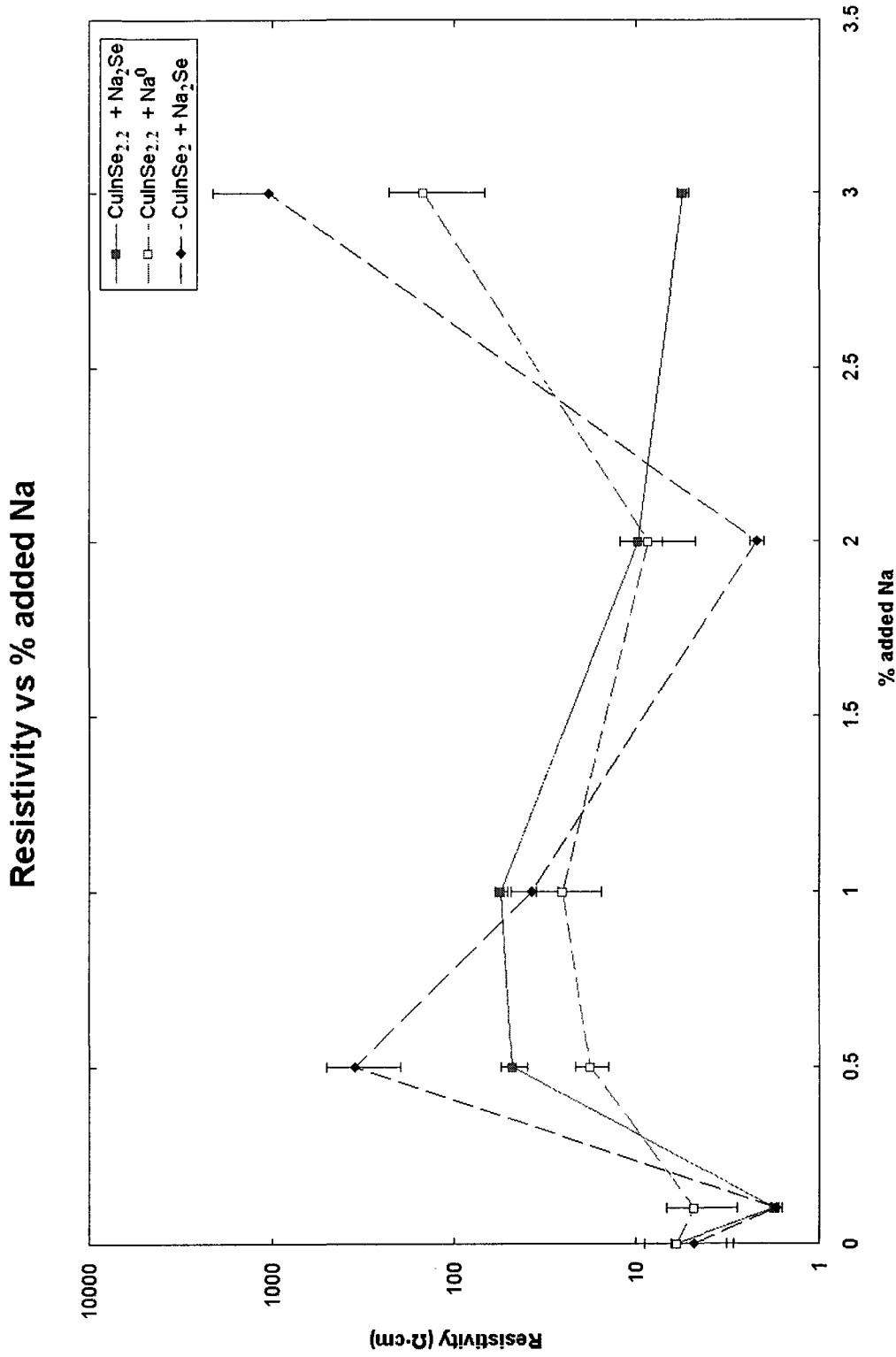


Fig. 5.19 Resistivity vs % added Na for all p-type samples. Note that there appears to be no discernable pattern which connects the resistivity of the samples with the amount of sodium, either in the form of Na₂Se or Na⁰, added to the melt.

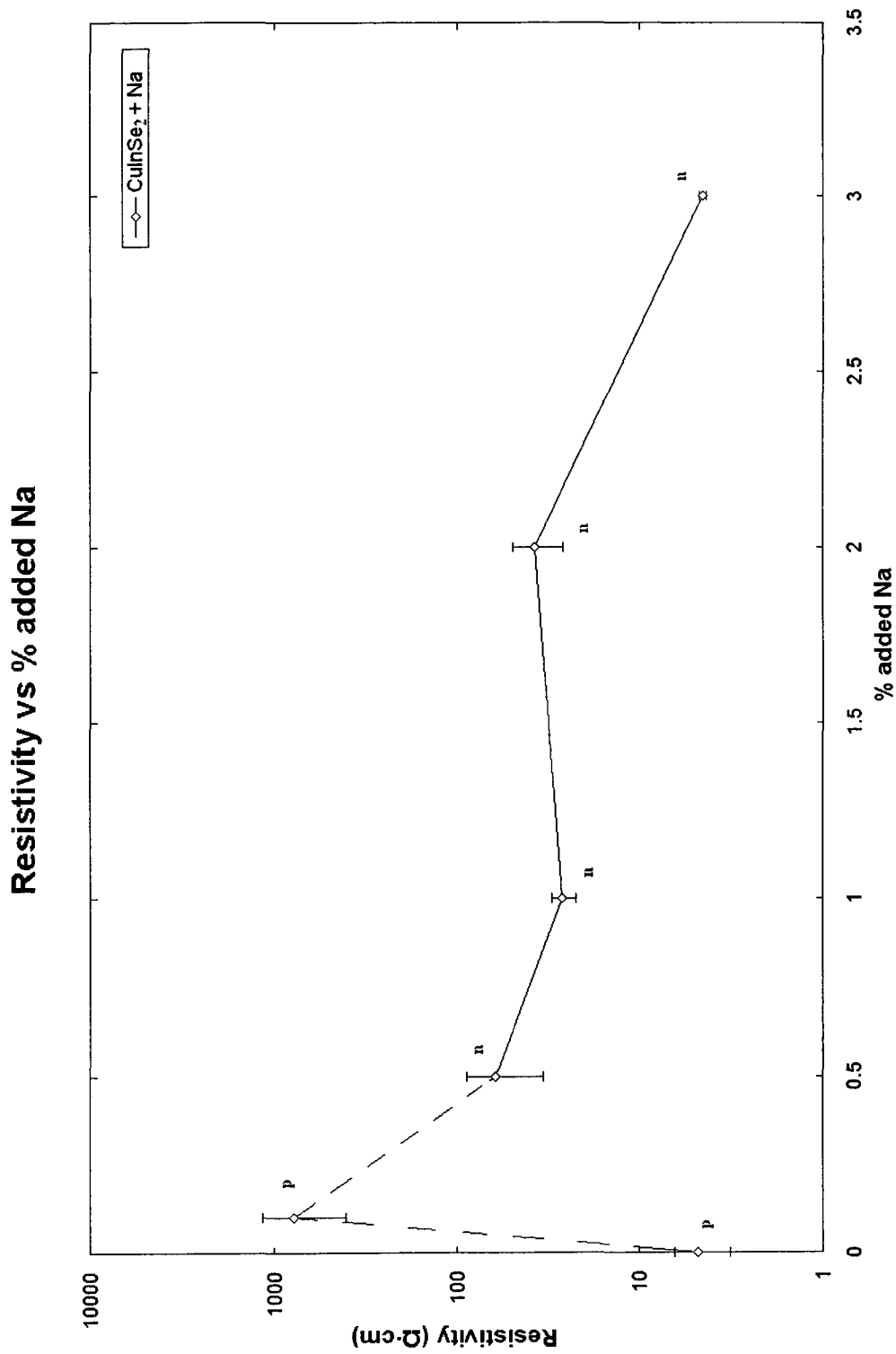


Fig. 5.20 Resistivity vs % added Na for the stoichiometric samples grown with Na^0 , which were seen to undergo a type change from p to n for sodium additions of 0.5% and greater. There would appear to be an overall decrease of resistivity with Na addition in the n-type samples.

Thermoelectric Power versus % added Na

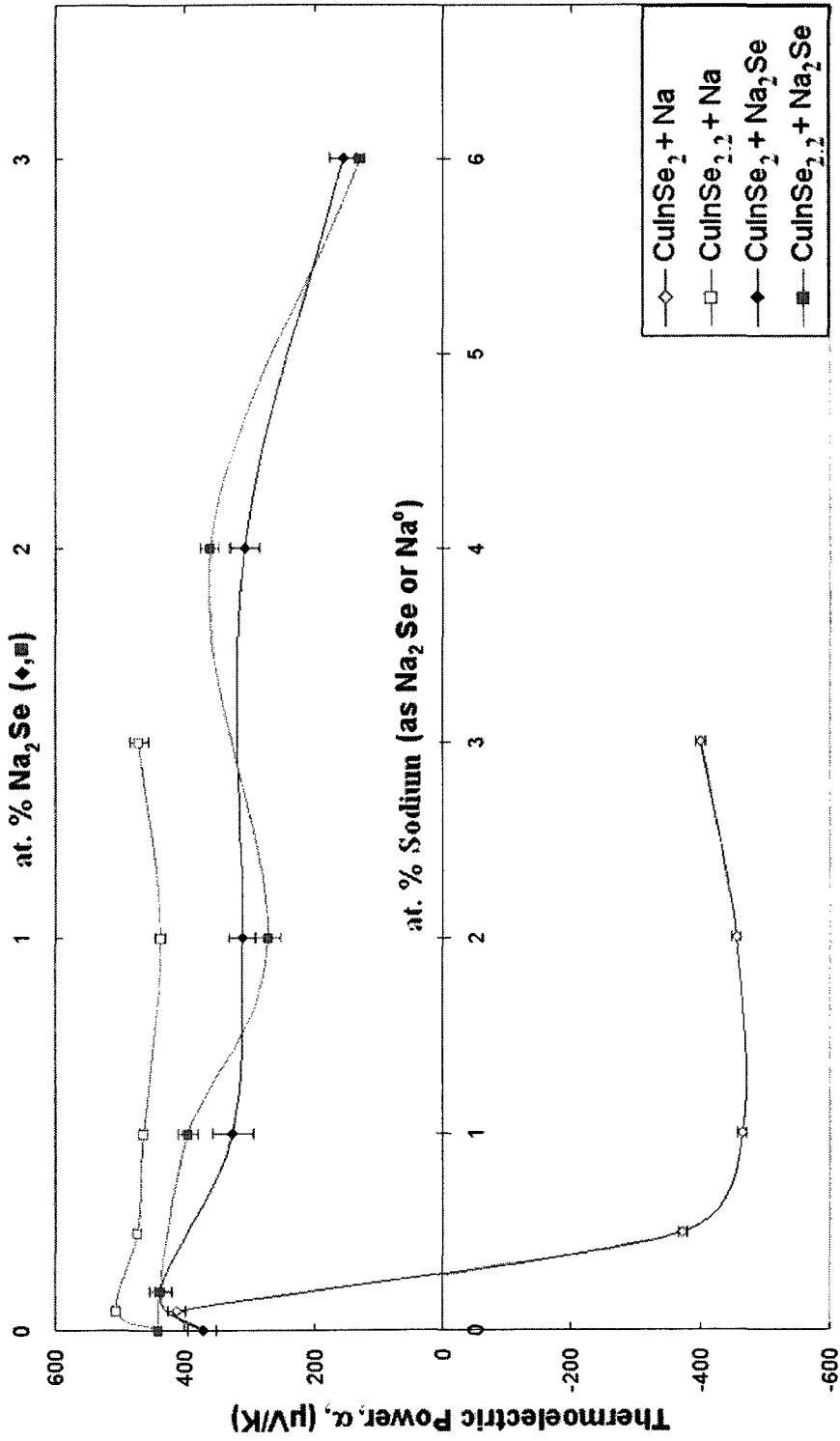


Figure 5.21 Measured thermoelectric power (α) plotted against atomic sodium content for all samples using the middle scale. The upper scale, with values half those of the middle scale, correspond only to samples with Na_2Se additions. The lines through the points represent guidance for the variation.

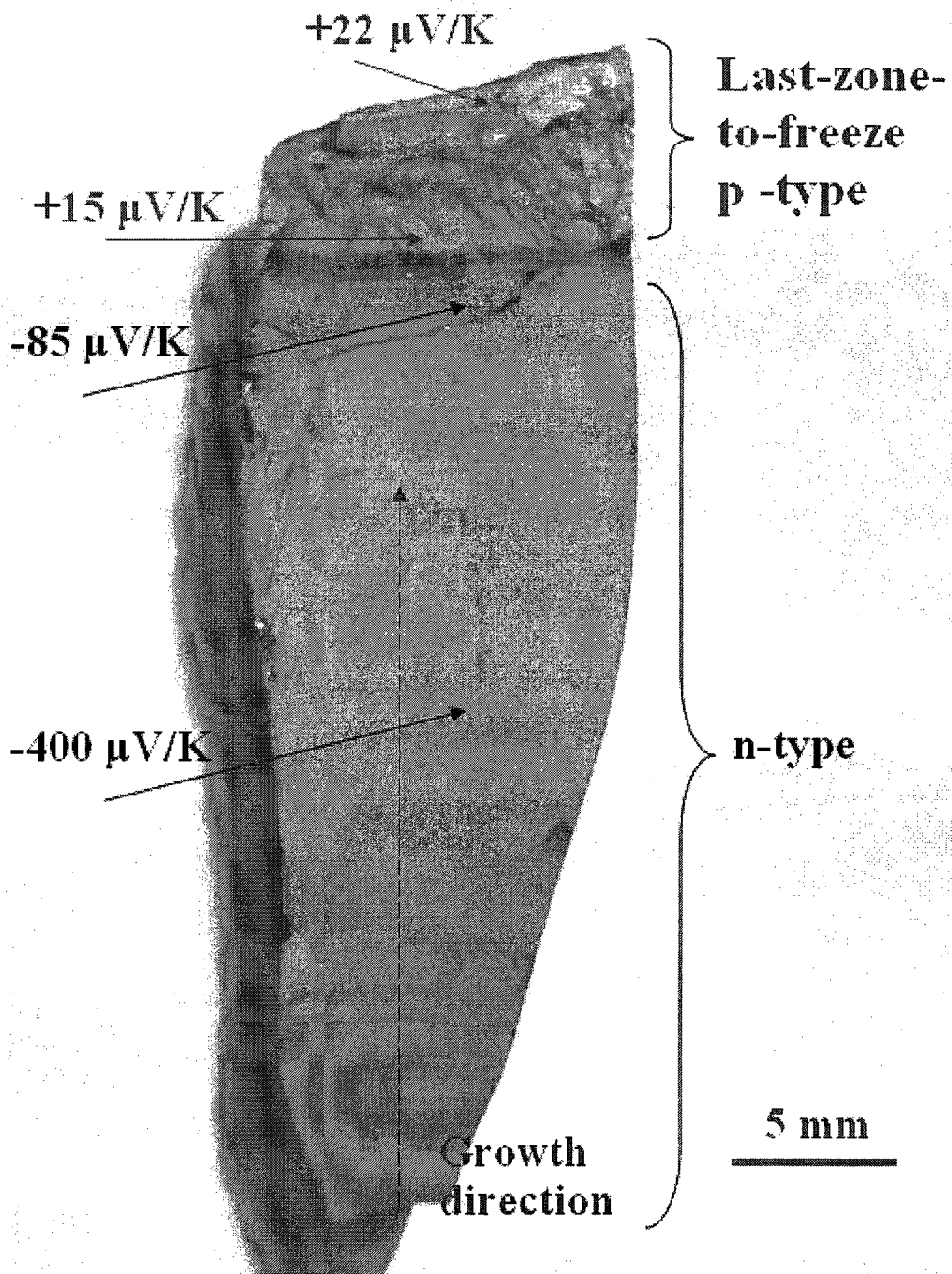


Figure 5.22 A cut surface of ingot HM-B26 (3 at. % Na^0 in stoichiometric CuInSe_2), depicting the n-type main part of the ingot, and the p⁺-type last-zone-to-freeze.

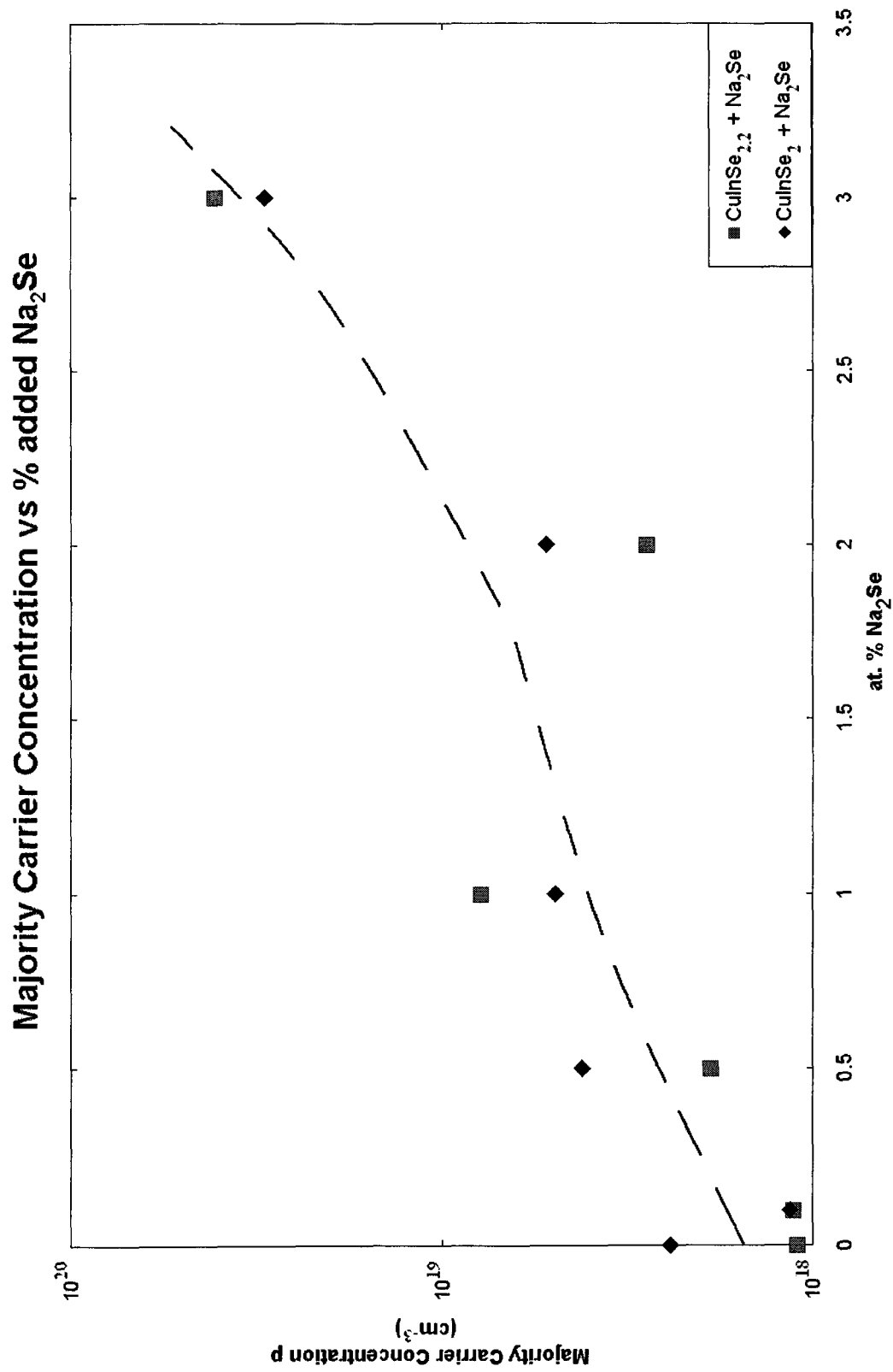


Figure 5.23 Calculated variation of hole concentration, from thermoelectric power, for the samples grown with the addition of Na₂Se.

Chapter 6

Discussion and Conclusions

6.1. INTRODUCTION

This final chapter consists of a discussion of the results of the study presented in this thesis, as reported in Chapter 5. Included at the end of this discussion is a description of a mechanism, detailing the reactions involved in each of the four sets of growth runs, which aims at reconciling all of the observations reported in this thesis. It could be stated that much of this mechanism is speculation and conjecture rather than fact; however, it is based on reported findings, from this study as well as from others. The chapter is ended with a few brief suggestions at how this work may be continued and expanded.

6.2. DISCUSSION OF RESULTS

The appearance of a white deposit on the inner walls of the ampoules grown with additions of Na, in either form, and the subsequent microstructural investigations of this film which revealed it to be essentially sodium (as well as containing Si, O, and C, but no Cu, In, or Se) is indicative of at least a portion of the added Na appearing outside the CuInSe_2 lattice after crystal growth. It may have been considered that the presence of this deposit represented the saturation with Na of the ingots. However, with the failure of XRD analysis to detect any Na within the crystals, even at additions of 3 at. %, it must be concluded that this study has found

no evidence of Na penetrating into the CuInSe_2 lattice. This is in agreement with numerous other studies [6.1-5] in which the same conclusion was reached.

The appearance of a red deposit on the outside surface of the ingots grown with Na was observed to increase with the amount of Na added to the melt, as well white deposit observed, within the same set of ingots. For example, stoichiometric CuInSe_2 plus 2 % Na_2Se produced more red and white deposit than stoichiometric CuInSe_2 plus 1 % Na_2Se . However, the amounts of red and white deposit were found to be inversely related to each other as the quantity of Se added to the ampoules was increased from one set of growth runs to the other. The implication here is that, when an abundance of selenium is present, a portion will bond to the Na within the ampoule, thus depleting the white deposit, before solidifying on the surface of the crystals during the cooling phase of growth. Indeed, Na, along with Se, was detected by XPS and SEM-EDX to be among the many constituents of the red deposit. However, evidence from SEM-EDX also suggests that large portions of this deposit contain copper as well. As a stoichiometric amount of Cu was added to the ampoule and therefore an excess or abundance of this element is not present, the indication is that Cu is somehow removed from the crystals and deposited on their surfaces, resulting in a slight Cu-deficiency. As the quantity of Na is increased, when sufficient Se is also present, more Cu is pulled from the material, which reacts with the Se to form copper selenides, resulting in even more red deposit. Several studies into the effects of Na on CIS have speculated that the formation of elemental copper accompanies any reaction occurring between the Na and the chalcopyrite [6.6-8].

Perhaps when this excess Se is present, the Cu, upon being removed from the material, forms selenides. In samples grown in the complete absence of excess Se, as in the stoichiometric ingots grown with metallic sodium, copper-resembling nodules were seen to form only with large additions of Na⁰.

With the condition of having a complete absence of excess selenium within a sealed ampoule coupled with the addition to this ampoule of Na⁰, it is believed that Na and Se will still form bonds. However, rather than depleting the white deposit, it is suggested that the main effect will be the depletion of Se from the material. D. Braunger et al [6.9] hypothesized that the presence of Na at the growth of CIS and CIGS thin-films results in the formation, and subsequent migration to the surface of said films, of Na₂Se_x. They suggest these compounds act as a reservoir of Se, facilitating its placement in the CuInSe₂ lattice. Among these compounds, Na₂Se may be the principal selenide in the growth runs performed during this work, as less selenium implies less Se partial pressures and therefore favors the formation of this tightly bonded and not easily broken compound over the formation of the “looser” Na₂Se_x, where $x > 1$ [6.9]. However, without selenium to replace the amount which was removed to form Na₂Se, the result may be the creation of V_{Se} donors in such numbers as they become the dominant defect in the material. Ingots grown in this environment would therefore undergo a type conversion from p to n. This was the hypothesis put forward by Wang et al [6.10] in order to explain their observation of this phenomenon. Further work by Champness et al [6.11] and Shukri et al [6.12] confirmed the n-type conductivity of CuInSe₂ grown with a deficiency of Se.

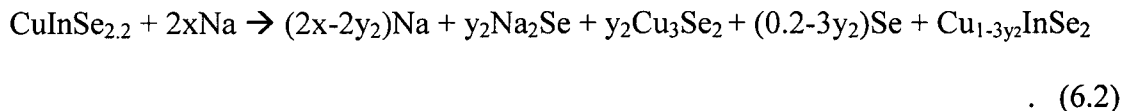
Lyahovitskaya et al [6.7], upon annealing n-type single crystals of CuInSe_2 with Se^0 vapour, observed these crystals to become p-type. However, rather than rationalize this as the removal of V_{Se} due to penetration of the vapour into the crystal, they attribute this type conversion to the creation of V_{Cu} acceptors. In this reaction, they propose that Se is deposited on the surface of the crystal, and that Cu is subsequently diffused to these areas of high Se concentration, leaving behind Cu-vacancies and coating the surfaces with a copper selenide film. In a separate experiment, when the crystals were annealed with Na^0 , the result was the formation of Na_2Se_x and $x\text{Cu}^0$, which deposited on the surface of the crystals, and therefore left them both copper and selenium deficient. These findings, coupled with the findings of this study as detailed in Chapter 5, as well as previous studies which investigated the properties of CuInSe_2 , particularly those of Wang et al [6.10] and Du [6.13], have given rise to the following speculations, aimed at accounting for all of the occurrences of these works:

During CuInSe_2 crystal growth, sodium atoms bond with or act as a sink for the selenium, thereby depleting a quantity of Se from the crystal, eventually depositing this element or a selenide on the surface. In this model, a very small amount of copper is also depleted by diffusion toward the Se-rich surface. The resulting ingots are primarily Se-deficient and therefore n-type. The sodium not involved in this reaction adheres to the sides of the ampoule in the form of a white deposit, while the copper and selenide mixture eventually becomes a red deposit at the last-zone-to-freeze. It is proposed that such a reaction may progress as follows:

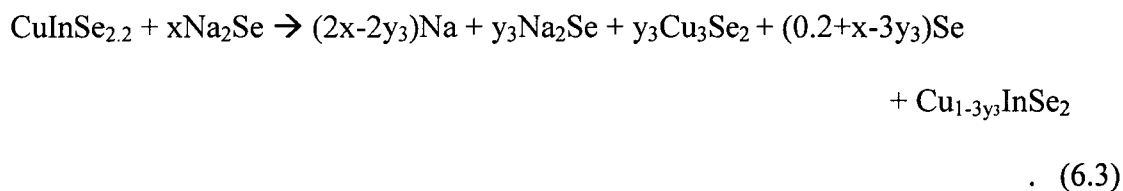


In this reaction the red deposit, of which there was very little, is represented as Na_2Se . This is an oversimplification, as the red deposit is comprised of many phases, including (from XPS) Se^0 , Cu^0 , CuSe and In^0 and, after oxidation, CuO , InO_x and SeO . Sodium was also seen in the red deposit. Cu_3Se_2 , previously identified by XRD in the grey dots of ingots grown with Na_2Se , might be included amongst the phases of the red deposit as well. The term y_1 is meant to represent a portion of Na^0 that bonds with or removes the Se; the remainder of the sodium ends up as the white deposit. Thus, it is the deficiency of selenium that is essentially responsible for the type change from p to n for large concentrations of Na. A slight deficiency of copper, which possibly occurs, is not accounted for in Eq. (6.1). This is to avoid detracting from the main activity in the ingot, which is the removal of selenium and hence the n-type behaviour.

It is further proposed that, if there exists sufficient selenium to replace the amount removed by the sodium, as provided by an excess of Se ($\text{CuInSe}_{2.2}$), the following reaction would take place:



In this equation, $y_2 < x < 0.2$. As well, y_2 is greater than y_1 , as there is more Se present for the Na to bond with or remove. As such, the amount of white powder is reduced, and the amount of red deposit is increased. The major difference is that the removal of selenium from the chalcopyrite no longer occurs. Any selenium that does not bond or remove with the sodium is left as a remainder, appearing as spots on the sides of the ampoule and black film on the ingot. Copper is also removed from the material, making it p-type due to the creation of copper vacancies. It has been suggested [6.14] that V_{Cu} is an acceptor in $CuInSe_2$. The copper may then bond with the excess Se, forming Cu_3Se_2 (umangite) which, along with Na_2Se , forms the red deposit. However, this may be a simplification. It was observed that as Na concentration is increased, corresponding in Eq. (6.2) to increases in x , more white and red deposits were produced. However, this did not result in a change in α , implying that the ratio of Cu, In and Se in the chalcopyrite remained essentially the same with increases of Na. It could be that the amount of copper removed here is more dependent on the $(0.2-3y_2)Se$ term than the Na_2Se , which changes little as x is increased. A similar reaction mechanism is to be interpreted for additions of Na_2Se rather than Na^0 , such as:



However, it is not immediately obvious, by examination of Eq. (6.2) and (6.3), that the hole concentration would increase with additions of Na_2Se but not Na^0 (see Fig. 5.21). It is possible that the quantity of Cu removed is greater in the latter case, implying y increases more with additions of Na_2Se than Na^0 , i.e. $y_3 < y_2$.

Alternatively, it has been hypothesized that, with the addition of Na_2Se , less Se is removed from the chalcopyrite, and so the remaining Se migrates to Cu-sites in the lattice, thus forming Cu_2Se_x , Cu_3Se_2 , etc. These compounds may then be precipitated from the chalcopyrite to the surface, resulting in the creation of V_{Cu} , thus increasing the density of acceptor sites in the material. This, however, might not happen with Na^0 and excess Se, as Na^0 is more successful in drawing out Se than Na_2Se . Therefore, with Na^0 , V_{Se} and V_{Cu} occur together, thereby compensating the acceptor effect of the creation of V_{Cu} and resulting in no significant increase in carrier concentration.

To summarize, an increase in hole concentration was observed for increases of sodium in the form of Na_2Se into melts of CuInSe_2 in both stoichiometric proportions and in the presence of excess Se. However, the same was not observed for elemental sodium Na^0 , which resulted in n-type ingots in stoichiometric CuInSe_2 , and no change in hole concentration for $\text{CuInSe}_{2.2}$. These observations would suggest important differences in the behaviour of CuInSe_2 to the presence of sodium in different forms, and under different conditions of availability of selenium.

6.3. FUTURE WORK

While the present research has obtained many interesting results, including confirmation of type conversion with the addition of sodium to stoichiometric CuInSe₂, it has not given a clear explanation of the beneficial effect of the element in CIS solar cells. To make further progress in this direction, photovoltaic cells will need to be fabricated and investigated, where the absorber substrate consists of monocrystalline p-type CuInSe₂, with and without sodium, either in elemental form or as Na₂Se. Accordingly, cells with the layer structure CuInSe₂-CdS-ZnO_{intrinsic}-ZnO_{doped} will be fabricated and examined in detail. Besides photovoltaic cells, further work should be done to find out why the addition of Na₂Se decreases the thermoelectric power, while Na also apparently does not. It is possible that oxygen plays a role in this difference, and this possibility ought to be explored. The accuracy of the thermoelectric power measurements should also be improved by having a thermocouple closer to the heated tip of the probe. Additionally, some Hall-effect measurements on selected samples should be done to help explain the thermoelectric power and conductivity results. As well, improvements in the four-point probe should be carried out, particularly by reducing the pin-to-pin distance to enable resistivity over smaller regions to be obtained. The source of the cracking of ampoules should also be looked into. Several uncertainties surrounding this cracking have yet to be answered, including whether the presence of the sodium weakens the quartz, or whether it mitigates the non-sticking effect of the boron nitride and thus causes the cracking by differential contraction during the cooling stage of the ingot preparation. Finally, further efforts should be made in the Bridgman-growth

procedure in order to obtain larger and higher quality CuInSe_2 monocrystals. The author hopes he will have the opportunity to devote himself to such a program of further investigation.

REFERENCES

- [1.1] C.H. Champness, *Physics in Canada*, **57**, 1 (2001) 29.
- [1.2] S.B. Zhang, S.H. Wei, A. Zunger, H. Katayama-Yoshida, *Phys. Rev. B*, **57**, 16 (1998) 9642.
- [1.3] R. Noufi, K. Zweibel, 4th WCPEC, **1** (2006) 317.
- [1.4] L. Kazmerski, K. Zweibel, Best Research Cell Efficiencies. http://www.nrel.gov/pv/thin_film/pn_general_interest.html#presentation (accessed Sept 2008).
- [1.5] W.S. Weng, L.S. Yip, I. Shih, C.H. Champness, *Can J. Phys.*, **67** (1989) 294.
- [1.6] L.S. Yip, I. Shih, C.H. Champness, *J. Crystal Growth*, **129**, 1-2 (1993) 102.
- [1.7] C.H. Champness, *Thin Solid Films*, **431-432** (2003) 172.
- [1.8] Z.A. Shukri, C.H. Champness, *Acta. Cryst. B*, **53** (1997) 620.
- [1.9] C.H. Champness, T. Cheung, I. Shih, 4th WCPEC, **1** (2006) 512.
- [1.10] Z.A. Shukri, C.H. Champness, *J. Crystal Growth*, **191**, 1-2 (1998) 97.
- [1.11] C.H. Champness, I. Shih, H. Du, *Thin Solid Films*, **431-432** (2003) 68.
- [1.12] H.P. Wang, I. Shih, C.H. Champness, 28th IEEE Photovoltaic Specialists Conf. Record (2000) 642.
- [1.13] M. Bodegård, L. Stolt, J. Hedström, 12th European PVSEC (1994) 1743.
- [1.14] B.M. Keyes, F. Hasoon, P. Dippo, A. Balcioglu, F. Abulfotuh, 26th IEEE Photovoltaic Specialists Conf. Record (1997) 479.
- [1.15] M.A. Contreras, B. Egass, P. Dippo, J. Webb, J. Granata, K. Ramanathan, S. Asher, A. Swartzlander, R. Noufi, 26th IEEE Photovoltaic Specialists Conf. Record (1997) 359.
- [1.16] L. Kronik, D. Cahen, H.W. Schock, *Adv. Mater.*, **10**, 1 (1998) 31.
- [1.17] D.J. Schroeder, A.A. Rockett, *J. Appl. Phys.*, **82**, 10 (1997) 4982.

- [1.18] B.J. Stanbery, S. Kincal, S. Kim, T.J. Anderson, O.D. Crissale, S.P. Ahrenkiel, G. Lippold, 28th IEEE Photovoltaic Specialists Conf. Record (2000).
- [1.19] V. Lyahovitskaya, Y. Feldman, K. Gartsman, H. Cohen, C. Cytermann, D. Cahen, J. Appl. Phys., **91**, 7 (2002) 4205.
- [1.20] A. Rockett, Thin Solid Films, 481 (2005) 2.
- [1.21] J.E. Granata, J.R. Sites, S. Asher, R.J. Matson, 26th IEEE Photovoltaic Specialists Conf. Record (1997) 387.
- [1.22] T. Nakada, D. Iga, H. Ohbo, A. Kunioka, Jap. J. Appl. Phys., **36**, 2 (1997) 732.
- [1.23] M. Ruckh, D. Schmid, M. Kaiser, R. Schäffler, T. Walter, H.W. Schock, 1st WCPEC (1994) 156.
- [2.1] C.H. Champness, T. Cheung, I. Shih, Conf. Rec. IEEE 4th World Conf. PVEC, **1** (2006) 512.
- [2.2] V.A. Johnson and K. Lark-Horovitz, Phys. Rev. **92**, 2 (1953) 226.
- [2.3] H. Neumann, R.D. Tomlinson, E. Nowak, N. Avgerinos, Phys. Stat. Sol. (a), **56** (1979) K137.
- [2.4] R.F. Pierret, *Modular Series on Solid State Devices Volume I Semiconductor Fundamentals*, 2nd ed.; Addison-Wesley Publishing Co: Reading, Ma, 1988; p 70.
- [2.5] L.B. Valdes, Proc. I.R.E. **42** (1954) 420.
- [3.1] H. Hahn, G. Frank, W. Klinger, A.D. Meyer, G. Störger, Zeif. F. Anorg. Allge. Chemie, **271** (1953) 11.
- [3.2] S. Wagner, J.L. Shay, P. Migliorato, H.M. Kasper, Appl. Phys. Lett., **25**, 8 (1974) 434.
- [3.3] J.L. Shay, S. Wagner and H.M. Kasper, Appl. Phys. Lett., **27**, 2 (1975) 89.
- [3.4] L.L. Kazmerski, F.R. White, G.K. Morgan, Appl. Phys. Lett., **29**, 4 (1976) 268.
- [3.5] J.L. Shay, B. Tell, H.M. Kasper, L.M. Schiavone, Phys. Rev. B, **7**, 10 (1973) 4485.

- [3.6] L.L. Kazmerski, M.S. Ayyagari, G.A. Sanborn, J. Appl. Phys., **46**, 11 (1975) 7865.
- [3.7] L.L. Kazmerski, P.J. Ireland, F.R. White, R.B. Copper, 13th IEEE Photovoltaic Specialists Conf. Record (1978) 184.
- [3.8] R.A. Mickelsen, W.S. Chen, Appl. Phys. Lett., **36**, 5 (1980) 371.
- [3.9] R.A. Mickelsen, W.S. Chen, Y.R. Hsiao, V.E. Lowe, IEEE Trans. Electron Devices, **ED-31**, 5 (1984) 542.
- [3.10] R.A. Mickelsen, W.S. Chen, Proc. 16th Photovoltaic Specialists Conf. (1982) 781.
- [3.11] W.E. Devaney, R.A. Mickelsen, W.S. Chen, 18th IEEE Photovoltaic Specialists Conf. Record (1985) 1733.
- [3.12] W.E. Devaney, W.S. Chen, J.M. Stewart, R.A. Mickelsen, IEEE Trans. Electr. Dev., **37**, 2 (1990) 428.
- [3.13] J. Hedström, H. Ohlsén, M. Bodegård, A. Kylner, L. Stolt, D. Hariskos, M. Ruckh, H.W. Schock, 23rd IEEE Photovoltaic Specialists Conf. Record (1993) 364.
- [3.14] J. Holz, F. Karg, H. von Philipsborn, 12th European PVSEC (1994) 1592.
- [3.15] L. Margulis, G. Hodes, A. Jakubowicz, D. Cahen, J. Appl. Phys., **66**, 15 (1989) 3554.
- [3.16] L. Stolt, M. Bodegård, J. Hedström, J. Kessler, M. Ruckh, K.O. Velthaus, H.W. Schock, 11th European PVSEC (1992) 120.
- [3.17] M. Bodegård, L. Stolt, J. Hedström, 12th European PVSEC (1994) 1743.
- [3.18] D.F. Dawson-Elli, C.B. Moore, R.R. Gay, C.L. Jensen, 1st WCPEC (1994) 152.
- [3.19] J.E. Granata, J.R. Sites, S. Asher, R.J. Matson, 26th IEEE Photovoltaic Specialists Conf. Record (1997) 387.
- [3.20] D. Rudmann, M. Kaelin, F.J. Haug, F. Kurdesau, H. Zogg, A.N. Tiwari, 3rd WCPEC (2003) 376.
- [3.21] A. Rockett, J.S. Britt, T. Gillespie, C. Marshall, M.M. Al Jassim, F. Hasoon, R. Matson, B. Basol, Thin Solid Films, 372 (2000) 212.

- [3.22] W.N. Shafarman, J. Zhu, Mater. Res. Soc. Symp. Proc., 668 (2001) H2.3.1.
- [3.23] M. Lammer, R. Kniese, M. Powalla, Thin Solid Films, 451 (2004) 175.
- [3.24] V. Probst, J. Rimmasch, W. Riedl, W. Stetter, J. Holz, H. Harms, F. Karg, H.W. Schock, 1st IEEE WCPEC (1994) 144.
- [3.25] T. Nakada, T. Kume, A. Kunioka, 25th IEEE Photovoltaic Specialists Conf. Record (1996) 893.
- [3.26] R. Kimura, T. Nakada, P. Fons, A. Yamada, S. Niki, T. Masuzawa, K. Takahashi, A. Kunioka, Sol. Energy Mat. Sol. Cells, 67 (2001) 289.
- [3.27] A. Rockett, M. Bodegård, K. Granath, L. Stolt, 25th IEEE Photovoltaic Specialists Conf. Record (1996) 985.
- [3.28] A. Rockett, Thin Solid Films, 481 (2005) 2.
- [3.29] D.W. Nilas, M. Al Jassim, K. Ramanathan, J. Vac. Sci. Technol. A, 17, 1 (1999) 291.
- [3.30] J.H. Scofield, S. Asher, D. Albin, J. Tuttle, M. Contreras, D. Nilas, R. Reedy, A. Tennant, R. Noufi, 1st WCPEC (1994) 164.
- [3.31] C. Heske, R. Fink, E. Umbach, W. Riedl, F. Karg, Appl. Phys. Lett., 68, 24 (1996) 3431.
- [3.32] V. Lyahovitskaya, Y. Feldman, K. Gartsman, H. Cohen, C. Cytermann, D. Cahen, J. Appl. Phys., 91, 7 (2002) 4205.
- [3.33] B.M. Keyes, F. Hasoon, P. Dippo, A. Balcioglu, F. Abulfotuh, 26th IEEE Photovoltaic Specialists Conf. Record (1997) 479.
- [3.34] T. Nakada, D. Iga, H. Ohbo, A. Kunioka, Jap. J. Appl. Phys., 36, 2 (1997) 732.
- [3.35] M. Ruckh, D. Schmid, M. Kaiser, R. Schäffler, T. Walter, H.W. Schock, 1st WCPEC (1994) 156.
- [3.36] D.J. Schroeder, A.A. Rockett, J. Appl. Phys., 82, 10 (1997) 4982.
- [3.37] H.P. Wang, I. Shih, C.H. Champness, 28th IEEE Photovoltaic Specialists Conf. Record (2000) 642.

- [3.38] U. Rau, M. Schmitt, D. Hilburger, F. Engelhardt, O. Seifert, J. Parisi, W. Riedl, J. Rimmasch, F. Karg, 25th IEEE Photovoltaic Specialists Conf. Record (1996) 1005.
- [3.39] S.B. Zhang, S.H. Wei, A. Zunger, H. Katayama-Yoshida, Phys. Rev. B, **57**, 16 (1998) 9642.
- [3.40] B.J. Stanbery, E.S. Lambers, T.J. Anderson, 26th IEEE Photovoltaic Specialists Conf. Record (1997) 499.
- [3.41] T. Tanaka, Y. Kitamura, T. Yamaguchi, A. Yoshida, 2nd WCPEC (1998) 608.
- [3.42] L. Kronik, D. Cahen, U. Rau, R. Herberholz, H.W. Schock, 2nd WCPEC (1998) S. 453.
- [3.43] L. Kronik, D. Cahen, H.W. Schock, Adv. Mater., **10**, 1 (1998) 31.
- [3.44] S.H. Wei, S.B. Zhang, A. Zunger, J. Appl. Phys., **85**, 10 (1999) 7214.
- [3.45] M.A. Contreras, B. Egaas, P. Dippo, J. Webb, J. Granata, K. Ramanathan, S. Asher, A. Swartzlander, R. Noufi, 26th IEEE Photovoltaic Specialists Conf. Record (1997) 359.
- [3.46] J.E. Granata, J.R. Sites, 2nd WCPEC (1998) 604.
- [3.47] D.W. Niles, K. Ramanathan, F. Hasoon, R. Noufi, B.J. Tielsch, F.E. Filghum, J. Vac. Sci. Technol. A, **15**, 6 (1997) 3044.
- [3.48] D. Braunger, D. Hariskos, G. Bilger, U. Rau, H.W. Schock, Thin Solid Films, 361-362 (2000) 161.
- [3.49] D. Braunger, S. Zweigart, H.W. Schock, 2nd WCPEC (1998) 1113.
- [4.1] Z.A. Shukri, *Bridgman growth of CuInSe₂ monocrystals for photovoltaic cell research*. Ph.D. Thesis, McGill University (1996).
- [4.2] G.I. Ahmed, *Electrical investigations on CuInSe₂ single crystals*. M.Eng. Thesis, McGill University (1996).
- [4.3] H.P. Wang, *Studies of compounds related to Cu(In_{1-x})Ga_xSe₂ solar cells*. Ph.D. Thesis, McGill University (2001).
- [4.4] V. Lyahovitskaya, Y. Feldman, K. Gartsman, H. Cohen, C. Cytermann, D. Cahen, J. Appl. Phys., **197**, (1999) 177.
- [4.5] Z.A. Shukri, C.H. Champness, I. Shih, J. Crystal Growth, **129** (1993) 107.

- [4.6] H. Du, *Study of photovoltaic cells fabricated with monocrystalline Bridgman-grown CuInSe₂*. M.Eng. Thesis, McGill University (2003).
- [4.7] T.C.H. Cheung, *Room temperature transport measurements on Bridgman-grown CuIn_{1-x}Ga_xSe₂*. M.Eng. Thesis, McGill University (2005).
- [4.8] S. Agilan, D. Mangalaraj, Sa.K. Narayandass, G. Mohan Rao, *Physica B: Condensed Matter*, **365**, 1-4 (2005) 93.
- [4.9] *CRC Handbook of Chemistry and Physics, 62nd ed.*; CRC Press: Boca Raton, Fl, 1982; p. F-67.
- [4.10] L. Rybach, F. Laves, *Geochim. Cosmochim. Acta*, **31** (1967) 539.
- [5.1] W.S. Weng, L.S. Yip, I. Shih, C.H. Champness, *Can J. Phys.*, **67** (1989) 294.
- [5.2] Z.A. Shukri, C.H. Champness, *Acta. Cryst. B*, **53** (1997) 620.
- [5.3] H. Du, C.H. Champness, I. Shih, *Thin Solid Films*, **480** (2005) 37.
- [5.4] S. Niki, P.J. Fons, Y. Lacroix, K. Iwata, A. Yamada, H. Oyanagi, M. Uchino, U. Suzuki, R. Suzuki, S. Ishibashi, T. Ohdaira, N. Sakai, H. Yokokawa, *J. Crystal Growth*, **201-202** (1999) 1061.
- [5.5] H.P. Wang, I. Shih, C.H. Champness, *28th IEEE Photovoltaic Specialists Conf. Record* (2000) 642.
- [5.6] J.E. Granata, J.R. Sites, *2nd WCPEC* (1998) 604.
- [5.7] Z.A Shukri, C.H. Champness, I. Shih, *J. Crystal Growth*, **129**, 1-2 (1993) 107.
- [5.8] V. Lyahovitskaya, Y. Feldman, K. Gartsman, H. Cohen, C. Cytermann, D. Cahen, *J. Appl. Phys.*, **91**, 7 (2002) 4205.
- [5.9] L. Garbato, F. Ledda, and R. Rucci, *Prog. Cryst. Growth Charact.* **15**, 1 (1987) 1.
- [5.10] T. Tanaka, Y. Kitamura, T. Yamaguchi, A. Yoshida, *2nd WCPEC* (1998) 608.
- [5.11] S.H. Wei, S.B. Zhang, A. Zunger, *J. Appl. Phys.*, **85**, 10 (1999) 7214.
- [5.12] F.M. Smits, *The Bell System Technical Journal*, **37** (1958) 711.
- [5.13] J. Holz, F. Karg, H. von Philipsborn, *12th European PVSEC* (1994) 1592.

- [5.14] V. Probst, J. Rimmasch, W. Riedl, W. Stetter, J. Holz, H. Harms, F. Karg, H.W. Schock, 1st IEEE WCPEC (1994) 144.
- [5.15] R. Kimura, T. Nakada, P. Fons, A. Yamada, S. Niki, T. Masuzawa, K. Takahashi, A. Kunioka, Sol. Energy Mat. Sol. Cells, 67 (2001) 289.
- [5.16] C.H. Champness, T. Cheung, I. Shih, Sol. Energy. Mat. Sol. Cells, **91**, 9 (2007) 791.
- [5.17] C.H. Champness, I. Shih, H. Du, Thin Solid Films, **431-432** (2003) 68.
- [5.18] L. Kronik, D. Cahen, H.W. Schock, Adv. Mater., **10**, 1 (1998) 31.
- [5.19] J.E. Granata, J.R. Sites, S. Asher, R.J. Matson, 26th IEEE Photovoltaic Specialists Conf. Record (1997) 387.
- [5.20] M. Ruckh, D. Schmid, M. Kaiser, R. Schäffler, T. Walter, H.W. Schock, 1st WCPEC (1994) 156.
- [5.21] H. Neumann, R.D. Tomlinson, E. Nowak, N. Avgerinos, Phys. Stat. Sol. (a), **56** (1979) K137.
- [6.1] M. Bodegård, L. Stolt, J. Hedström, 12th European PVSEC (1994) 1743.
- [6.2] A. Rockett, Thin Solid Films, 481 (2005) 2.
- [6.3] D.W. Niles, M. Al Jassim, K. Ramanathan, J. Vac. Sci. Technol. A, **17**, 1 (1999) 291.
- [6.4] J.H. Scofield, S. Asher, D. Albin, J. Tuttle, M. Contreras, D. Niles, R. Reedy, A. Tennant, R. Noufi, 1st WCPEC (1994) 164.
- [6.5] C. Heske, R. Fink, E. Umbach, W. Riedl, F. Karg, Appl. Phys. Lett., **68**, 24 (1996) 3431.
- [6.6] J.E. Granata, J.R. Sites, 2nd WCPEC (1998) 604.
- [6.7] V. Lyahovitskaya, Y. Feldman, K. Gartsman, H. Cohen, C. Cytermann, D. Cahen, J. Appl. Phys., **91**, 7 (2002) 4205.
- [6.8] S.H. Wei, S.B. Zhang, A. Zunger, J. Appl. Phys., **85**, 10 (1999) 7214.
- [6.9] D. Braunger, D. Hariskos, G. Bilger, U. Rau, H.W. Schock, Thin Solid Films, 361-362 (2000) 161.

- [6.10] H.P. Wang, I. Shih, C.H. Champness, 28th IEEE Photovoltaic Specialists Conf. Record (2000) 642.
- [6.11] C.H. Champness, I. Shih, H. Du, Thin Solid Films, **431-432** (2003) 68.
- [6.12] Z.A. Shukri, C.H. Champness, J. Crystal Growth, **191**, 1-2 (1998) 97.
- [6.13] H. Du, *Study of photovoltaic cells fabricated with monocrystalline Bridgman-grown CuInSe₂*. M.Eng. Thesis, McGill University (2003).
- [6.14] S.B. Zhang, S-H Wei, A. Zunger, Phys. Rev. B, **57**, 16 (1998) 9642.